Doctor of Engineering

Development of Low-cost and High Sensitive Platform for Rapid Disease Diagnosis

질병 신속 진단을 위한 저비용, 고감도 플랫폼 개발

The Graduate School
of the University of Ulsan

Department of Medicine
Jin, Choong Eun

Development of Low-cost and High Sensitive Platform for Rapid Disease Diagnosis

Supervisor : Shin, Yong

A Dissertation

Submitted to
the Graduate School of the University of Ulsan
In partial Fulfillment of the Requirements
for the Degree of

Doctor of Engineering

by

Jin, Choong Eun

Department of Medicine
Ulsan, Korea
August, 2019

Development of Low-cost and High Sensitive Platform for Rapid Disease Diagnosis

This certifies that the dissertation
of Jin, Choong Eun is approved

Committee Chair Dr. **Kim, Sung-Han**

Committee Member Dr. **Park, In Ja**

Committee Member Dr. **Shin, Yong**

Committee Member Dr. **Lee, Tae Yoon**

Committee Member Dr. **Park, Yun-Yong**

Department of Medicine
Ulsan, Korea
August, 2019

ABSTRACT

Background

In order to manage and treat diseases rapidly, it is important to identify the cause of a disease accurately and quickly. In particular, emerging infectious diseases and cancers are the main causes of death, and treatment and management differ depending on the presence of targeted pathogens or mutations. For these reasons, accurate diagnosis is necessary. Currently developed diagnostic methods are high-cost, time-consuming methods with low sensitivity and specificity. In addition, in cases of emerging infectious diseases, the current method of diagnosis requires complex equipment and technology, despite the need for rapid on-site diagnosis. To overcome these limitations, rapid and accurate disease diagnostic approach was developed using a sample preparation technology-based microfluidic platform and bio-optical sensor based silicon microring resonator.

Method

For clinical sample preparation, a microfluidic platform was developed that enabled pathogen enrichment and nucleic acids extraction using homobifunctional imidoester reagents. HI reagents bind to pathogens or nucleic acids via covalent bonding and electrostatic interactions. To validate the clinical utility of this platform and compare its performance with that of conventional methods, we obtained plasma samples from patient with ST and SFTS patients, 10 nasopharyngeal samples from patient with HAdV infection, 12 environmental swab samples exposed to patients with hPIV-3, and 20 saliva and 14 plasma samples from paateints with HZ. A microfluidic platform that can isolate cell-free DNA from the plasma of patients with cancer without a cell lysis step was also developed. cfDNA isolated using this platform can be analyzed oncogenic mutations (*BRAF*, *KRAS*). Moreover, the Oncopanel result of isolated cfDNA compared to WES result of tissue specimens from patient with colorectal cancer. Finally, for detecting nucleic acids, a bio-optical sensor using the isothermal PCR method was developed. This sensor was validated using DNA from patients with ADV, HZ and genomic DNA or cfDNA from patients with cancer.

Result

Sample preparation using a microfluidic platform could handle various

clinical samples within 50 min using one chip. This platform can increase the enrichment ratio more than 80% compared to that with a conventional kit. Its clinical utility in large sample volumes was demonstrated in 46 clinical specimens including environmental swabs, saliva, and blood plasma. This system showed higher sensitivity with these samples and could detect pathogens that were below the threshold of detection using other methods. Moreover, after isolation of cfDNA from the plasma of patients with cancer using the microfluidic platform, the detection efficiency of circulating tumor DNA was increased because of decreased background DNA compared to that using a conventional kit. When the WES result of tissue from patients was compared, the concordance ratio of mutations was 71.4%. With the increasing sensitivity of ctDNA detection, oncogenic mutations in cfDNA can be identified using sequencing or PCR without high-cost NGS analysis. Last, when detecting pathogens or mutations using the bio-optical sensor, the sensitivity of detection is 10-100 times higher compare to that of the qPCR method. By combining the sample preparation using the microfluidic platform, the possibility of a fast and highly sensitive diagnostic platform was confirmed.

Conclusion

In this study, a microfluidic platform enabling sample preparation within 50 min was integrated with a bio-optical sensor for detecting nucleic acids within 20 min. This integrated assay led to rapid and sensitive disease diagnosis technology in clinical specimens. Integrated systems such as this have considerable potential as POC based pathogen diagnostic systems that could have diverse clinical applications in humans and also in animal healthcare. It could also be useful for the clinical diagnosis and monitoring of cancer and infectious disease treatment.

CONTENTS

LIST OF FIGURES

Chapter 4. Rapid Nucleic Acids Detection with Bio-optical Sensor

LIST OF TABLES

Chapter 5. Conclusions

ABBREVIATIONS

ADC	Assembled double microfluidic disposable chips
APDMS	3-aminopropyl diethoxymethylsilane
APTES	3-aminopropyltriethoxysiane
CFU	Colony forming unit
cfDNA	Cell-free DNA
ctDNA	Circulating tumor DNA
Ct	Cycle threshold (Cycle number)
CRC	Colorectal cancer
DI	De-ionized
DMA	Dimethyl adipimidate
DMP	Dimethyl pimelimidate
DMS	Dimethyl suberimidate
DTBP	Dimethyl 3,3'-dithiobispropionimidate
dNTP	Deoxynucleotide triphosphate
EtBr	Ethidium bromide
HAdV	Human adenovirus
HI	Homobifunctional imidoester
hPIV	Human parainfluenza
HZ	Herpes zoster
μTAS	Micro total analysis system
NA	Nucleic acid
NGS	Next generation sequencing
PCR	Polymerase chain reaction
POC	Point-of-care
qPCR	Quantitative real-time PCR
qRT-PCR	Quantitative RT real-time PCR
RPA	Recombinase polymerase amplification
RT	Reverse transcription
SMR	Silicon microring resonator
ST	Scrub typhus
SFTS	Severe fever with thrombocytopenia syndrome
VZV	Varicella-zoster virus
WES	Whole exome sequencing

Chapter 1. General Information

1.1. Homobifunctional imidoester

Crosslinking is the process of chemically joining two or more molecules by a covalent bond. Crosslinking reagents contain reactive ends to specific functional groups (primary amines, sulfhydryls, etc.) on proteins or other molecules. Crosslinkers are commonly used to modify nucleic acids, drugs and solid surfaces. Crosslinking reagents have been used to assist in determination of near-neighbor relationships, three-dimensional structures of proteins, solid-phase immobilization, hapten-carrier protein conjugation and molecular associations in cell membranes (1-3).

Crosslinkers can be either homobifunctional or heterobifunctional. Homobifunctional crosslinkers have two identical reactive groups and often are used in one-step reaction procedures to crosslink proteins, to each other or to stabilize quaternary structure, in solution (4-6).

Imidoester crosslinkers react with primary amines to form amidine bonds. The resulting amidine is protonated and, therefore, has a positive charge at physiological pH. Imidoester crosslinkers react rapidly with amines at alkaline pH to form amidine bonds but have short half-lives. As the pH becomes more alkaline, the half-life and reactivity with amines increases, making crosslinking more efficient when performed at pH 10 than at pH 8. Reaction conditions below pH 10 may result in side reactions, although amidine formation is favored between pH 8-10. Studies using monofunctional alkyl imidates reveal that at pH <10, conjugation can form with just one imidoester functional group. An intermediate N-alkyl imidate forms at the lower pH range and will either crosslink to another amine in the immediate vicinity, resulting in N,N'-amidine derivatives, or it will convert to an amidine bond. At higher pH, the amidine is formed directly without formation of an intermediate or side product (4-6).

DMA, DMP, DMS and DTBP are water soluble, membrane permeable homobifunctional crosslinkers. DMA, DMP and DMS are non-cleavable forms of imidoester crosslinkers. By contrast, DTBP can be cleaved by reducing the disufide bond of the spacer arm (Fig. 1.1).

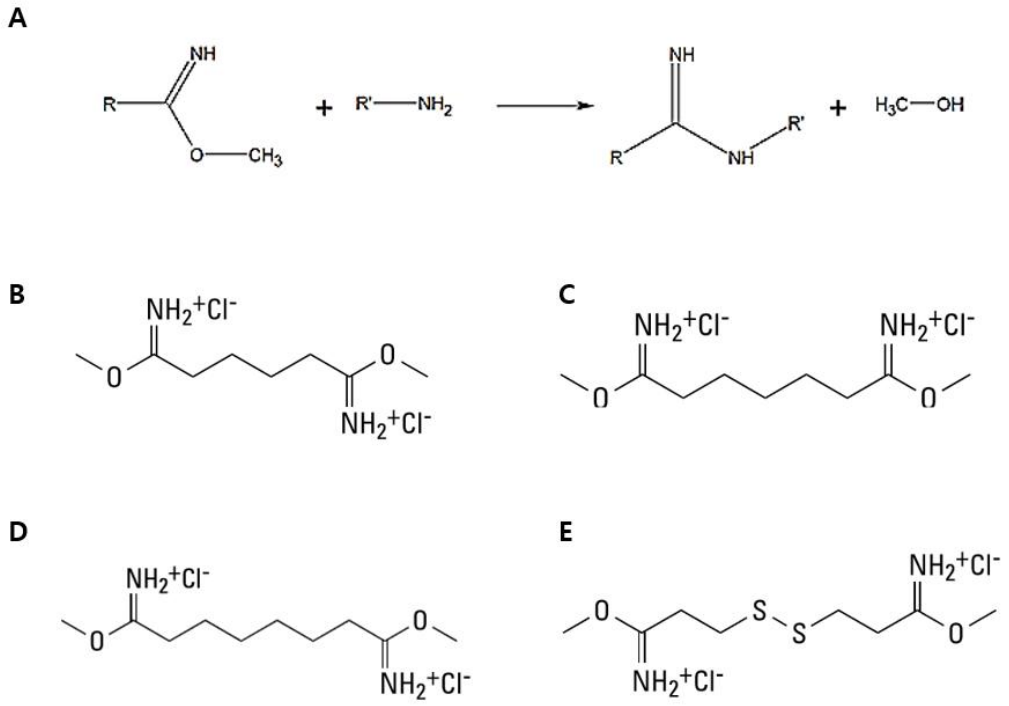

Figure 1.1. Structure of homobifunctional imidoesters. (A) Interaction imidoester with amine. (B) DMA. C) DMP. (D) DMS. (E) DTBP.

1.2 Sample preparation

1.2.1. Diagnosis for infectious disease

The infectious disease is the second leading cause of death in the world, and two-thirds of the victims from infectious diseases are children under five years old (7). Therefore, rapid and accurate diagnosis and treatment of infectious diseases is very important. For diagnosing infectious disease, various diagnosis method was developed for detecting pathogens. Conventional assay for diagnosing infectious disease include blood culture, Dipstick assay, and ELISA, which have low sensitivity and specificity, or require additional test (8, 9). Hence, the gold-standard method for laboratory diagnosis of infectious disease is pathogen isolation in cell cultures. But, this usually requires 1-2 weeks for delivering the infection result. Alternatively, antibody-based immunoassay and PCR methods are relatively more rapid and sensitive than the cell culture method, however, these are not sufficient for the detection of pathogens because of their lack of sensitivity and specificity, as well as their technical complexity (8). Also, they are not suitable for the early diagnosis of pathogens in humans. A rapid and accurate method to

quickly detect this pathogen is needed therefore to enable the rapid and appropriate treatment of diseases in different clinical situations. When a clinical sample for disease diagnosis is obtained, it is subjected to go through three steps of pathogen enrichment, nucleic acid extraction and detection (10). However, in the process of going through these three steps, the expensive equipment such as ultra-centrifuge, PCR and sequencer and skilled techniques are required, which makes this whole process take a few hours or days (10, 11). Therefore, for a long period of time until the accurate diagnosis is made, the patient have to suffer without proper prescription.

One of the diagnostic methods currently in use for infectious disease is point-of-care testing. Briefly, this diagnosis method is a way to confirm whether the patient is sick or not and rapidly respond accordingly without having to go to the hospital. It is simple and easy to use method. Also, the global diagnostic market for point-of-care testing is now increasing significantly. According to World Health Organization (WHO), it is recommended that point-of-care testing should be rapid, sensitive, specific to target, affordable, user-friendly, and equipment-free (12, 13). Although there are many of technologies being used by applying point-of-care testing, but they have still many limitations.

To overcome these limitations, it is important to develop new diagnosis technologies which enable to sample preparation and detection with high sensitivity, rapidity and simplicity.

1.2.2. Cell-free DNA for diagnosing cancer

Since the identification of cell-free nucleic acids (cfNAs) in 1948, detection of cfNAs, including circulating tumor DNA (ctDNA), mRNA, and miRNAs, from liquid biopsies of human plasma has been employed for diagnosing various cancers, monitoring drug resistance, and quantifying minimal residual disease (14-17). Liquid biopsies can overcome the limitations of tumor tissue biopsies, such as sampling bias, intratumoral heterogeneity, and difficulty in repeatedly obtaining samples (18-20). In particular, cfNAs are released in the blood by cell apoptosis and necrosis in both normal and cancer patients and can be considered as diagnostic markers (15). Among the cfNAs in blood plasma, ctDNA has been used for mutation genotyping in various cancers (21, 22). Because ctDNA exists at low levels in plasma, detection methods, such as next-generation sequencing (NGS), droplet digital PCR, and BEAMing, have been developed to analyze ctDNA with high sensitivity (0.01%-0.001%)

(23-25). However, these methods are not considered for cfDNA sampling (23-25).

One major technical issue in cfDNA analysis is the efficiency of the extraction procedure in obtaining the DNA from plasma. Most studies have used affinity column-, magnet-, and polymer-based methods to perform cfDNA extraction (14-16). These methods are expensive, time-consuming, and complex and require additional instruments such as centrifuge or vacuum pump. In addition, they require chaotropic reagents for blood cell lysis that can lead to the release of DNA from non-cancerous cells, which can strongly affect ctDNA analysis. To overcome this issue, procedures of cfDNA sampling from blood plasma need to be standardized to obtain a sufficient amount of DNA and reduce the cellular background, which would subsequently improve the detection sensitivity of ctDNA mutation profiling; however, such methods have been underexplored.

1.3. Microfluidic platform

1.3.1 Characterization of microfluidic platform

A microfluidic system can handle small volumes of body fluids for medical diagnosis with accuracy and rapidity. In addition, microfluidic technologies are cost-effective, portable, and easy to use for sample preparation (26-28). Additionally, given the contagious nature of virus samples, the platform can be disposable to protect end-users from exposure to bio-hazards during the operation. Despite the advantages of microfluidic technologies, many microfluidic-based sample preparation systems are not suitable for obtaining viruses from complex clinical samples with extremely low concentrations that are used in many clinical applications. This is because these systems involve complicated steps for device fabrication, non-biocompatible materials, additional substances, including beads, and require the use of a micropump and microvalves (26-28). Nevertheless, an ideal microfluidic-platform for the purification and isolation of pathogens that can overcome the above limitations is crucial because it can efficiently enhance the detection limit of the detection system.

1.3.2. Fabrication of microfluidic platform

A low-cost thin-film device for use as a microfluidic system (closed system) was fabricated with a CO_2 laser-cutting machine (VLS3.50 (610 ×

305 mm); Universal Laser Systems, Scottsdale, AZ) and comprised microfluidic chambers in a single microchannel in combination with HI for nucleic acid extraction (Fig. 1.2). In contrast to the Qiagen kit (open system), the microfluidic chamber of this system is based on a closed platform to prevent the contamination caused by an open platform. During the washing and elution steps, the reaction samples remain in the microfluidic chamber with the closed platform, which reduces contamination. The shape of the microfluidic chamber was designed to facilitate cell lysis and sample dispersion via inducing the passive micromixing during the nucleic acid extraction. Repeated sudden expansion and contraction in flow cross-sectional area can create microvortices at liquid sample injection. Thirty-five slot-type microwells were connected to each other with expansion and contraction ratios of 1:5.6 and 5.6:1, respectively, in the chamber to extract the nucleic acids (DNA or RNA) from the sources. The design of the microfluidic chip was first drawn using AutoCAD (Autodesk, Inc., San Rafael, CA) and then printed with a laser-cutting machine, which can be used for the fabrication of rapid prototyping devices with low cost, simplicity, and rapidity. In order to fabricate a 3D disposable chip with three layers (Fig. 1.2), the laser-cutting machine (10.6 μ CO_2 laser sources ranging in power from 10 to 50 W) created the three layers comprising 300-μm-thick double-sided tape (Adhesive 300LSE9495LE, 3M, U.S.A.) as an inner layer and two 100-μm-thick thin films (Kemafoil hydrophilic film, HNW-100, COVEME, Italy) as outer layers (Fig. 1.2). The outer layers were attached to the permanent adhesive surfaces of the top and bottom of the inner layer (double-side tape) to generate a 3D disposable chip for the HI reaction (Fig. 1.1). Accordingly, the chamber height was set to approximately 300 μm, and the total volume was 300 μL (Figure 1.2).

Moreover, to control the sample flow in the microchannel, a cast acrylic sheet (MARGA CIPTA, Indonesia) with 3 mm-thickness, attached to the double-sided tape on one side, was cut and drilled by the laser cutting machine. The fabricated adapters were attached to the inlet and outlet of the 3D disposable chip. Thereafter, precut Tygon tubing (AAC02548; Cole-Parmer, Vernon Hills, IL) was placed in the hole of the adapter and sealed using epoxy (EP-05, AXIA EPOXY GLUE, Japan), thermally stable at 120 ℃. Second, for easy handling of the thin-film platform for nucleic acid extraction, a plastic cartridge was fabricated using the laser cutting machine. The plastic cartridge (upper and lower parts) held the 3D disposable chip during the

assay; the dimensions were 105 mm long, 60 mm wide, and 10 mm high. The layout of each plastic component was first designed using AutoCAD (Fig. 1.2). A milling machine patterned the designed structures on transparent acrylonitrile butadiene styrene (ABS) sheets. After mounting the chip on the lower plastic portion, they were assembled with the upper plastic part using four wrench bolts to build the system.

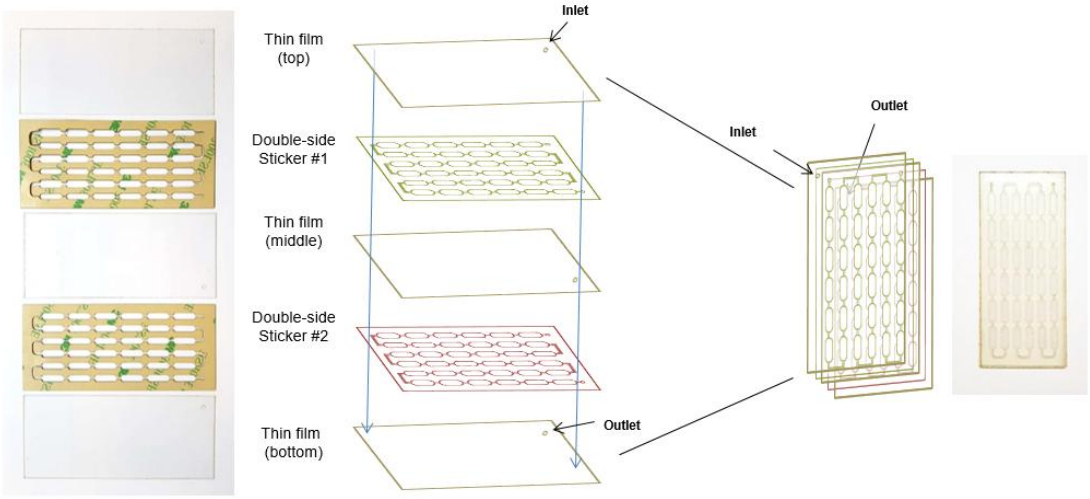

Figure 1.2. An example of microfluidic platform

Finally, in order to use the HI (Fig. 1.1) as a nonchaotropic reagent with the thin film platform for nucleic acid extraction, the surface modification protocol was optimized. Briefly, in order to create an amine group at the inner surface of the 3D disposable chip, the surface was first treated with oxygen plasma (Covance Model, Femtoscience) for 3, 5, 7, and 10 min to change the surface properties of the inner film from being hydrophobic to hydrophilic, and immersed in a solution of 2% APTES or APDMS, Sigma-Aldrich) in H_2O solution for 10-60 min at 65 ℃, followed by thorough rinsing with deionized water. After silanization with APTES or APDMS on the inner surface for 60 min at 65 ℃, the surface hydrophilicity was increased (approximately 30-40°), as reported previously (4, 29). At this point, the system was prepared for the extraction of nucleic acids from various sources. This system can be stored at room temperature until use.

1.3.3. Optimization of microfluidic platform

For isolation of NA from a single sample, a design optimization of microwell for enhancement of bio-molecule binding efficiency is desired. Thus, five microfluidic channels were designed with different micro-well sizes from channel (Ch1 to Ch5) (Fig. 1.3A) to select optimal design of microfluidic channel for bio-molecule isolation. The efficiency of NA binding with HI was examined using five microfluidic channels. Extracted genomic DNA from AGS cell line was diluted with elution buffer, and mixed with the DMP solution. The mixture was injected into the platform with various channels and incubated for interacting between DMP and microwell. After DNA elution with 10mM sodium bicarbonate (<pH 10.6) for breaking the crosslinking, the concenteration of DNA was measured using Nanodrop. In fig. 1.3B, the capture efficiency of DNA showed higher value with smaller size of microwell. Especially, the DNA is captured 100% using Ch4 system against input DNA (Fig. 1.3B). Design of Ch4 was selected for NA extraction and pathogen enrichment in this study.

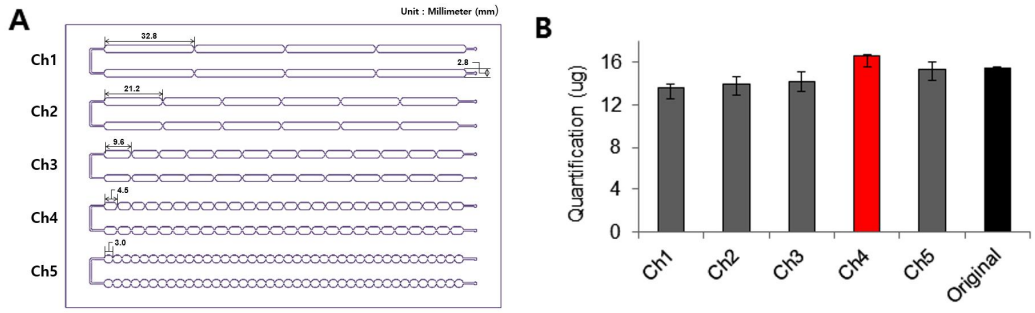

Figure 1.3. The size optimization of microfluidic system. (A) Testing different types of design for optimal capturing of the bio-molecules [Ch1-Ch5]. (B) Recovery testing with the different types of design.

1.4. Bio-optical sensor based on silicon microring resonator

1.4.1. Principles of the isothermal PCR

The isothermal DNA amplification techniques have emerged as an alternative to PCR in molecular diagnostics in order to bypass thermal constraints. Isothermal amplification methods do not require thermal cycling and instead use enzymes for DNA synthesis. Many isothermal amplification methods have been developed to allow exponential amplification at both constant and low temperature including nucleic acid sequence-based amplification (NASBA)

(30), loop-mediated isothermal amplification (LAMP) (31), rolling circle amplification (RCA) (32), helicase-dependent amplification (HDA) (33), and recombinase polymerase amplification (RPA) (34). With the exception of HDA and RPA, most isothermal technologies require an initial denaturation step at 95 ℃ to separate the double-strand DNA. As an isothermal method, RPA does not require thermal cycling and operates at a constant temperature of 37 -42 ℃. The advantage of RPA is that it is able to form a complex consisting of a primer and a recombinase enzyme to extend the DNA, which negates the need for a polymerase and cycle repetition (34, 35). The RPA technique has been applied to the amplification of DNA from bacteria and/or viruses by integration with either microfluidics (36) or lateral flow paper (37). It has not yet been applied to testing of genetic variation (i.e., SNPs, mutations). Recent studies of the amplification of bacterial or viral DNA using RPA techniques have shown that they require less time to attain completion (20-30 min) and have a limit of detection of about 10 copies by using the foil based centrifugal microfluidic cartridge (38), the digital SlipChip (39), and the lateral flow paper (37). Therefore, the high sensitivity of the isothermal RPA technique indicates that it could be useful for the detection of DNA biomarkers in human diseases in POC fields (26).

1.4.2. Preparation of the bio-optical sensor

The bio-optical sensor is combined with the isothermal nucleic acid amplification technique which can detect pathogen or oncogenic mutation in human clinical samples within 30 min. The principle of this bio-optical sensor involves the simultaneous amplification and detection of nucleic acid in a label-free and real-time manner without any additional steps (26-28, 40). The SMR sensor device was obtained from One BioMed Pte Ltd. Briefly, the structures of the SMR sensor were patterned on commercially available silicon on insulator wafer with a 220-nm-thick top silicon layer and 2 mm-thick buried oxide layer by 248-nm deep ultraviolet lithography. The structures were then etched into the buried oxide layer using a reactive ion-etching process, followed by the deposition of 1.5-mm high-density plasma oxide as a top cladding layer. Four microrings were designed that were connected to an input waveguide (through), so that each ring then had an output waveguide (drop). For a reference sensor, 1 ring was left under the SiO_2 cladding to monitor temperature-induced drift. The 3 remaining rings were collected through a vertical grating coupler connected to a single-mode

fiber optic probe.

Next, the sensing chip was prepared using a 3-step process to operate as the bio-optical sensor (Fig. 1.4). First, the surface of the sensing chip was functionalized with an amine group for the immobilization of the primer using an asymmetric technique. The sensors were treated with oxygen plasma for cleaning and surface oxidation and were then immersed in a solution of 2% APTES in a mixture of ethanol-H_2O (95%:5%, v/v) for 2 h, followed by thorough rinsing with ethanol and DI water. To cure the sensors, they were dried under a nitrogen stream and heated to 120 ℃ for 15 min. The sensors were then incubated with 2.5% glutaraldehyde (GAD; Sigma-Aldrich) in DI water containing 5 mM sodium cyanoborohydride (Sigma-Aldrich) for 1 h, followed by rinsing with DI water. All the primers used for the amplification were custom-synthesized (IDT, USA) and are listed in Table 1.1. For DNA primer immobilization, the sensor surface was prepared by incubation with the forward primer in PBS (1 mM) containing 5 mM sodium cyanoborohydride for 16 h at room temperature. Following incubation, unbound DNA probes were removed using PBS, and the sensors were dried using nitrogen. An acrylic well [6 mm × 61.5 mm × 61 mm] was then pasted onto the chip to enclose the bio-optical sensor area. For an optimized reaction, 29.5 μL of rehydration buffer, 15 μL of nuclease-free water, and 2.5 μL of forward primers (10 μM) were combined. One dried enzyme pellet (TwistDX, UK) was added to each solution and vortexed. Subsequently, 2.5 μL of magnesium acetate solution (280 mM) was dispensed into the cap of each tube. A unidirectional shake-mode mixing protocol guaranteed the homogeneous distribution of the molecules that were necessary for the reaction in the buffer. After mixing, 50 μL of the reaction buffer were distributed into five 10 μL aliquots. To initiate the reactions, 5 μL of genomic DNA sample, extracted from clinical samples, were added to each 10-μL reaction aliquot and RPA solutions containing the DNA targets were added to the acrylic well at room temperature. Mineral oil then added to protect the solution from evaporation during amplification. The bio-optical sensor was then placed on a thermo-electric cooler (TEC) with a controller (Alpha Omega Instruments) to maintain a constant temperature (38 ℃) through the application of a constant DC voltage. The wavelength shift was acquired every 5 min for up to 30 min to monitor the amplification and detection of pathogens (HAdV and HZ) or oncogenic mutation (*BRAF* and *KRAS*).

Figure 1.4. Principles of bio-optical sensor

Table 1.1 The list of primer sequence for bio-optical sensor.

Targets	Sequence (5' → 3')
ADV	F: $NH_2-(CH_2)_{12}$-AGT GGT CTT ACA TGC ACA TCG CCG GGC ACC A
	R: GGC CAC GGT GGG GTT TCT AAA CTT GTT TCC CA
KRAS (G12D)	F: $NH_2-(CH_2)_{12}$-CTG AAT ATA AAC TTG TGG TAG TTG GAG CTG A
	R: $NH_2-(CH_2)_{12}$-CTC ATG AAA ATG GTC AGA GAA ACC TTT ATC
KRAS (G13D)	F: $NH_2-(CH_2)_{12}$-CTG AAT ATA AAC TTG TGG TAG TTG GAG CTG GTG AG
	R: $NH_2-(CH_2)_{12}$-CTC ATG AAA ATG GTC AGA GAA ACC TTT ATC
HZ	F: $NH_2(CH_2)_{12}$-CCC GGG TAC AGG TTG GCA AAC GCA GTC
	R: $NH_2-(CH_2)_{12}$-CCG GGG CCG TCG AGT ATC TAG GCT CGC GGT TGG CC

1.5. Testing Samples

For testing the utility of the system with various samples, cancer cell lines (AGS [stomach, ATCC_CRL-1739], HCT116 [colorectal, ATCC_CCL-247], and MCF7 [breast, ATCC_HTB-22]) were maintained in plastic culture dishes with high-glucose Dulbecco's Modified Eagle's Medium (DMEM, Life Technology), supplemented with 10% fetal bovine serum (FBS), in a 37 ℃ humid incubator with 5% ambient CO_2. After culturing, the cells were used for nucleic acid extraction with the system and Qiagen kit.

Escherichia coli (ATCC 25922) was inoculated in nutrient broth (NB) medium and incubated overnight at 37 ℃ under shaking conditions. I calculated CFU using plate count agar (PCA) medium after incubation at 37 ℃ for overnight and extracted genomic *E. coli* DNA from 100 μL of medium broth containing 10^1 to 10^8 CFUs/mL.

1.6. Purpose of this study

In recent years, emergence of emerging infectious disease and variant disease is increasing due to the climate change and vigorous human and physical exchanges between countries. When people are exposed to these infectious diseases, the current technology does not only require much time to diagnose, but also has limitations in proper prescription and treatment due to low sensitivity and its complicated process. This does not only bring physical and economic pain to patients, but also become an important cause of the increased mortality rate due to such infectious diseases.

Moreover, Cancer is the first leading cause of death in the world and the death rate from cancer is increasing continuously. There are two methods for the diagnosis of cancer in patients : tissue biopsy and liquid biopsy. Tissue biopsy is the gold standard for tumor characterization, but it may have inconsistent results due to tumoral heterogeneity. As the samples are obtained during surgery, the process requires more time, is more difficult, and results in pain and risk for the patient. On the other hand, liquid biopsy is a non-invasive method, which takes less time, minimalizes pain, and can investigate tissue profiling. Liquid biopsy can be applied to predictive screening with CTC and cfDNA, cancer diagnosis, targeted-therapy, prognosis and monitoring. When cfDNA used for detecting mutation, sample preparation step for removing PCR inhibitors or debris and detecting mutation step with high sensitivity are very important.

To rapid and accurate diagnosis of diseases, new diagnosis technique

containing sample preparation step and NA detection step which can be applicable infectious disease as well as cancer was developed. To validate this technique, cell lines, bacteria and the clinical samples include plasma, environmental swab, saliva, nasopharyngeal sample and frozen tissue from patients were used. The experimental process in this study was shown as table 1.2.

Table 1.2. The experimental process in this study.

	Samples	Sample preparation (Microfluidic platform)		Bio-optical sensor (RPA+SMR sensor)
		Pathogen Enrichment	NA extraction	NA detection
Infectious diseases	ST (Plasma)		DNA extraction	Hexon protein gene
	SFTS (Plasma)		RNA extraction	
	ADV (Nasopharyngeal sample)		DNA extraction	
	HPIV-3 (Environmental swab)	Virus enrichment	RNA extraction	
	HZ (Saliva)	Bacteria enrichment	DNA extraction	
	HZ (Plasma)	Bacteria enrichment	DNA extraction	Hemagglutinin-neuraminidase gene
Cancer (CRC)	Frozen tissue			*KRAS* (G12D, G13D)
	Plasma (cfDNA)		cfNA isolation	*KRAS (G12D, G13D)*

Chapter 2. Nucleic Acids (NAs) Extraction Based Combination of Homobifunctional Imidoester (HI) and Microfluidic Platform

2.1. Introduction

Recent advances in innovative technologies for clinical diagnostics have enabled the rapid and accurate diagnosis of several human diseases. Nevertheless, emerging diseases caused by novel pathogens (i.e., bacteria, viruses) remain a major threat to human life, due to the lack of appropriate diagnostic tools for clinical use at the early disease stage. Hence, various technologies have been evaluated for the diagnosis of diseases such as cancer, as well as neurological and infectious diseases (41−43). However, there are several unmet needs in terms of diagnosis with the existing technologies due to constraints such as low sensitivity and specificity, labor−intensive nature, high cost, need for highly skilled technicians, and need for automation and portability of the system that requires the integration of sample preparation and detection techniques (44−47).

In order to overcome these constraints, most studies have focused on the improvement of detection technologies (48−53), and accordingly, advancements in detection technologies are being continuously made. In contrast, only few efforts have focused on the development of sample preparation (nucleic acid extraction) technologies (54−57), which are also a major requirement. Extraction of NA (DNA, RNA) is important not only for clinical diagnostics but also for life sciences research, such as for the identification of DNA biomarkers, assessment of DNA−based therapeutics, and understanding gene−disease relationships (58−62). Hence, the high quality and quantity of NAs extracted from various human samples using innovative technologies would be desired for the improvement of the sensitivity and specificity of the diagnostics tools. Moreover, an ideal nucleic acid extraction technique should be useful for various sample volumes (one drop to microliter scale) and should be easy to integrate with detection techniques for developing POC diagnostic devices.

Different techniques based on the use of hazardous chemicals such as chaotropic reagents and organic solvents, either with liquid phase−based methods (63−65) or solid phase−based methods (66−68) (including filter/membrane and particles), have been developed for nucleic acid extraction. These hazardous chemicals lead to the degradation of biomolecules

and inhibition of the PCR reaction (69-72). To avoid the use of hazardous chemicals, the incorporation of chitosans as nonchaotropic reagents into solid materials has enabled the successful extraction of nucleic acids. However, the binding and release of nucleic acids to and from the chitosan depends on the change in the buffer pH (73-75). Based on the present status of the nucleic acid extraction techniques, the current methods, including conventional (liquid phase-based) (63-65) and recently developed (solid phase based) methods (66-68), for nucleic acid extraction are useful but have many limitations, including the degradation of nucleic acids by organic solvents; 30-36 high risk of contamination; requirement of instruments including centrifuge, vacuum, and others; requirement of prepreparation steps including fabrication steps for fiter/membrane, particles, and reagent coating; labor-intensive and time-consuming nature, including the sample handling steps; and unsuitable platform for POC testing including the difficulty of integration with the detection technique (76-77).

In this report on the use of a simple and inexpensive method with HIs (DMP, DMS, DTBP) for the extraction of nucleic acids (RNA and DNA) in combination with a microfluidic-based thin-film platform, to overcome the limitations of nucleic acid extraction from various samples using the existing methods. This approach is a method of using HIs as a nonchaotropic reagent to avoid the use of hazardous chemicals in the chaotropic assays (i.e., conventional nucleic acid extraction assays), and to set up an inexpensive microfluidic platform with thin-film material (created with a laser cutting machine) for NA extraction. HIs are used as a capturing reagent for NA (both RNA and DNA) extraction from several sources (cancer cells, bacteria, and viruses).

Furthermore, to overcome the limitations of conventional assays, such as the high risk of contamination, need for instruments and prepreparation steps, labor-intensive and time consuming nature, and difficulty of integration with the detection technique for POC testing (76-77), the HIs reagent are coupled with the microfluidic system using a thin-film platform to create a μTAS. The μTAS offers a completely closed system that minimizes the risk of sample contamination, and allows for the portability of the analytical method. Although the μTAS has been found to have these advantages, several complex steps remain unexplored, including the need for valves and pumps, bonding, and micro-channel fabrication (78-80). The thin-film-based rapid prototyping method in the present study was used to create a closed single

microfluidic channel system to extract nucleic acids from the samples without any contamination. Hence, this system is based on the combination of HIs for capturing nucleic acids and a thin-film-based microfluidic system as a platform for nucleic acid extraction in a single channel microfluidic platform without any instruments. This would lead to a major change in the sample processing techniques used in the clinical settings.

2.2. Materials and methods

2.2.1. Clinical samples

To validate the ability of the system in human clinical samples, 140 μL of blood plasma samples from human disease patients were mixed with 200 μL of the assay solution, and then injected into the system for viral RNA and bacterial DNA extraction. The plasma samples from the patients who had either severe fever with SFTS (Huaiyangshan virus) for RNA or ST (*Orientia tsutsugamushi*) and Nasopharyngeal samples from patients infected with adenovirus (HAdV) for DNA were obtained using protocols approved by the institutional review board of Asan Medical Center, Republic of Korea. Institutional approval and written informed consent from the patients were obtained. All experiments were performed in accordance with the relevant guidelines and regulations.

For DNA extraction, the DNA was extracted from the clinical samples using proteinase K to break down unwanted proteins and QIAamp DNA mini kit (Qiagen, Germany). End-point PCR and qPCR were performed to assess the quantity and purity of DNA for downstream analysis. For RNA extraction, RNA was extracted from cells using proteinase K, DNase I to break down unwanted proteins and DNAs, and the QIAamp Viral RNA mini kit (Qiagen, Germany). The viral DNA samples were extracted from 10 samples from patients with HAdV infection using the QIAamp DNA mini kit according to the manufacturer's instructions. Each sample had a starting volume of 200 μL and was eluted to approximately 100 μL using an elution buffer. The extracted DNA was then aliquoted and stored at −20 ℃ until use. End-point PCR and qPCR were performed to assess the quantity and purity of the viral DNA for downstream analysis. All the primers used for conventional PCR assays are described in Table 2.1

Table 2.1. Primer Sequences of DNA and RNA amplification

NA	Targets	Sequence (5' → 3')
DNA	β-actin	F: ATG GTG GGC ATG GGT CAG A
		R: GCC ACA CGC AGC TCA TTG
	ST (*Orientia tsutsugamushi*)	F: GCA GCA GCT GTT AGG CTT TT
		R: TTG CAG TCA CCT TCA CCT TG
	E. coli	F: CAA CTC TGG CTC CGT CTC TG
		R: CAT CAT GCA AGC GGC CTC TG
	KRAS (G12D)	F: TGT GGT AGT TGG AGC TGA
		R: TCA TGA AAA TGG TCA GAG AAA CC
	KRAS (G12D)	F: TGT GGT AGT TGG AGC TGG TGA G
		R: TCA TGA AAA TGG TCA GAG AAA CC
	HAdV	F: GCC ACG GTG GGG TTT CTA AAC TT
		R: GCC CCA GTG GTC TTA CAT GCA CAT C
	HZ	F: GTT CGC CCG GGT ACA GGT TGG
		R: TTT GCC GGG GCC GTC GAG TAT CTA
RNA	*18S rRNA*	F: GCT TAA TTT GAC TCA ACA CGG GA
		R: AGC TAT CAA TCT GTC AAT CCT GTC
	STFS (Huaiyangshan virus)	F: CAG CCA CTT TAC CCG AAC AT
		R: GGC CTA CTC TCT GTG GCA AG
	hPIV-3	F: TGA TGA AAG ATC AGA TTA TGC ATA TC
		R: CCG CGA CAC CCA GTT GTG

2.2.2. Development and optimization of nucleic acids extraction using microfluidic platform

To extract nucleic acids using the system, the assay solution is optimized. For an optimized reaction, a lysis buffer (100 mM Tris-HCl (pH 8.0), 10 mM ethylenediaminetetraacetic acid, 1% sodium dodecyl sulfate, and 10% Triton X-100) with either proteinase K for DNA or proteinase K and DNase I for RNA to break down unwanted proteins and DNAs was mixed with various concentrations (50, 100, 150, 200, and 250 mg/mL) of HIs as the reaction solution. To conduct the reaction, 100-140 μL of sample from mammalian cells, bacteria, or clinical samples was mixed with 200 μL of the assay solution, and then injected into the system by the syringe with hands. For RNA extraction, the system was placed at room temperature for 10 min to extract RNA from the sources. For DNA extraction, the system was placed in an incubator at 56 ℃ for 20 min to extract DNA from the sources. The HI can capture the nucleic acids through a complex on the surface. After washing with PBS at 50 μL/min of flow rate to remove the debris from the samples using syringe pump (KD Scientific, MA), an elution buffer (10 mM sodium bicarbonate, pH < 10.6, flow rate; 50 μL/min) was used to collect the nucleic acids that were extracted within a few minutes. The quantity and purity of the nucleic acids extracted were measured using the ratio of the optical densities of the samples at 260 and 280 nm, with NanoDrop (Thermo Fisher Scientific, Waltham, MA). The amount of protein in the sample was measured optical density using spectrophotometer at 595 nm after the mixing with Bradford reagent (Sigma-Aldrich). To compare the system with a conventional nucleic acid extraction method, either QIAamp Viral RNA Mini Kit or QIAamp DNA mini kit was used according to the manufacturer's protocol (Qiagen, Germany).

2.2.3. The isolation of cfNA using microfluidic platform

To isolate cfNA, the plasma sample with DTBP as the reaction solution insert into microfluidic platform and incubate 10 min for reaction with DTBP and cfNA. After washing with PBS to remove debris from the sample, an elution buffer (10 mM sodium bicarbonate, pH <10.6) was used to collect the nucleic acids within a few minutes through breaking crosslinking with DTBP and amine group of APDMS. The isolated cfNAs were stored −20 ℃ until use. The concentration of isolated cfDNA was measured using Qubit 3.0 fluorometer (Thermo Fisher scientific) and size and purity of cfDNA was

checked using High Sensitivity D1000 ScreenTape System (Agilent, Germany).

2.2.4. Measurement of cell-free DNA integrity and cellular DNA background

To measure cfDNA integrity, cfDNA is amplified with two types of *Alu* primer sets using real-time PCR (81). The cfDNA samples were analyzed using the *Alu* 247/115 ratio. A ratio close to 1.0 indicated that the cfDNAs are not truncated, whereas that close to 0.0 indicated that cfDNAs were truncated. For real-time PCR, the following procedure modified from the AriaMx real-time PCR instrument protocol (Agilent Technologies) was used. Five microliters of cfDNA were amplified in a total volume of 20 μL containing 10 μL of 2× Brilliant III SYBR Green QPCR master mix, 25 pmol of each primer, and deionized water. The PCR conditions were as follows: initial denaturation at 95 ℃ for 10 min and 35 cycles of denaturation, annealing, and elongation at 95 ℃ for 30 s, 64 ℃ for 30 s, and 72 ℃ for 30 s, respectively, followed by a cooling step at 40 ℃ for 30 s. The SYBR Green signals of the amplified products were acquired using the AriaMx real-time PCR (Agilent Technologies) (4-6). To measure the cellular DNA background, the β-actin gene is amplified (400 bp) using qPCR. When the cellular DNA contaminated the cfDNA pools, the C_T value from qPCR was lower than that of the non-contaminated samples. The PCR conditions were as follows: initial denaturation at 95 ℃ for 10 min and 40 cycles of denaturation, annealing, and elongation at 95 ℃ for 10 s, at 55 ℃ for 20 s, and at 72 ℃ for 20 s, respectively, followed by a cooling step at 40 ℃ for 30 s. The SYBR Green signals of the amplified products were acquired using the AriaMx real-time PCR (Agilent Technologies). The primer sets of genes used in this study are described in Table 2.2.

Table 2.2. Primer sets used for conventional PCR and Sanger sequencing

Target gene		Sequence (5' → 3')
Alu	247 bp	F: GTG GCT CAC GCC TGT AAT C
		R: CAG GCT GGA GTG CAG TGG
	115 bp	F: CCT GAG GTC AGG AGT TCG AG
		R: CCC GAG TAG CTG GGA TTA CA
β-actin		F: GCA CCA CAC CTT CTA CAA TGA
		R: TGT CAC GCA CGA TTT CCC
BRAF	Exon 15	F: TCA TAA TGC TTG CTC TGA TAG GA
		R: GGC CAA AAT TTA ATC AGT GGA
KRAS	G12D	F: TGT GGT AGT TGG AGC TGG
		R: TCA TGA AAA TGG TCA GAG AAA CC
	G13D	F: TGT GGT AGT TGG AGC TGG TGA G
		R: TCA TGA AAA TGG TCA GAG AAA CC
	Exon 2	F: TCA TTA TTT TTA TTA TAA GGC CTG CT
		R: CAA GAT TTA CCT CTA TTG TTG GAT C
18S rRNA		F: GCT TAA TTT GAC TCA ACA CGG GA
		R: AGC TAT CAA TCT GTC AAT CCT CTC
GADPH		F: CCT GGA GAA ACC TGC CAA GTA TG
		R: AGA GTG GGA GTT GCT TTG AAG TC

2.2.5. Whole exome sequencing (WES) analysis

To develop the simple and low-cost cfNA-sampling platform for clinical use, the primary tissues and blood plasma from 14 CRC patients are collected, blood samples from 10 healthy controls, frozen plasma samples from 11 CRC patients (with OncoPanel results from the primary tissues), and blood plasma from five CRC patients (no primary tissue testing result) from the BRC of the Asan Medical Center (Seoul, Korea) after approval from the Institutional Review Board. The samples were obtained by a colorectal surgical team and were randomly selected according to cancer stage. The characteristics of all patients and mutation information based on WES results of the 14 tissue samples are described in Table 2.3. cfDNA obtained from the patients' plasma was analyzed for hot-spot mutations using SCODA (Theragen, Suwon, Kora) (82).

Table 2.3. Clinicopathologic characteristics and sequencing results from primary tissue and plasma (ctDNA) samples obtained from 14 colorectal cancer patients.

Nr.	Age	Gender	Pathologic Stage	Tissue (IS)	ctDNA	
					Column	DTBP
T1	68	M	2	WT	WT	WT
T2	62	M	2	WT	WT	WT
T3	54	M	4	***BRAF* (V600E)**	WT	***BRAF* (V600E)**
T4	62	M	3	***KRAS* (G12V)**	WT	WT
T5	42	M	4	WT	***KRAS* (G13D)**	***KRAS* (G13D)**
T6	42	M	2	WT	WT	***KRAS* (G13D)**
T7	48	F	4	***KRAS* (G12V)**	WT	WT
T8	34	F	4	***BRAF* (V600E)**	WT	***BRAF* (V600E)**
T9	40	M	3	***KRAS* (G13D)**	***KRAS* (G13D)**	***KRAS* (G13D)**
T10	65	M	4	***KRAS* (G12D)**	***KRAS* (G12D)**	***KRAS* (G12D)**
T11	64	F	2	WT	WT	WT
T12	42	M	3	WT	WT	***KRAS* (G12D)**
T13	72	F	3	***KRAS* (G13D)**	***KRAS* (G13D)**	***KRAS* (G13D)**
T14	56	M	4	WT	WT	WT

Bold text indicates detected mutations.

WT: wild type

2.2.6. Application of the simple and low-cost method for circulating tumor DNA (ctDNA) analysis

Eleven blood plasma samples obtained from CRC patients, which contained *BRAF* and *KRAS* mutations, as detected using OncoPanel were tested. All ctDNA was isolated from the plasma samples using the DTBP platform that was combined with Sanger sequencing for simple and low-cost ctDNA analysis. For Sanger sequencing, all ctDNA samples were amplified using the sequencing primer of *BRAF* exon 15 (annealing temperature, 58 ℃) and *KRAS* exon 2 (annealing temperature, 55 ℃). The samples were directly sequenced using BigDyeTerminal chemistry with the forward sequencing primer of detectable *BRAF* and *KRAS* mutations. The DNA sequencing reaction mixtures were electrophoresed using ABI's 3730XL DNA analyzer (Applied Biosystems, USA) at the Macrogen Sequencing Center (Macrogen Inc.,). The DTBP platform was also applied to conventional PCR methods for simple and low-cost ctDNA analysis. To compare the sensitivity of mutation detection between the column-based method and the DTBP platform, isolated ctDNA from blood plasma samples of five CRC patients in which mutations had not been identified were amplified with *KRAS* mutation specific primer sets and mutations were identified using PCR and Sanger sequencing. For conventional PCR, 5 μl of DNA was amplified in a total volume of 25 μL, containing 10× PCR buffer (Qiagen), 2.5 mM $MgCl_2$, 0.25 mM deoxynucleotide triphosphate, 25 pmol of each primer, and 1 unit of Taq DNA polymerase (Qiagen). The PCR program for the *KRAS* mutation was performed as follows: initial denaturation at 95 ℃ for 15 min and 45 cycles of denaturation, annealing, and elongation at 95 ℃ for 30 s, 58 ℃ (for G12D) and 60 ℃ (for G13D) for 30 s, and 72 ℃ for 30 s, respectively, followed by final elongation at 72 ℃ for 7 min. Gel electrophoresis was used to separate the PCR products on a 2% agarose gel containing ethidium bromide. The gel was visualized using a GelDoc System (Clinx Science Instruments).

2.3. Results and discussion

2.3.1. Optimization of the HI platform

The HI was used as nonchaotropic reagents for the extraction of both RNA and DNA using a thin-film-based microfluidic platform (Figure 2.1). The chemical structure of HIs (DMS, DMP) consists of methylene groups and bifunctional imidoester groups (Figure 2.1A) (4-6). The use of the thin-film-based microfluidic platform involves sample lysis, washing, and elution in a single closed micro-channel with a syringe pump only. To extract RNA and DNA from samples with the HI system (Figure 2.1C-D), a mixed solution of sample, the lysis buffer, and HI (DMS or DMP) was added via pipetting into the system, which was previously activated with amine reactive groups on the surface to capture the complex of nucleic acids and DMP. Amino groups of DMP capture the nucleic acids by electrostatic adsorption due to the large numbers of negative charges on the nucleic acids. In addition, HIs react with amine groups of ends of the fragmented DNA, which contains a few base pairs of single stranded DNA at each end of the fragment during lysis reaction, through covalent bonding. Therefore, DMP can capture the nucleic acid by both electrostatic interaction and covalent bonding. The system mixture was then incubated at room temperature for 10-20 min to extract RNA (Figure 2.1C) or at 56 ℃ for 20 min to extract DNA (Figure 2.1D) according to the Qiagen protocol; subsequently, the amino groups of the nucleic acids interact with the bifunctional groups of the DMP to form cross-links (i.e, covalent bonds) due to use of proteinase K and DNase I in the mixing solution for breaking down the unwanted proteins and DNAs. After the incubation, the purification step was completed by PBS washes to remove the debris and unbound molecules. Finally, the elution buffer (pH 10.6) was added to collect the extracted nucleic acids (RNA or DNA) by breaking the interaction between the complex and inner surface of the system that can be used for the downstream analysis of biomolecules.

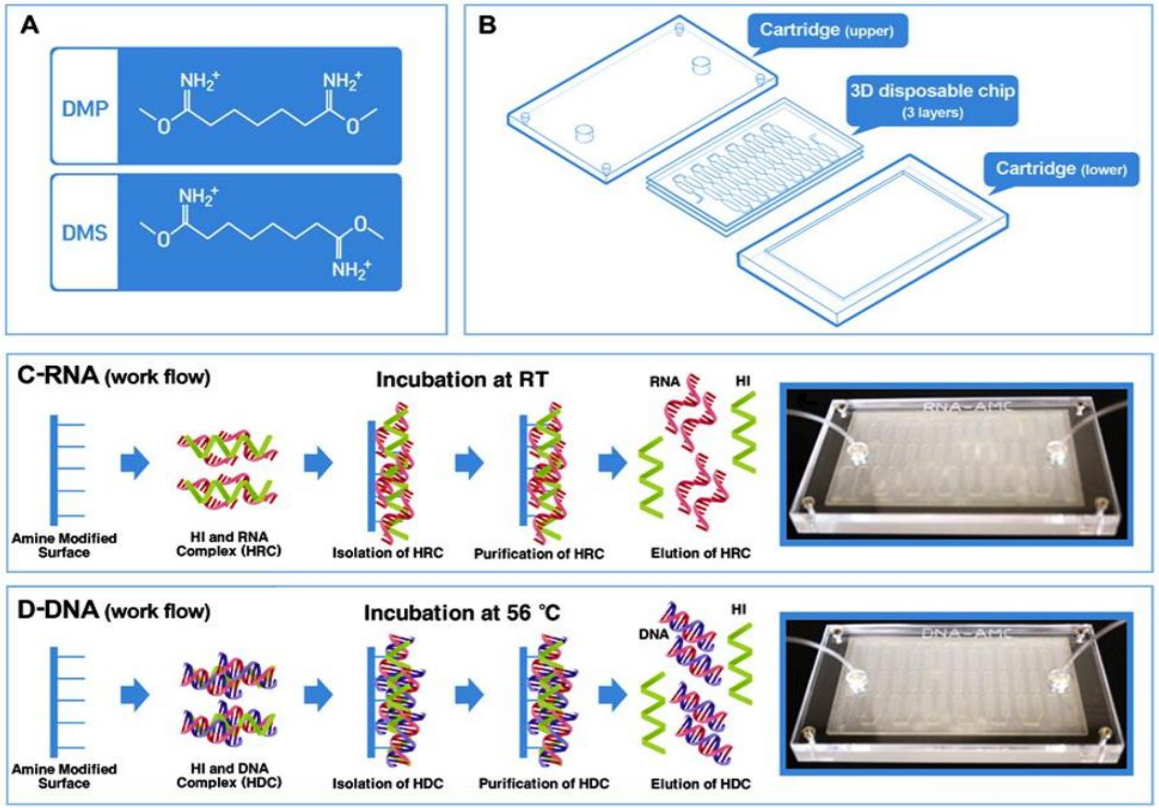

Figure 2.1. Schematic representation of the principle of the microfluidic system for nucleic acid extraction. (A) Chemical structure of HIs (DMS and DMP) (B) A plastic type microfluidic cartridge with a 3D disposable chip that was fabricated using a laser cutting machine for nucleic acid extraction. (C-D) Schematic work flows of the microfluidic system for RNA (C) and DNA (D) extraction. (C-D) A photograph of the working prototype of the microfluidic system for RNA and DNA extraction.

2.3.2. Characterization of the HI platform

First, in order to investigate whether the HI system can useful for the extraction of nucleic acids (RNA and DNA), the fundamental characterization of the system was performed in several cancer cell lines and bacterial cells. In Fig. 2.2A, the recovery rate of the input DNA (1 μg of human genomic DNA) was measured with and without HIs (DMS and DMP). More than 95% of the DNA was recovered with both DMS (black) and DMP (gray), and <50% of DNA was recovered without HIs via electrostatic interaction (Fig. 2.2A). The cancer cell line (1×10^6 cells of the breast cancer cell line) was used to optimize the system protocol for the extraction of human genomic DNA and RNA. Based on the results of the characterization (Fig. 2.2), the system protocol was optimized in terms of oxygen plasma time (10 min) for the formation of hydrophilicity on the surface of the inner microfluidic channel (Fig. 2.2B), the flow rate (50 μl/min, Fig. 2.2C) for the elution of nucleic acids, and concentration of HIs (100 mg/ml, Fig. 2.2D−E) for the extraction of high quality and quantity of nucleic acids.

In contrast to DNA extraction, RNA extraction is more difficult due to the easy degradation of RNA in all environmental conditions. Nevertheless, the HI system with either DMS or DMP can be used for the extraction of RNA at two concentrations of cancer cells (1×10^3 and 1×10^6). For PCR compatible testing, the RNA extracted from the system with 2 concentrations was used for the amplification of the 18S rRNA gene, which serves as a good internal control due to the reduced variance in expression (83, 84), with both one−step RT−PCR and one−step qRT−PCR. I observed that the 18S rRNA gene was strongly amplified in both the 10^6 (C_T: 18.42 ± 0.46 in DMS, C_T: 17.86 ± 0.32 in DMP) and 10^3 (C_T: 32.15 ± 0.09 in DMS, C_T: 31.60 ± 0.2 in DMP) concentrations of cells (Fig. 2.2F). For the extraction of DNA using the HI system, cancer cells (1×10^3 and 1×10^6) at different concentrations with DMS (range, 50-250 mg/ml) were also used. For PCR compatible testing, I used the DNA extracted from the system at 2 concentrations for the amplification of the β−actin gene, with both end−point PCR and qPCR (Fig. 2.2G). The β−*actin* gene was amplified at all concentrations of DMS with 1×10^6 cells (C_T: 22.11 ± 0.31; Fig. 2.2E) and 1×10^3 cells (C_T: 31.73 ± 0.01; Fig. 2.2H).

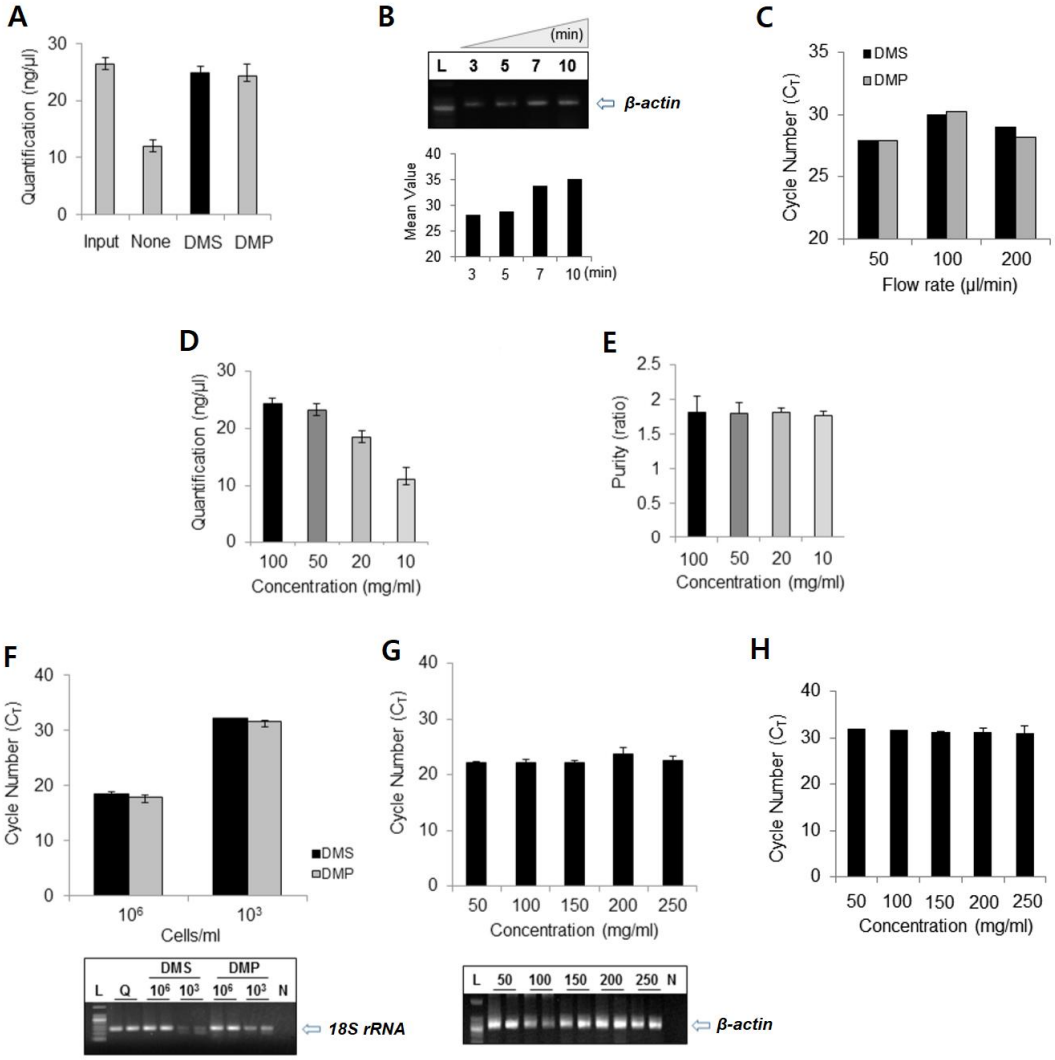
A
Quantification (ng/μl)
30
20
10
0
Input None DMS DMP
B
(min)
L 3 5 7 10
β-actin
Mean Value
40
35
30
25
20
3 5 7 10 (min)
C
DMS
DMP
Cycle Number (CT)
35
30
25
20
50 100 200
Flow rate (μl/min)
D
Quantification (ng/μl)
30
20
10
0
100 50 20 10
Concentration (mg/ml)
E
Purity (ratio)
2.5
2
1.5
1
0.5
0
100 50 20 10
Concentration (mg/ml)
F
Cycle Number (CT)
40
30
20
10
0
DMS
DMP
10^6 10^3
Cells/ml
L Q DMS 10^6 10^3 DMP 10^6 10^3 N
18S rRNA
G
Cycle Number (CT)
40
30
20
10
0
50 100 150 200 250
Concentration (mg/ml)
L 50 100 150 200 250 N
β-actin
H
Cycle Number (CT)
40
30
20
10
0
50 100 150 200 250
Concentration (mg/ml)

Figure 2.2. Fundamental characterization of the microfluidic system for RNA and DNA extraction. (A) Recovery amounts of the input DNA with HIs (DMS or DMP). (B) The efficiency of DNA extraction depends on the plasma oxidation time (3, 5, 7, and 10 min) for the surface modification of the thin film. (C) The efficiency of DNA extraction depends on the flow rate of the elution step (50, 100, and 200 μl/min) using a syringe pump. (D–E) The quantity (D) and purity (E) of the DNA extracted from the cells (HCT116, colorectal cancer cell line) using different concentration of DMS (100, 50, 20, and 10 mg/ml). (F) Downstream analysis for RNA genetic testing with the 18S rRNA gene, using RNAs extracted from the cancer cells, with the system was performed using qRT–PCR (D–upper, DMS: black, DMP: gray) and end–point PCR (D–lower). Gel electrophoresis analysis of the one–step reverse transcript end–point PCR products with the 18S rRNA gene. (L: DNA size marker; Q: RNA from the Qiagen kit, with 1×10^6 and 1×10^3 cells using DMS, and 1×10^6 and 1×10^3 cells using DMP; and N: negative control). (G) Downstream analysis for DNA genetic testing with the β–actin gene, using DNAs extracted from cancer cells (1×10^6 cells) with the system, was performed using qPCR (E–upper) and end–point PCR (E–lower). Gel electrophoresis analysis of the end–point PCR products with the β–actin gene. (L: DNA size marker/HI concentration of 50, 100, 150, 200, and 250 mg/ml; N: negative control) (H) Downstream analysis for DNA genetic testing with the β–actin gene using the DNAs extracted from the cancer cells (1×10^3 cells) with the system, was performed using qPCR with different concentrations of HI (50, 100, 150, 200, and 250 mg/ml). All error bars indicate standard deviation of the mean based on at least 3 independent experiments.

2.3.3. Application in the variety of sample sources

Thereafter, to further evaluate the capacity of the HI system as an RNA extraction assay, RNA extracted from three cancer cell lines was tested, including AGS (gastric), HCT116 (colorectal), and MCF7 (breast), with serial dilutions ranging from 1×10^1 to 1×10^5 cells, in a volume of 100 μl (Fig. 2.3A–C). The quantity of the RNA extracted with the microfluidic system is observed depends on the number of cells. In order to assess the sufficient removal of PCR inhibitors in the RNAs extracted with the microfluidic system for use in downstream analysis, both conventional PCR assays for the analysis of the 18S rRNA gene are performed. The gene was found to be strongly amplified on PCR of RNA extracted from 3 different cell lines (Fig. 2.3D). Fig. 2.3E indicates the dependence of the cycle number (C_T) in the one–step qRT–PCR on the concentrations of the HCT116 cells. Good linearity (R^2=0.9907) between C_T and the concentrations was observed. The error in the measurement was calculated based on three independent experiments and the error bars represent the standard deviation.

To further evaluate the capacity of the HI system as a DNA extraction assay, the DNA extracted from MCF7, AGS, and HCT116 cells were tested using conventional PCR assays. To assess the critical parameters of the DMS and DMP assay for downstream analysis, the purity, quantity, and PCR compatibility of the DNA extracted from the system were tested. The HI system with the Qiagen kit using the same concentration of cells (1×10^6) was compared. The DNA extracted from the HI system with both DMS and DMP was comparably amplified with that obtained from the Qiagen kit in AGS and HCT116 cells (Fig. 2.4A–B). Fig. 2.4C–E showed that the DNA extracted with DMS was sufficient for PCR, and similar to the amount of DNA extracted with DMP. Moreover, the HI system (either with DMS or DMP) with sample solutions containing HCT116 cells in concentrations ranging from 1×10^1 to 1×10^6 cells in a volume of 100 μL was evaluated. In qPCR, I observed that the DNA extracted from the HI system either with DMS (Fig. 2.4F) or DMP (Fig. 2.4G) was amplified gradually, depending on the serial dilution of the cells. Moreover, I examined whether the point mutation of *KRAS* gene, which is a well–known biomarker in cancer (85, 86), can be detected from the DNAs extracted through the system (Fig. 2.5). The DNAs from AGS cells, which carry the G12D substitution mutation with no codon 13 mutation, and HCT116 cells, which carry the G13D substitution mutation with no codon 12 mutation, were used as templates. When a codon

12 mutation primer set (G12D) was used, the amplification only occurred in the AGS cells with the Qiagen, DMS, and DMP assays, and not in the HCT116 cells. In contrast, when the codon 13 mutation primer set (G13D) was used, the amplification only occurred in the HCT116 cells with the Qiagen, DMS, and DMP assays, and not in the AGS cells (Fig. 2.5A).

Furthermore, to test the flexibility of the system in various sample sources, the bacterial DNA extracted from *E. coli*, in concentrations ranging from 1×10^3 to 1×10^8 CFUs in a volume of 100 μl was tested. The *E. coli* gene was strongly amplified using the DNAs extracted from the serially diluted samples. The efficiency of the amplification was comparable for the extracted DNA from both the HI system and the Qiagen kit (Fig. 2.4H). Moreover, storage testing to assess the duration for which the extracted nucleic acid can be stored for downstream analysis was performed. The extracted nucleic acids from the HI system could be used within 20 days under storage conditions (Fig. 2.5B). Although the HI system does not require the use of large instruments including centrifuges, vortexes, and others, the system involves the use of a syringe pump for optimal results. However, sample processing does not require any instrument system for POC testing in actual settings, and does not need electricity. Therefore, the proof of concept of the system without instruments (by hand control) was examined. In end-point PCR, the DNAs extracted from the HI system, either with DMS or DMP, without the syringe pump were also well amplified. Moreover, the efficiency of amplification in the no syringe pump group was similar to that in the syringe pump group (Fig. 2.5C).

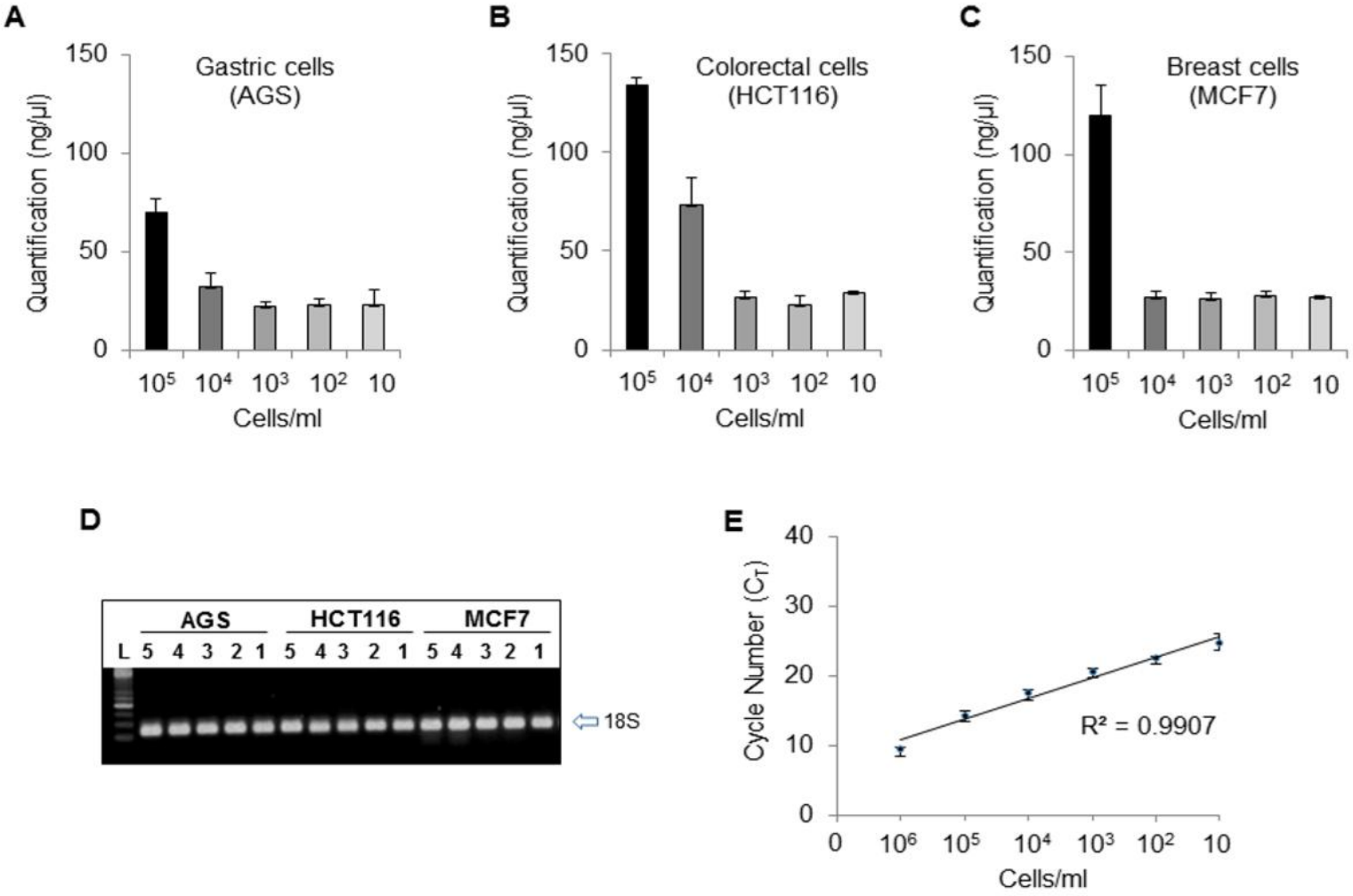
A
Gastric cells
(AGS)
Quantification (ng/μl)
150
100
50
0
10^5 10^4 10^3 10^2 10
Cells/ml
B
Colorectal cells
(HCT116)
Quantification (ng/μl)
150
100
50
0
10^5 10^4 10^3 10^2 10
Cells/ml
C
Breast cells
(MCF7)
Quantification (ng/μl)
150
100
50
0
10^5 10^4 10^3 10^2 10
Cells/ml
D
AGS
HCT116
MCF7
L 5 4 3 2 1 5 4 3 2 1 5 4 3 2 1
18S
E
Cycle Number (C_T)
40
30
20
10
0
R² = 0.9907
0 10^6 10^5 10^4 10^3 10^2 10
Cells/ml

Figure 2.3. Application of the microfluidic system for RNA extraction with cancer cell lines. (A–C) Capacity of the system with (A) AGS (gastric cancer cell line), (B) HCT116 (colorectal cancer cell line), and (C) MCF7 (breast cancer cell line) cells, in concentrations ranging from 1×10^1 to 1×10^5 cells. The quantity of the RNA extracted from the cells was measured using NanoDrop. (D) Downstream analysis for RNA genetic testing with the 18S rRNA gene using the RNAs extracted from 3 cancer cells with the microfluidic system, was performed using one-step RT-PCR. (L: DNA size marker; 1: RNA from 1×10^1 cells; 2: RNA from 1×10^2 cells; 3: RNA from 1×10^3 cells; 4: RNA from 1×10^4 cells; 5: RNA from 1×10^5 cells using DMS) (E) Downstream analysis for RNA genetic testing with the 18S rRNA gene, using RNAs extracted from HCT116 cancer cells in concentrations ranging from 1×10^1 to 1×10^6 cells with DMP, was performed using one-step qRT-PCR. The experiment was repeated 3 times for each concentration, and only one curve for each concentration is shown. The solid line is a linear fitting curve with $R^2=0.9907$, showing good linear dependence. All error bars indicate the standard deviation of the mean based on at least 3 independent experiments.

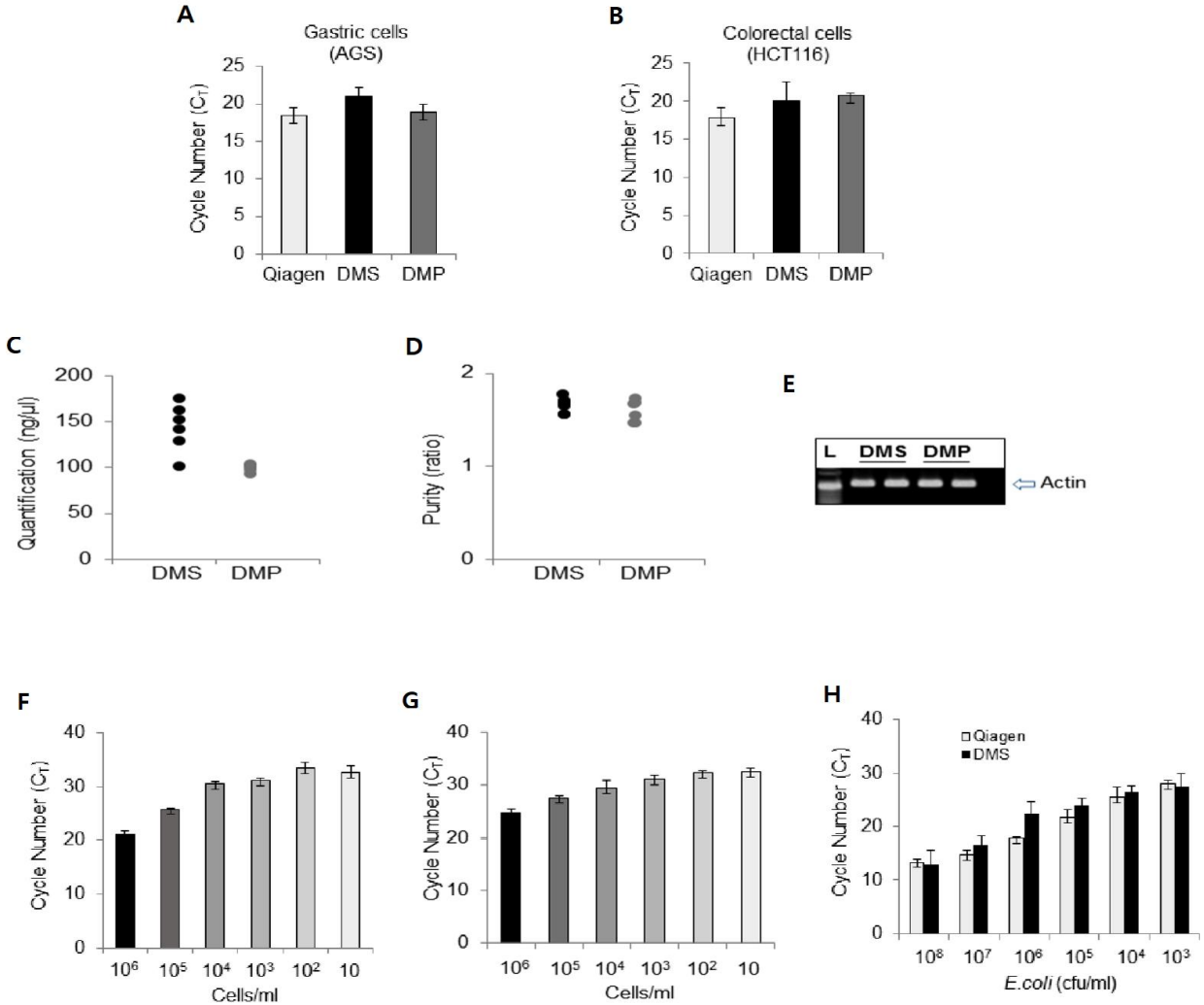
A
Gastric cells
(AGS)
Cycle Number (C_T)
25
20
15
10
5
0
Qiagen
DMS
DMP
B
Colorectal cells
(HCT116)
Cycle Number (C_T)
25
20
15
10
5
0
Qiagen
DMS
DMP
C
Quantification (ng/μl)
200
150
100
50
0
DMS
DMP
D
Purity (ratio)
2
1
0
DMS
DMP
E
L
DMS
DMP
Actin
F
Cycle Number (C_T)
40
30
20
10
0
10^6
10^5
10^4
10^3
10^2
10
Cells/ml
G
Cycle Number (C_T)
40
30
20
10
0
10^6
10^5
10^4
10^3
10^2
10
Cells/ml
H
Qiagen
DMS
Cycle Number (C_T)
40
30
20
10
0
10^8
10^7
10^6
10^5
10^4
10^3
E.coli (cfu/ml)

Figure 2.4. Application of the microfluidic system for DNA extraction with cancer cell lines. (A−B) The capacity of the microfluidic system with (A) AGS (gastric cancer cell line) and (B) HCT116 (colorectal cancer cell line) for DNA extraction using qPCR. (Qiagen: white, DMS: black, DMP: gray). (C−D) Capacity of the system with MCF7 (breast cancer cell line) cells for DNA extraction. The quantity (C) and purity (D) of the DNA extracted were measured using NanoDrop. (DMS: black, DMP: gray). (E) Gel electrophoresis analysis with the Actin gene using the DNA extracted from the microfluidic system. (F−G) Capacity of the system using DMS (F) or DMP (G) with HCT116 cells in concentrations ranging from 1×10^{1} to 1×10^{6} cells by using qPCR. (H) Capacity of the HI system with *E. coli* in concentrations ranging from 1×10^{3} to 1×10^{8} cfu by using qPCR. (Qiagen: white, DMS: black). All error bars indicate the standard deviation of the mean based on at least 3 independent experiments.

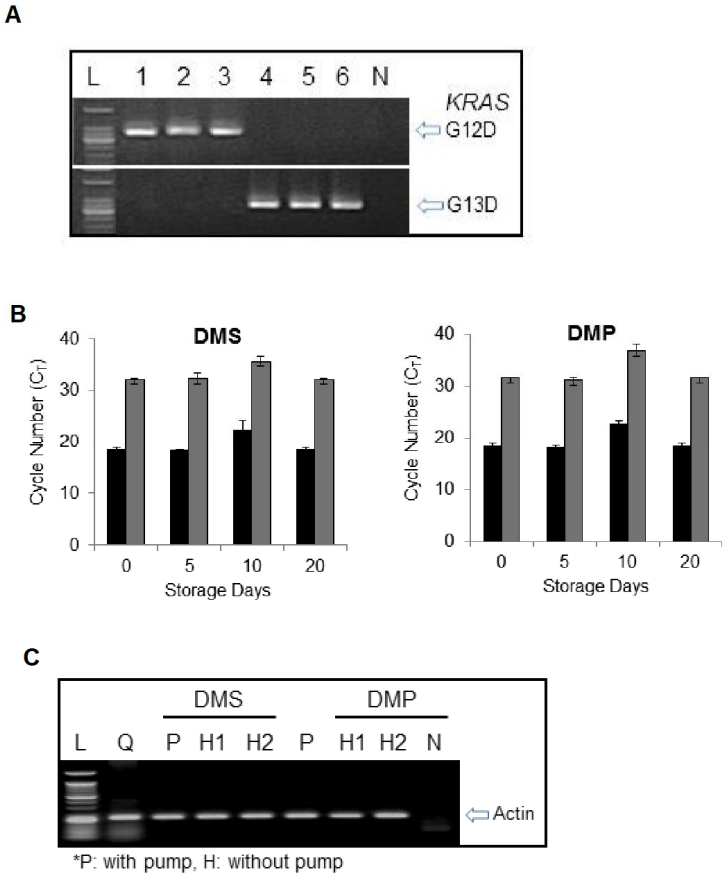

Figure 2.5. Validation of the microfluidic system. (A) Genetic analysis with *KRAS* gene point mutations (codon 12 [G12D] and codon 13 [G13D]) using the DNAs extracted from the microfluidic system. DNA amplification with mutation primer pairs in AGS cells containing the G12D mutation and HCT116 cells containing the G13D mutation. (L: DNA size marker; 1: AGS cells with the Qiagen kit; 2: AGS cells with the DMS assay; 3: AGS cells with the DMP assay; 4: HCT116 cells with the Qiagen kit; 5: HCT116 cells with the DMS assay; 6: HCT116 cells with the DMP assay; N: negative control). (B) The storage condition of the DNA extracted from the system. The DNAs extracted from the DMS and DMP assays were stored at 4°C for 0, 5, 10, and 20 days. The colors represent the 1×10^6 cells (black) and 1×10^3 cells (gray) of the HCT116 line. All error bars indicate the standard deviation of the mean based on at least 3 independent experiments. (C) Capacity testing of the system without the syringe pump. Gel electrophoresis of the β-*actin* products using end-point PCR. (L: DNA size marker; Q: Qiagen kit; P: with the pump; H1&H2: without the pump in the DMS and DMP assay; N: negative control).

2.3.4. Validation in clinical samples

Finally, to validate clinical utility, the microfluidic system can be used to extract either viral or bacterial nucleic acids (DNA and RNA) from tick-borne diseases such as SFTS and ST (87). The viral RNA was extracted from the blood plasma of SFTS patients using both the Qiagen kit and the microfluidic system with DMS. The amplification efficiency of qPCR with the DMS assay was 2-3 cycles longer as compared to that with the Qiagen kit (Fig. 2.6A). This could be relayed to the degradation of RNA in the microfluidic system, which needs to be optimized. Bacterial DNA was also extracted from the blood plasma of ST patients using the Qiagen kit, DMS, and DMP. The amplification efficiency of qPCR for the extraction of bacterial DNA with the HI system was comparable with that with the Qiagen kit (Fig. 2.6B).

Also, the microfluidic system could be used to extract viral DNA form clinical samples. Viral DNAs were extracted from 10 HAdV nasopharyngeal samples using the Qiagen kit and the microfluidic system with DMS. The amplification efficiency of end-point PCR for the extraction of viral DNA with the microfluidic system was comparable with that of the Qiagen kit (Fig. 2.6C). However, the end-point PCR assay is not suitable for quantifying the viral DNA obtained from both assays. Hence, the amplification efficiency of the viral DNAs obtained from both assays using qPCR was examined. Although the amplification efficiency of the DMS assay was 2-3 cycles longer than or comparable (depending on the viral load of the samples) to that of the Qiagen kit (Fig. 2.6D), The DMS assay can be useful for the extraction of viral DNA from the clinical samples.

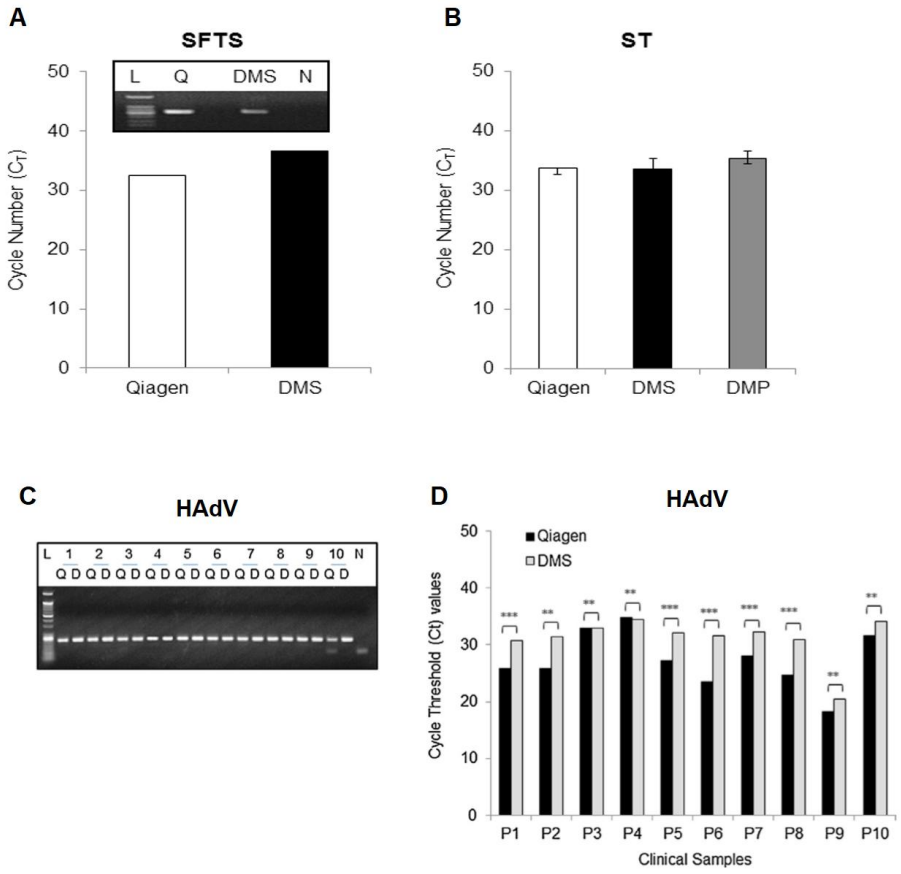

Figure 2.6. Validation of the microfluidic system in clinical samples. (A) Viral RNA extraction from the blood plasma of a severe fever with thrombocytopenia syndrome patient. (B) Bacterial DNA extraction from the blood plasma of a scrub typhus (*Orientia tsutsugamushi*) patient. The colors represent the Qiagen kit (white), DMS assay (black), and DMP assay (gray). (C) Gel electrophoresis analysis of end-point PCR products of viral DNAs extracted from 10 human specimens of adenovirus infection using the Qiagen kit and the DMS platform (L: 50 bp DNA ladder, 1-10: human specimens, Q: extracted with the Qiagen kit, D: extracted with the DMS platform, and N: negative control). (D) Fluorescence signal obtained by qPCR for amplified viral DNAs extracted from 10 specimens using both the Qiagen kit (black) and the DMS platform (gray).

2.3.5. Isolation cell-free nucleic acids (cfNA) for cancer diagnosis

The cfNA (both cfDNA and cfRNA) isolation platform is based on the combination of a capture agent and a solid substance. The cfNA isolation assay includes four steps: 1) chip surface modification, 2) sample mixing, 3) binding, and 4) washing and elution steps that can be performed in a single DTBP platform (Fig. 2.7). After the surface modification with APDMS, the capture agent used is the nonchaotropic reagent DTBP for amine group-mediated nucleic acid capture without any additional preparation (i.e., immobilization) prior to operation. The binding reaction between DTBP and cfNAs can be explained as follows: 1) the positively charged DTBP attracts negatively charged cfNA by electrostatic coupling, and 2) two imidoester groups in the structure of DTBP bind to the primer amine groups of nucleic acids to form amidine by covalent bonding (Fig. 2.7) (88). In order to collect the isolated cfNA, sodium bicarbonate (pH < 10.6) was then used as an elution buffer, since it can break the crosslinking of DTBP and cfNA complex from the surface of the platform (Fig. 2.7). The solid substance used is a thin-film microfluidic platform for the purification of cfNAs and DTBP complexes with a microchannel to streamline the processing. Use of the DTBP platform without a cell lysis buffer and instruments allows the isolation of cfNA from blood plasma within 15 min by overcoming the limitations of the column-based method, such as the increased cellular background owing to cell lysis, the requirements of chaotropic reagents, large sample volume, and the use of instruments (i.e., vacuum pump and centrifuge) (89).

The capture efficiency of the column-based method and the DTBP platform using the amplicon of the *Alu* element (115 base pair; bp) was examined, which was used to determine the integrity of cfDNA in blood (Fig. 2.8A-C). the capture efficiency among the various HI reagents, such as DTBP and DMA, DMS, and DMP was first compared. The C_T value from the DTBP-based platform was lower than that using other HI reagents (Fig. 2.8A). The C_T value obtained using the DTBP method was also lower than

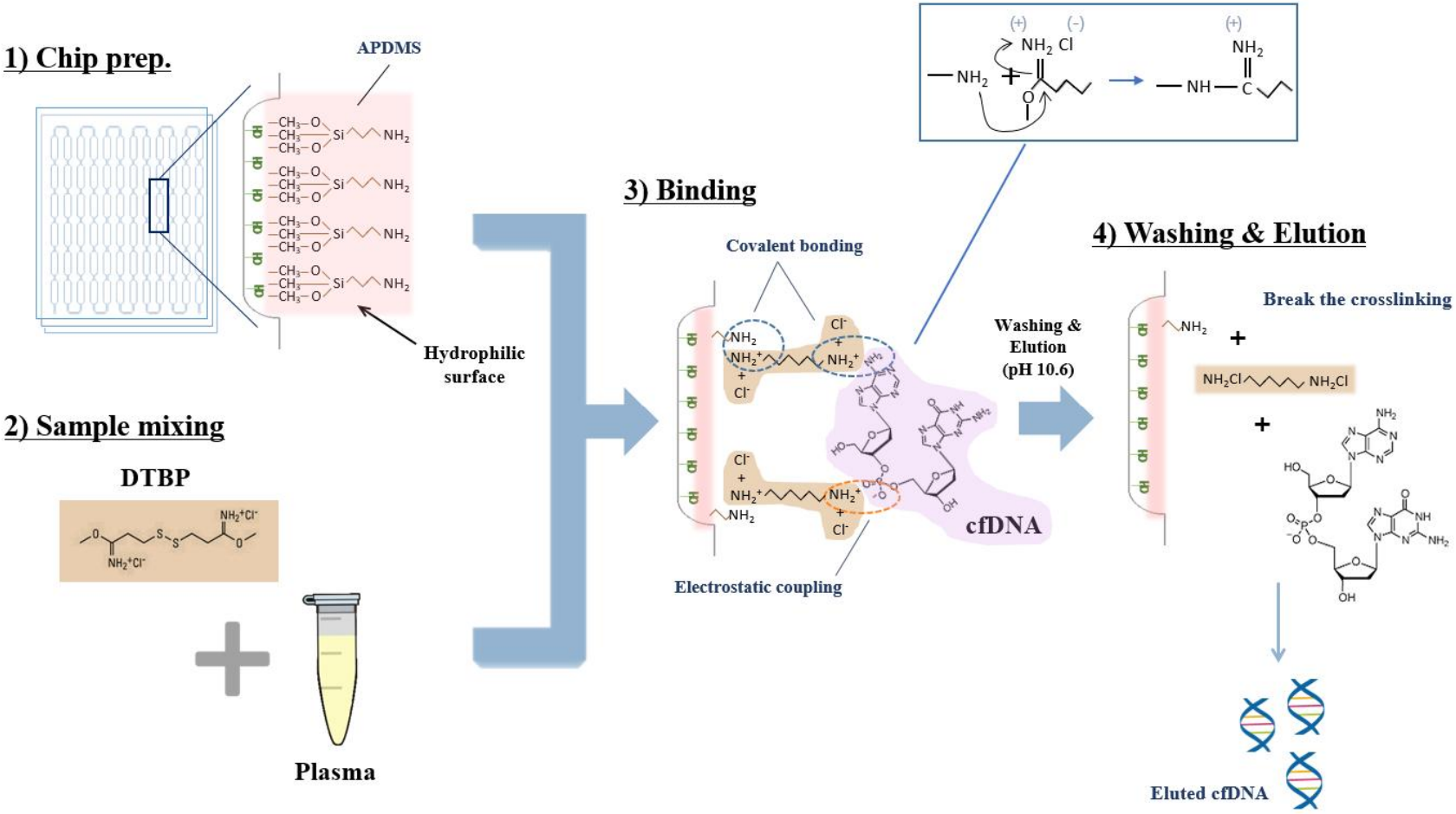
1) Chip prep.
APDMS
Hydrophilic surface
2) Sample mixing
DTBP
Plasma
3) Binding
Covalent bonding
Electrostatic coupling
cfDNA
Washing & Elution (pH 10.6)
4) Washing & Elution
Break the crosslinking
Eluted cfDNA

Figure. 2.7. Operation principles of a cfNA isolation based microfluidic system with DTBP. 1) Chip preparation: assembling the microfluidic platform and inner surface modification with APDMS for binding the amine group of DTBP. 2) Sample mixing: blood plasma samples were mixed with DTBP solution (30 mg/mL) and injected into the platform. 3) Binding: DTBP binds to the amine group of both APDMS and nucleic acids by covalent bonding and electrostatic coupling. 4) Washing and elution: after washing with PBS, elution buffer leads to the breakage of the cross-linking, thus eluting cfDNA (or cfRNA)

that from the column-based method, and was similar to the input as an absolute value (Fig. 2.8E). Thus, DTBP was selected as an optimal capture agent and evaluated the optimal protocol for the isolation of cfDNA under the best experimental conditions (i.e., 30 mg/mL of DTBP and 20 μL/L of APDMS). cfRNA can be isolated using the conditions of the DTBP platform (Fig. 2.8D).

The column-based method uses a chaotropic reagent-based lysis buffer, which leads to an increased cellular background and degrades the cfDNA. This consequently reduces the ctDNA detection rate (90, 91). To address this issue, the utility of the DTBP platform was evaluated for cfDNA isolation without the use of a lysis buffer and large instruments from 24 blood plasma samples, including 14 samples from prospective CRC patients, and 10 from healthy controls. The cfDNA concentration obtained from the DTBP platform was much higher than that obtained from the column-based method (Table 2.3). The integrity of cfDNA and the amount of background cellular DNA from both the DTBP and column-based methods was examined. To measure the cfDNA integrity in plasma, two sets of *Alu* element primers, which amplified 115 and 247 bp products were used. *Alu* 247 bp represents the absolute amount of longer fragments of plasma DNA, whereas *Alu* 115 bp represents the total amount of cfDNA in plasma (92, 93). The DNA integrity was calculated using the *Alu* 247/115 ratio, with a ratio value that was close to 0, thus indicating that most of the DNA was truncated (92, 93). In Fig. 2.8F, the *Alu* 247/115 ratio of cfDNA obtained from the CRC patients was lower than that obtained from healthy controls, and the cfDNA obtained from the CRC patients was more truncated with the DTBP platform than with the column-based method. This result indicates that more cfDNA can be isolated from the DTBP platform (Fig. 2.8F; Table 2.4).

Moreover, 420 bp of the β-actin gene was amplified using qPCR to investigate the amount of background cellular DNA in the isolated cfDNA population. In the case of both healthy controls and CRC patients, the C_T value of the isolated cfDNA from the DTBP platform was more delayed than that from the column-based method (Fig. 2.8F; Table 2.4). This means that the cellular background was smaller in value when the DTBP platform was compared to the case when the column-based method was used (Fig. 2.8G). To evaluate the quality of isolated cfDNA from plasma using the DTBP platform, the size of DNA fragments was analyzed using the electrophoreogram in Figure 2.8H. The observed size of the cfDNA fragments

was ≈165 bp (mean = 163 bp; range = 153-186 bp). Taken together, the simple and low-cost sampling platform could isolate high quality cfNA at increased quantities from liquid biopsies of cancer patients.

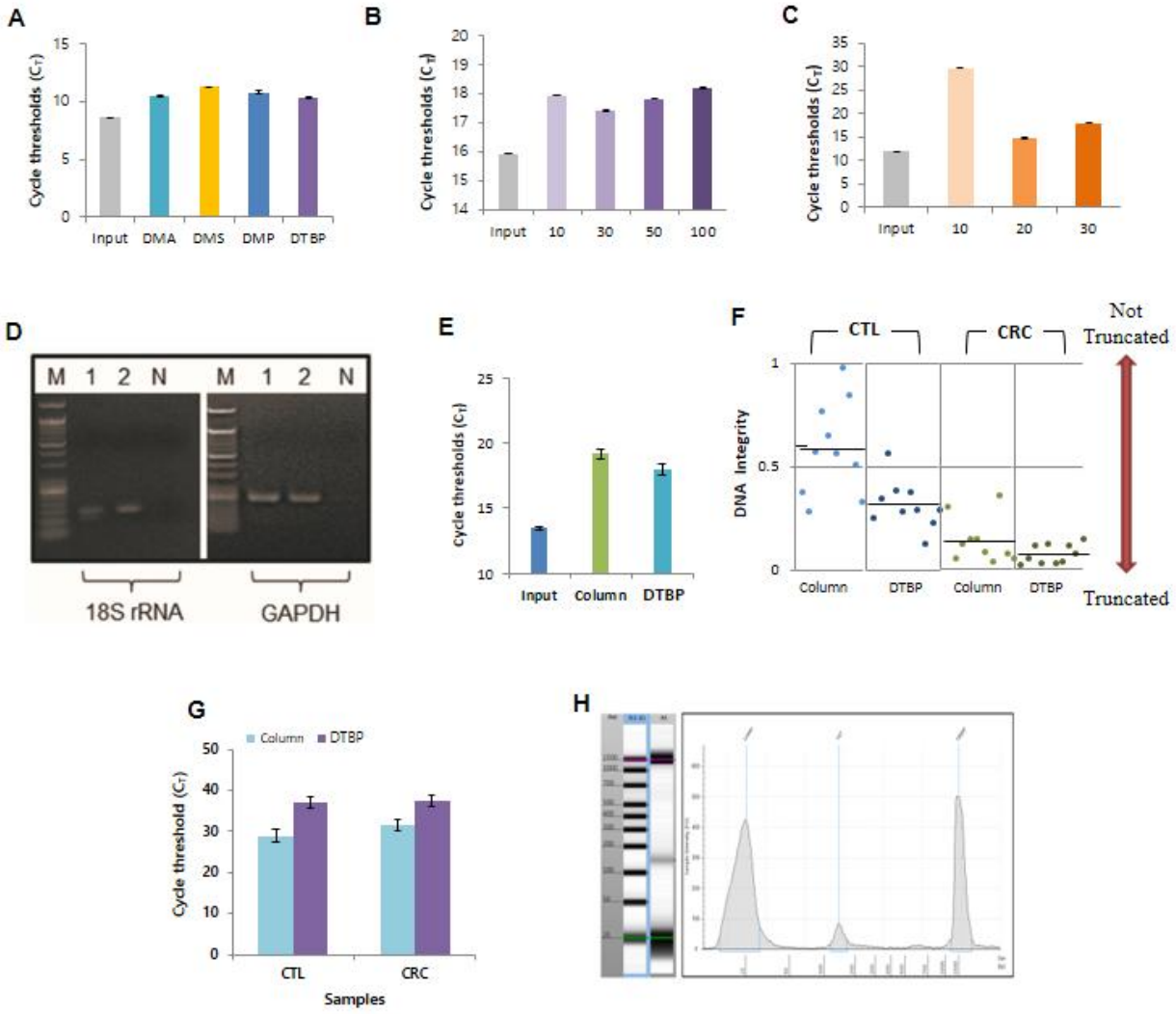
A
Cycle thresholds (CT)
15
10
5
0
Input
DMA
DMS
DMP
DTBP
B
Cycle thresholds (CT)
20
19
18
17
16
15
14
Input
10
30
50
100
C
Cycle thresholds (CT)
35
30
25
20
15
10
5
0
Input
10
20
30
D
M 1 2 N M 1 2 N
18S rRNA
GAPDH
E
Cycle thresholds (CT)
25
20
15
10
Input
Column
DTBP
F
CTL
CRC
Not Truncated
DNA Integrity
1
0.5
0
Column
DTBP
Column
DTBP
Truncated
G
Column
DTBP
Cycle threshold (CT)
50
40
30
20
10
0
CTL
CRC
Samples
H

Figure 2.8. Characterization of the DTBP platform for simple and low-cost cfNA isolation. (A) The amplification efficiency of this platform is dependent on the type of homobifunctional imidoester reagents. (B-C) The cfDNA capture rate is dependent on the DTBP concentration (mg/mL) (B) and APDMS concentration (μL/mL) (C). The error bars indicate the standard deviation from the mean, based on at least three independent experiments. (D) cfRNA isolation from blood plasma using the DTBP platform. (M: size marker, 1: plasma #1, 2: plasma #2, N: negative control). (E) Comparison of the capture efficiency with the *Alu* element amplicon using the column-based and DTBP platform. The error bars indicate the standard deviation from the mean, based on at least three independent experiments. (F) The integrity of isolated cfDNA using the column-based method and the DTBP platform (CTL: 10 healthy control samples, CRC: 14 colorectal cancer samples). (G) qPCR fluorescence signals for amplified *Actin* gene (400 bp) with the isolated cfDNA using the column-based method and the DTBP platform for checking the cellular DNA background. The error bars indicate the standard deviation from the mean, based on at least three independent experiments. (H) Electrophoreogram of the isolated cfDNA using the DTBP platform. Lower peak is 25 bp and upper peak is 1500 bp for size reference.

Table 2.4 Comparison of the characteristics of cfDNA isolated using the column-based method and the DTBP platform from 14 colorectal cancer (CRC) samples and 10 healthy control (CTL) samples.

	Nr.	Concentration (ng/μl)		Integrity (*Alu* 247/115 ratio)		*β-actin* C_T	
		Column	DTBP	Column	DTBP	Column	DTBP
CRC (Patients)	T1	0.574	1.12	0.18	0.14	29.95	37.98
	T2	0.297	1.13	0.26	0.06	31.57	39.19
	T3	1.10	1.34	0.31	0.03	30.71	37.25
	T4	0.626	1.08	0.05	0.06	31.93	34.96
	T5	0.882	1.09	0.12	0.12	30.46	37.43
	T6	0.616	0.641	0.15	0.15	30.19	33.91
	T7	0.667	0.786	0.15	0.12	29.7	34.98
	T8	0.337	1.01	0.08	0.03	33.52	37.9
	T9	0.763	1.09	0.04	0.03	31.76	38.61
	T10	0.298	1.46	0.36	0.12	32.11	35.18
	T11	0.271	0.98	0.26	0.08	31.65	38.84
	T12	0.217	0.686	0.08	0.06	33.96	38.3
	T13	0.237	1.39	0.06	0.04	32.77	34.93
	T14	0.248	1.13	0.35	0.1	30.47	37.28
CTL (Healthy)	C1	0.307	0.529	0.38	0.29	30.29	39.11
	C2	0.278	1.06	0.28	0.34	30.89	38.97
	C3	0.427	0.403	0.58	0.57	28.18	35.84
	C4	0.361	0.406	0.77	0.38	28.15	36.83
	C5	0.259	0.191	0.65	0.28	30.35	36.81
	C6	0.509	0.523	0.56	0.38	25.96	35.09
	C7	0.596	0.578	0.98	0.29	27.49	35.36
	C8	0.472	0.592	0.85	0.13	28.07	36.85
	C9	0.404	0.937	0.51	0.23	28.58	37.94
	C10	0.265	0.681	0.33	0.3	30.55	37.09

2.3.6. Correlation of ctDNA detection in tissue and liquid biopsies

The clear advantage of the DTBP platform is that it can effectively and rapidly capture cfDNA. I further evaluated whether ctDNA could be sensitively detected from the cfDNA population. For this purpose, I prospectively collected the matched cancer tissues and blood plasma samples from 14 CRC patients and compared the correlation of the mutation profiling between the column-based method and the DTBP platform (Fig. 2.9A). I extracted genomic DNA from the tissues and identified cancer-related mutations using WES methods. The WES results of the 14 studied samples are shown in Fig. 2.10. Ten of the 14 samples revealed various mutations, including known CRC-related mutations, *BRAF* (two samples), *CTNNB1* (one sample), *KRAS* (five samples), *PIK3CA* (five samples), and *TP53* (one sample) (Table 2.5). Subsequently, 500 μL of blood plasma samples from CRC patients was used to obtain cfDNA using both the DTBP and column-based methods. To check the correlation of hot-spot mutations (i.e., *BRAF* and *KRAS*) between the tissue and blood samples, *KRAS* mutations (G12D, G12V, and G13D), and a *BRAF* mutation (V600E) with a sequence-specific synchronous coefficient of drag alteration (SCODA) mutation panel (88), were used in both methods (Table 2.5). In particular, the *BRAF* mutation identified in matched tissue samples was detected in two plasma samples (T3 and T8) using the DTBP platform but not using the column-based method. The *BRAF* mutation that was investigated using the column method was under the detection limit of the SCODA calculation (Fig. 2.9B, left) that was used to compare quality and mutation ratios with WES results (94). In addition, the *KRAS* G12D mutation was detected in one sample (T10) by the column-based method and in two samples (T10 and T12) by the DTBP platform. The *KRAS* G12D mutation in the T10 sample was identified using both methods, but the mutation ratio revealed by the DTBP platform was 4-10 times higher than that revealed by the column-based method (Fig. 2.9B, middle). Even the mutation in the tissue sample of T12 that could not be detected by the column-based method was successfully detected by the DTBP platform that elicited an increased ratio (Fig. 2.9B, middle). The *KRAS* G13D mutation was detected in three samples (T5, T9, and T13) by the column-based method and in four samples (T5, T6, T9, and T13) by the DTBP platform. The mutation results of the two samples (T9 and T13) were correlated in tissues and plasma samples by both methods. Although the mutation could not be detected in the tissues of the two samples (T5 and

T6), it was detected in either the column-based method or the DTBP platform. The *KRAS* G13D mutation ratio was shown to be much higher by the DTBP platform than by the column-based method in all four samples (Figure 2.9B, right). In several studies, plasma analyses have revealed *KRAS* mutations that were not seen in the tissues owing to sampling heterogeneities (94, 95). No mutations were detected in the 10 healthy plasma samples. A higher concordance in the statuses of *BRAF* and *KRAS* between primary tumor and plasma samples was identified by the DTBP platform (71.4%) than by the column-based method (57.1%) (Figure 2.9C and Table 2.5).

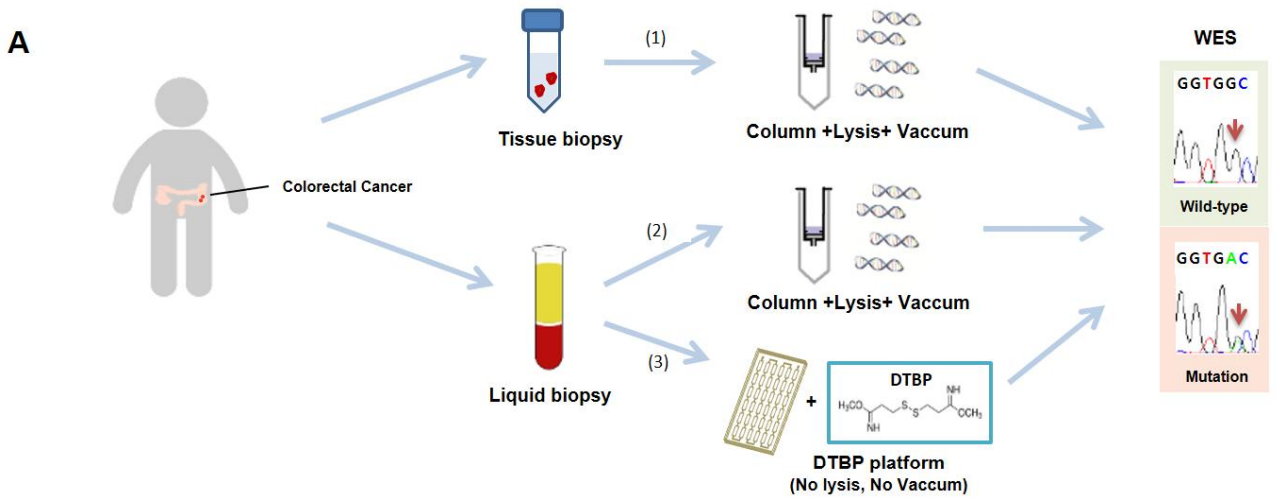

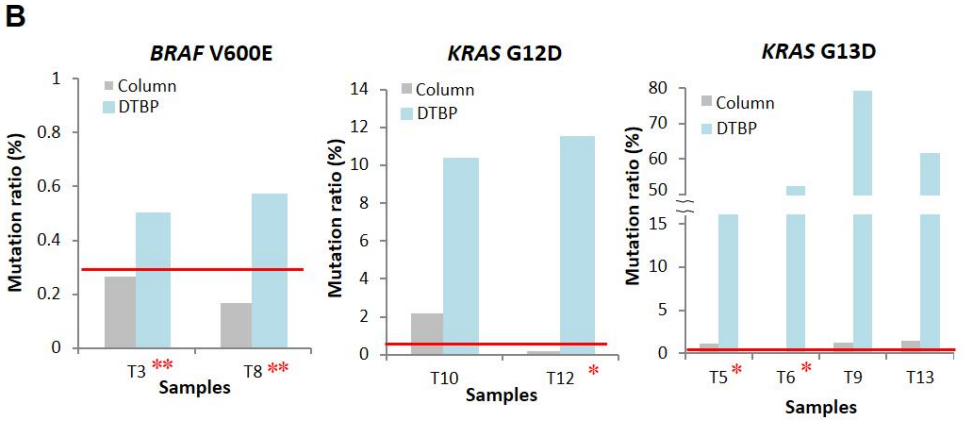

C

	Tissue	ctDNA	
		Column	DTBP
Mutation	50% (7/14)	28.6% (4/14)	57.1% (8/14)
Correlation with Tissue	-	57.1% (4/7)	71.4% (5/7)

Figure 2.9. Application of the DTBP platform for cfDNA isolation and ctDNA analysis. (A) Scheme of the work-flow of 14 clinical samples, including primary tissues and blood plasma from colorectal cancer patients. (1) Mutation screening using the column-based method for extraction from tissue biopsies and whole exome sequencing (WES) for detection. (2) Mutation screening using the column-based method for extraction from blood plasma and whole exome sequencing for detection (3) Mutation screening using the DTBP platform for extraction from blood plasma and whole exome sequencing for detection. (B) Mutation ratio of the isolated ctDNA using the column-based method (gray) and the DTBP platform (sky blue) for detecting *BRAF* V600E (left), *KRAS* G12D (middle), and *KRAS* G13D (right) mutations. The red line represents the cut-off (criterion) for reporting a sample as mutation (positive/negative) detected. The asterisk (*) represents samples from which the mutation was detected in only cfDNA and not in tissue DNA. The dual asterisks (**) represent samples from which mutations were detected only in cfDNA using the DTBP platform but not using the column-based method. (C) Correlation between WES results of primary tissues and plasma among 14 clinical samples with the ctDNA isolated using the column-based method and the DTBP platform.

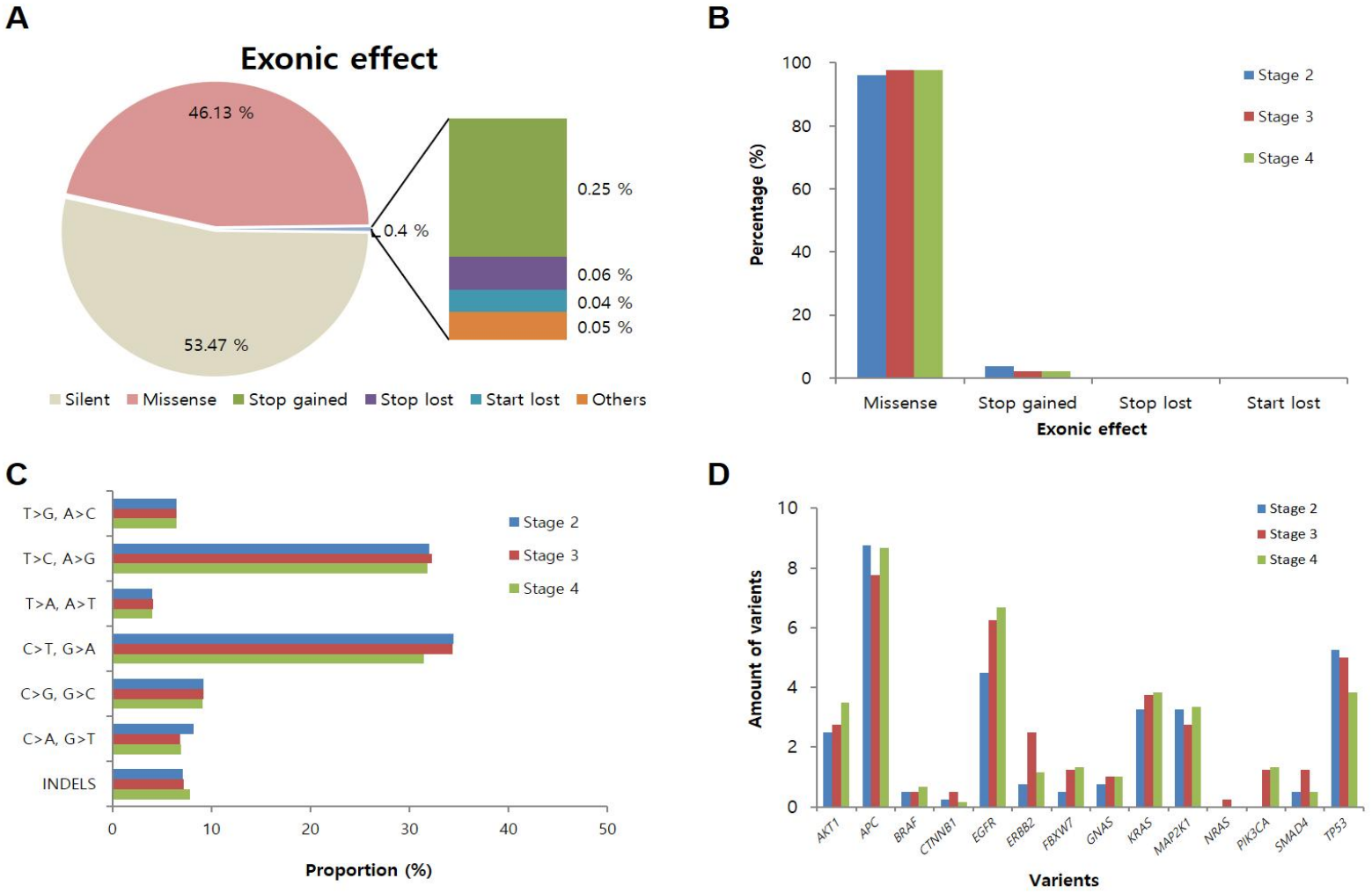
A
Exonic effect
46.13 %
0.4 %
53.47 %
0.25 %
0.06 %
0.04 %
0.05 %
Silent
Missense
Stop gained
Stop lost
Start lost
Others
B
Percentage (%)
100
80
60
40
20
0
Stage 2
Stage 3
Stage 4
Missense
Stop gained
Stop lost
Start lost
Exonic effect
C
T>G, A>C
T>C, A>G
T>A, A>T
C>T, G>A
C>G, G>C
C>A, G>T
INDELS
Stage 2
Stage 3
Stage 4
0
10
20
30
40
50
Proportion (%)
D
Amount of varients
10
8
6
4
2
0
Stage 2
Stage 3
Stage 4
AKT1
APC
BRAF
CTNNB1
EGFR
ERBB2
FBXW7
GNAS
KRAS
MAP2K1
NRAS
PIK3CA
SMAD4
TP53
Varients

Figure 2.10. Genetic characteristics of 14 primary tissue samples from colorectal cancer patients determined using whole exome sequencing. (A) Number of exonic effects from 14 tissues. (B) Exonic effect dependent on the cancer stage of colorectal cancer (CRC) patients. (C) Number of nucleotide substitution classes dependent on the cancer stage. (D) Mutation frequencies in CRC samples dependent on the cancer stage.

Table 2.5. Clinicopathologic characteristics and sequencing results from primary tissue and plasma (ctDNA) samples obtained from 14 colorectal cancer patients.

Nr.	Age	Gender	Pathologic Stage	Tissue (IS)	ctDNA	
					Column	DTBP
T1	68	M	2	WT	WT	WT
T2	62	M	2	WT	WT	WT
T3	54	M	4	*BRAF* (V600E)	WT	*BRAF* (V600E)
T4	62	M	3	*KRAS* (G12V)	WT	WT
T5	42	M	4	WT	*KRAS* (G13D)	*KRAS* (G13D)
T6	42	M	2	WT	WT	*KRAS* (G13D)
T7	48	F	4	*KRAS* (G12V)	WT	WT
T8	34	F	4	BRAF (V600E)	WT	*BRAF* (V600E)
T9	40	M	3	*KRAS* (G13D)	*KRAS* (G13D)	*KRAS* (G13D)
T10	65	M	4	*KRAS* (G12D)	*KRAS* (G12D)	*KRAS* (G12D)
T11	64	F	2	WT	WT	WT
T12	42	M	3	WT	WT	*KRAS* (G12D)
T13	72	F	3	*KRAS* (G13D)	*KRAS* (G13D)	*KRAS* (G13D)
T14	56	M	4	WT	WT	WT

2.3.7. Development of the simple and low-cost ctDNA analysis method

Highly sensitive detection technologies, including NGS, are needed to detect ctDNA after cfDNA isolation because ctDNA exists at low levels in blood plasma. However, NGS is an expensive method and requires large plasma volumes (>10 mL) for ctDNA detection. To address this issue, I developed a simple and low-cost ctDNA detection platform that combined the DTBP platform with Sanger sequencing or PCR (Fig. 2.11A). The Sanger sequencing results of isolated cfDNA are shown in Fig. 2.11B. When the Sanger sequencing was performed on one blood sample obtained from a CRC patient, the *KRAS* mutation G12D could be identified in the cfDNA that was isolated using only the DTBP platform (Fig. 2.11C). To validate the reproducibility of the DTBP platform, the process with plasma samples was repeated obtained from the same patients in different sample tubes and showed that the reproducibility of this platform was sufficient for use of the platform in clinical practice (Fig. 2.11D). Next, 11 plasma samples (frozen and long-term storage) of the CRC patients were tested whose tissue samples showed hot-spot mutations, as confirmed by the OncoPanel assay (96). The OncoPanel results of the tissue samples revealed a *BRAF* V600E mutation in one sample, *KRAS* G12D mutation in three samples, *KRAS* G12V mutations in two samples, and a *KRAS* G13D mutation in one sample. Using the simple and low-cost ctDNA detection platform with Sanger sequencing, a *BRAF* V600E mutation was detected in one sample, a *KRAS* G12D mutation in two samples, a *KRAS* G12V mutation in one sample, and *KRAS* G13D mutations in two samples. This simple and low-cost method with Sanger sequencing yielded a 71.4% correlation in the mutation profiles of the tissues and frozen blood plasma samples obtained from 11 CRC patients (Table 2.6).

Finally, to validate the clinical utility of this simple and low-cost platform, five blood plasma samples prospectively collected from CRC patients were tested. *KRAS* G12D or G13D mutations were identified using both the Sanger sequencing (Fig. 2.11E) and PCR (Fig. 2.11F), but I could not identify them with the column-based method. Although I could not confirm the mutations in the matched tissue samples because tissue samples were not available, *KRAS* G12D and G13D mutations were detected in all five plasma samples by the DTBP platform. These results showed that compared with the commercial column methods, simple and low-cost sampling from the plasma of cancer patients via the DTBP platform is useful for the rapid detection of ctDNA mutations with high sensitivity.

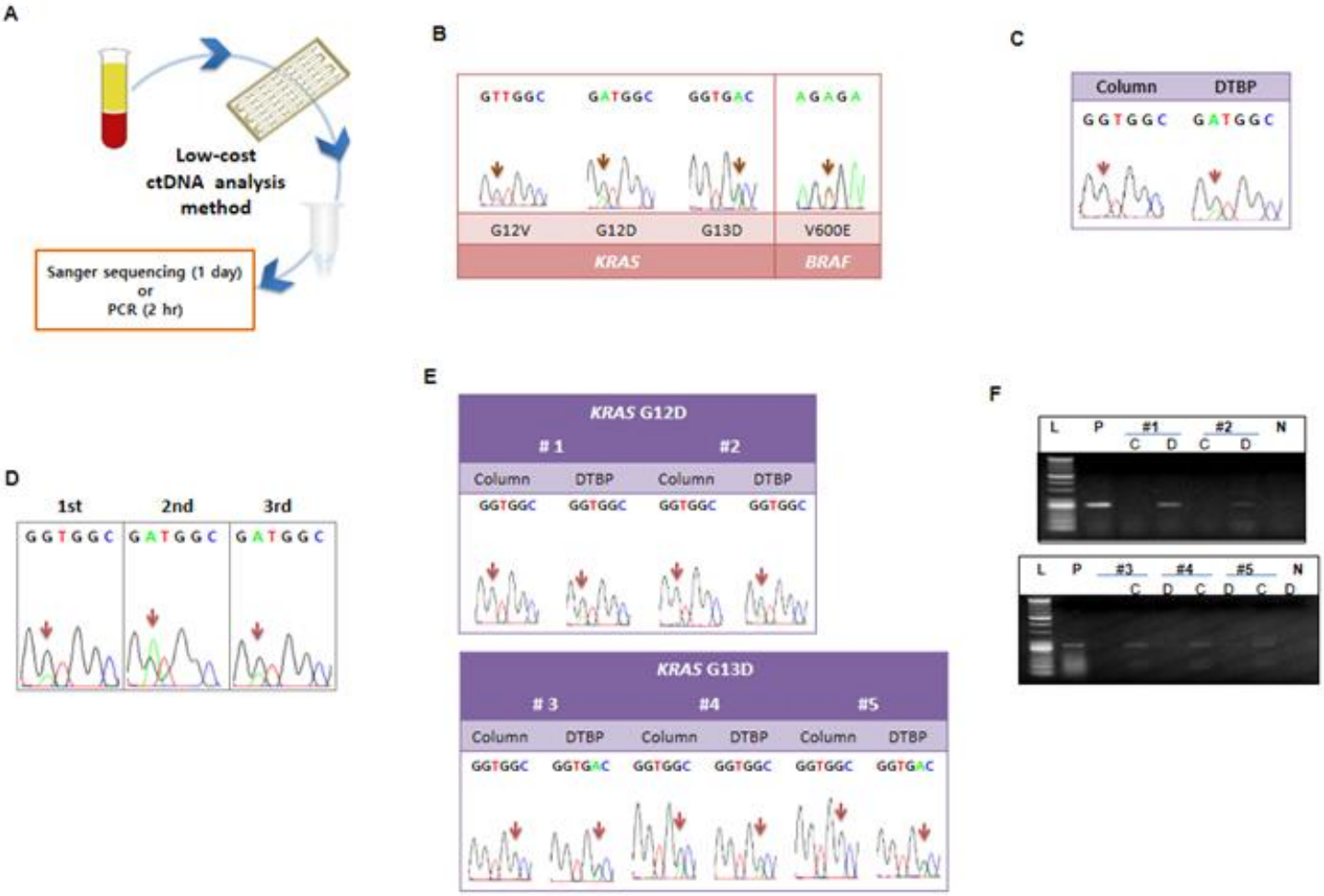
A
Low-cost
ctDNA analysis
method
Sanger sequencing (1 day)
or
PCR (2 hr)
B
GTTGGC
GATGGC
GGTGAC
AGAGA
G12V
G12D
G13D
V600E
KRAS
BRAF
C
Column
DTBP
GGTGGC
GATGGC
D
1st
2nd
3rd
GGTGGC
GATGGC
GATGGC
E
KRAS G12D
1
#2
Column
DTBP
Column
DTBP
GGTGGC
GGTGGC
GGTGGC
GGTGGC
KRAS G13D
3
#4
#5
Column
DTBP
Column
DTBP
Column
DTBP
GGTGGC
GGTGAC
GGTGGC
GGTGGC
GGTGGC
GGTGAC
F
L
P
#1
#2
N
C
D
C
D
L
P
#3
#4
#5
N
C
D
C
D
C
D

Figure 2.11. Simple and low-cost ctDNA analysis for clinical diagnosis. (A) Combination of the DTBP platform and Sanger sequencing for low-cost ctDNA analysis. (B) ctDNA was isolated from 11 plasma samples of colorectal cancer patients using the DTBP platform, and then Sanger sequencing was performed for ctDNA analysis. The mutation sequence identified using the DTBP platform. (C) Sequencing result of ctDNA for the *KRAS* mutation using the column-based method and DTBP platform. (D) Reproducibility of the DTBP platform with a different sample tube of the same patient. (E) Validation of this simple and low-cost ctDNA analysis using five plasma samples in which mutation were not identified in the column-based method. (F) Gel electrophoretic analysis of the PCR products with *KRAS* G12D (left) and *KRAS* G13D (right) mutations extracted from five CRC patients using the column-based method and the DTBP platforms (L: 500bp DNA ladder, P: positive control, #1-2: plasma samples for the G12D mutation, #3-5: plasma samples for the G13D mutation, C: column-based method, D: DTBP platform, and N: negative control).

Table 2.6 Results of simple and low-cost ctDNA analysis of samples from 11 colorectal cancer patients using the DTBP platform and Sanger sequencing.

Nr.	Tissue OncoPanel		ctDNA Sanger sequencing	
	BRAF	*KRAS*	*BRAF*	*KRAS*
S1	WT	G12D	WT	G12D
S2	WT	G12D	WT	G12D
S3	WT	WT	WT	WT
S4	WT	G12D	WT	WT
S5	WT	G12V	WT	G12V
S6	WT	WT	WT	WT
S7	V600E	WT	V600E	WT
S8	WT	WT	WT	WT
S9	WT	G12V	WT	WT
S10	WT	G13D	WT	G13D
S11	WT	WT	WT	WT

Chapter 3. Development of sample preparation microfluidic platform for rapid pathogen enrichment and NA extraction

3.1. Introduction

Pathogenic bacteria and viruses can cause significant levels of disease even at very low blood concentrations and ultimately lead to unexpected deaths and huge economic losses (97, 98). Past outbreaks such as Severe Acute Respiratory Syndrome have resulted in a total of 775 deaths since 2002 and Middle East Respiratory Syndrome infected 186 cases and caused 39 deaths within one month in 2015 in Korea. Emerging infectious diseases such as these caused by new or unknown pathogens will continue to significantly threaten human life because of the absence of appropriate diagnostic tools (99−102). Innovative clinical techniques for the rapid detection and efficient monitoring of both known and unknown pathogens are thus highly desirable to manage and minimize their spread (98, 103).

In general, the pathogen concentrations are extremely low at the early stages of disease and require highly sensitive and specific detection systems for early diagnostic and surveillance purposes. Recent advances with various PCR based techniques and NGS methods have assisted with this (40, 104, 105). However, these approaches are labor−intensive, require bulky instruments, are expensive to perform, and cannot readily be applied to large volume samples (106). In real clinical settings, only volumes of 100−200 μL can be effectively analyzed for pathogen infection with a PCR or sequencing method. When the concentration of pathogen is low and the original sample is over 1 mL, the threshold of detection may not be reached for these methods. Techniques for simultaneous pathogen enrichment, concentration, and extraction are therefore needed for clinical applications.

To date, if the required sample volume is large and a pathogen needs to be enriched for detection, the conventional sample preparation assays use immunological capture or physical separation (107, 108). Immunological capture requires antibodies based on previous knowledge of the targets and it therefore limited when identifying new or emerging virus strains. Ultracentrifugation is the most commonly used method for enriching pathogens from clinical samples but is an expensive method requiring a long processing time and bulky equipment. These techniques cannot therefore be used at the point−of−care due to their complexity and equipment requirements

(109, 110). The gold standard method in hospitals for the diagnosis of pathogens is a culture-based method, but this is also very time-consuming (from several hours to several days) and cannot be used for culture-negative bacteria (111). Although several recent methods for enriching pathogens using nanoparticles and magnetic beads have now been introduced, the preprocessing steps are lengthy and costly, require specific antibodies for pathogen capture and have stability issues under harsh sample conditions (112, 113).

An ideal pathogen diagnostic system that can be used at the point-of-care needs to be rapid, accurate, low-cost, and be able to process the entire clinical sample volume from the patient, including urine, saliva, and blood. However, these fluids usually contain elements that inhibit the amplification of DNA and RNA and rapid and simple techniques that can accurately isolate and enrich pathogens are thus needed to properly diagnose infectious diseases (114). A combination of such an enrichment and concentration method with sample preparation would significantly increase the pathogen detection sensitivity in a clinical application.

In this study, a simple, label-free and instrument-free pathogen enrichment technique via the use of HIs using a microfluidic (SLIM) system was described for ultrasensitive pathogen detection in various clinical specimens. HI reagents including DMA, DMP and DMS with assembled double microfluidic disposable chips (ADC) are used to effectively capture pathogens (bacteria and viruses) from the clinical samples within 10 min. All HI reagents consist of positive charge groups that can directly and selectively bind negatively charged pathogens in a 1-2 mL volume without the need for detergents or bulky instruments. In addition, the ADC microfluidic platform was used to streamline the processing of larger sample volumes and thereby save time and expense.

Nucleic acids were extracted with the SLIM system using a solution of HI reagents with lysis buffer from the pathogens enriched on this same system. DMA and DMP are known as cross-linking reagents and contain two imidoester groups, which react with amine groups of nucleic acids, proteins and cells to form amidine bonds (4-6). Accordingly, the SLIM system can be used for enrichment and extraction within 50 min on a single platform with a reduced risk of external contamination, and without the need for complicated procedures or separate equipment. The clinical utility of SLIM system was demonstrated to process 46 clinical specimens including environmental swabs,

saliva, and blood plasma which showed at least a 2-fold higher sensitivity for pathogen detection than existing methods. The clinical utility of this combination system was validated for the enrichment and detection of pathogens in 17 plasma samples including 14 HZ and 3 non-HZ controls. Our approach is not only enriched pathogens in a sample by at least 10-fold to enable the rapid and ultrasensitive detection of pathogens at the POC in the clinic.

3.2. Materials and methods

3.2.1. Amplification of bacterial DNA

The DNA extracted from the *E. coli* was amplified using PCR and qPCR. The PCR cycling conditions consisted of an initial denaturation step at 95 ℃ for 15 min; 40 cycles at 95 ℃ for 30 s, 58 ℃ for 30 s, and at 72 ℃ for 30 s; and a final elongation step at 72 ℃ for 7 min. Five microliters of DNA were amplified in a total volume of 25 μL containing 10X PCR buffer (Qiagen), 2.5 mM $MgCl_2$, 0.25 mM dNTP, 25 pmol of each primer, and one unit of Taq DNA polymerase (Qiagen). Electrophoresis was used to separate the PCR products on a 2% agarose gel containing EtBr. The gel was visualized using a GelDoc System (Clinx Science Instruments, Shanghi, China). The qPCR procedure was modified from the AriaMx real-time PCR Instrument protocol (Agilent technologies). Briefly, 5μL of DNA were amplified in a total volume of 20 μL containing 10 μL of 2X Brilliant III SYBR Green QPCR master mix, 25 pmol of each primer, and deionized water. An initial pre-incubation at 95 ℃ for 10 min was followed by 50 cycles at 95 ℃ for 10 s, at 58 ℃ for 20 s, and at 72 ℃ for 20 s, and by a cooling step at 40 ℃ for 30 s. The SYBR Green signals of the amplified products were acquired using AriaMx real-time PCR (Agilent technologies). The forward and reverse primers for the amplification of several genes were synthesized at a usual length of approximately 24 bps.

3.2.2. Clinical samples

To test the applicability of our SLIM system to the testing of various clinical samples, environmental swab samples from patients infected with human parainfluenza virus type 3 (hPIV-3), and the saliva and plasma samples from HZ patients were obtained using protocols approved by the institutional review board of Asan Medical Center, Republic of Korea. Institutional approval of the protocols used and written informed consent from the patients was also obtained (115, 116). The viral DNA and RNA samples were extracted using either the QIAamp DNA mini kit or QIAamp viral RNA mini kit in accordance with the manufacturer`s instructions. Each sample had a starting volume of 200 μL for DNA or 140 μL for RNA and was eluted to approximately 50 μL for DNA or 50 μL for RNA using an elution buffer. The extracted DNA and RNA were stored at −20 ℃ until use. For enrichment using the SLIM system, 2 ml of an environmental swab sample from hPIV-3

patients and 1 ml of saliva and plasma samples from HZ patients were used and the nucleic acids were eluted at the same volumes used with the Qiagen kit. The PCR assays for detecting hPIV-3 and VZV were performed using previously reported protocols (115, 116).

3.2.3. Optimization of enrichment platform

The assay conditions and solution was optimized, used to enrich pathogens using the SLIM system. All HI groups such as DMA, DMS and DMP were tested to compare their ability to directly bind pathogens. All HI reagents were purchased from Sigma-Aldrich. To conduct the reaction, a 1 mL preparation of *E. coli* (ATCC 25922) diluted in PBS was mixed with 300 μL of each HI solution (100 mg/mL) and then injected into the SLIM system using a syringe pump (KD Scientific, Holliston, MA) at 100 μL/min. The system was then placed at room temperature for 10 min to enable pathogen capture followed by elution with 10 mM sodium bicarbonate, pH < 10.6, at a flow rate of 50 μL/min).

To extract nucleic acids from the enriched pathogen solution, a QIAamp DNA mini kit (Qiagen, Germany) or nucleic acid extraction using our microfluidic platform with HIs was conducted as described previously. Briefly, the enriched pathogen sample was mixed with proteinase K, in-house lysis buffer (100 mM Tris-HCl (pH 8.0), 10 mM ethylenediaminetetraacetic acid, 1% sodium dodecyl sulfate, and 10% Triton X-100) and HI reagent (100 mg/mL). After incubating the system at 56 ℃ (for DNA) or room temperature (for RNA) for 20 min, PBS was used to wash the system to remove debris from the samples. Elution buffer (pH > 10.6) was used to collect the extracted NAs within a few minutes. The quantity and purity of the extracted nucleic acids were measured using both Qiagen kit and the microfluidic platform, based on the ratio of the optical densities of the samples at 260 nm and 280 nm measured with a Nano Drop spectrometer (Thermo Fisher Scientific, Waltham, MA).

3.2.4. Integration of enrichment and extraction step in one-platform

To enrich and concentrate the pathogens from a large volume samples via the SLIM system, a pre-mixed solution of sample and HI is introduced onto the ADC platform which has been pre-activated with amine reactive groups on its surface to electrostatically capture complexes of negatively charged pathogens and negatively charged HI reagents (Fig. 3.1A, right). As the

suspension flows through the platform, pathogen capture occurs on the inner surface while other substances flow through (Fig. 3.1A, right).

Second, after the enrichment process at room temperature for 20 min to selectively capture pathogens, a lysis buffer with additional HIs is added to isolate nucleic acids (DNA and RNA) from the captured pathogens by covalent bonding on the same platform at 56 ℃ for 20 min. Elution buffer is added to collect the nucleic acids by breaking the interaction between the complex and the inner surface of the platform. The SLIM system can thus capture and extract nucleic acids from pathogens from 1 or 2 mL samples without the need for other instruments such as centrifuges and vortexes.

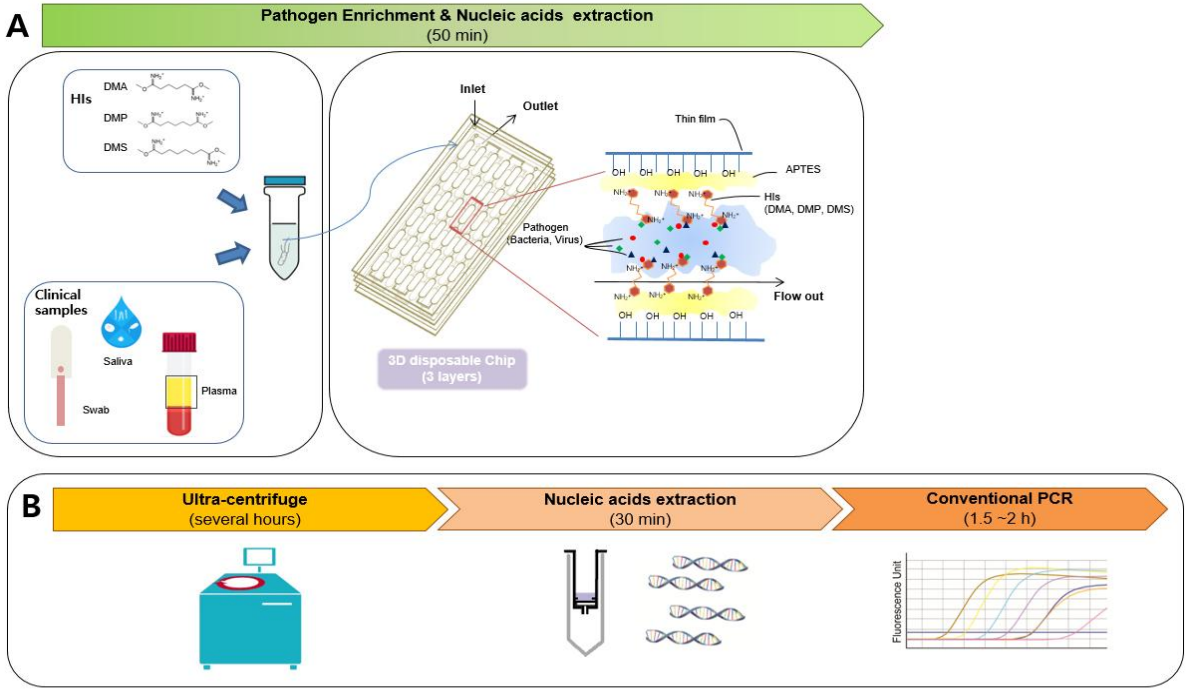

Figure 3.1. Schematic representation of the principle of ultrasensitive pathogen detection in clinical specimens. (A) Ultrasensitive pathogen detection system combining a simple and label-free system via homobifunctional imidoesters (HIs) with a microfluidic (SLIM) platform. A mixture clinical sample and HI reagent is added to the SLIM system to enrich the pathogen and extract the DNA/RNA within 50 min without the need for detergents or bulky instruments. (B) Work flow of conventional methods for detection of pathogens with enrichment via ultracentrifugation, nucleic acid extraction on a column, and pathogen detection by qPCR

3.3. Results and discussion

3.3.1. Characterization of SLIM platform

Commonly used pathogen detection assays for clinical samples include conventional PCR and pathogen cultures. A limitation of these established approaches However is their ability to detect true pathogens at very low concentrations in the sample. In actual clinical settings in which the patient sample volumes often range from at least 1 mL to as high as 10 mL depending on sources such as saliva, urine, and blood, researchers have typically used maximum volumes of only 200 μL due to the capacity limitations of available methods. Thus, the detection of low concentration pathogens has remained a challenge.

I investigated whether the SLIM system could enrich the pathogens from a large volume simply and rapidly and with high sensitivity and specificity. I tested this by loading 1 mL of *E. coli* samples (10^4 CFU/mL) onto the SLIM platform and enriched and re-suspended these organisms with 200 μL of elution buffer. The enriched sample was then subjected to nucleic acid extraction with a Qiagen kit. Different concentrations of DMA (one of the HIs) and various incubation times were tested to optimize this enrichment step and then amplified the *rodA* gene of the enriched *E. coli* using qPCR (Fig. 3.2). The qPCR C_T value and capture rate, depending on the concentration of DMA (50, 100 or 200 mg/mL), were measured for the 1 mL *E. coli* preparation (10^4 CFU/mL). A 100 μL volume of sample (10^5 CFU/mL) without pathogen enrichment was tested in the real-time PCR as a reference absolute value. Following SLIM enrichment, higher amplification efficiency at 100 mg/mL concentration of DMA was observed (Fig. 3.2A). The capture rate of *E. coli* was about 80% of the absolute value at this DMA level (Fig. 3.2B). The C_T value and capture efficiency of the system at different incubation times (5, 10 and 20 min) were tested. I observed a better amplification efficiency with the 20 min incubation time that was almost 80% enriched compared to the absolute value (Fig. 3.2C-D).

Next, the optimal HI reagents (DMA, DMP or DMS) were evaluated to use for pathogen enrichment again using a 1 mL preparation of *E. coli* (10^4 CFU/mL). DMP was found to be the most efficient of these reagents for pathogen enrichment and gave real-time result about 4 cycles earlier than that of the Qiagen kit without any enrichment (Fig. 3.2E-F).

Our system protocol was thus optimized for the concentration (100 mg/mL;

Fig. 3.2A, B) of reagent, incubation time (20 min; Fig. 3.2C, D) and selection of HI reagent (DMP; Fig. 3.2E, F) for enriching pathogens from a large sample volume.

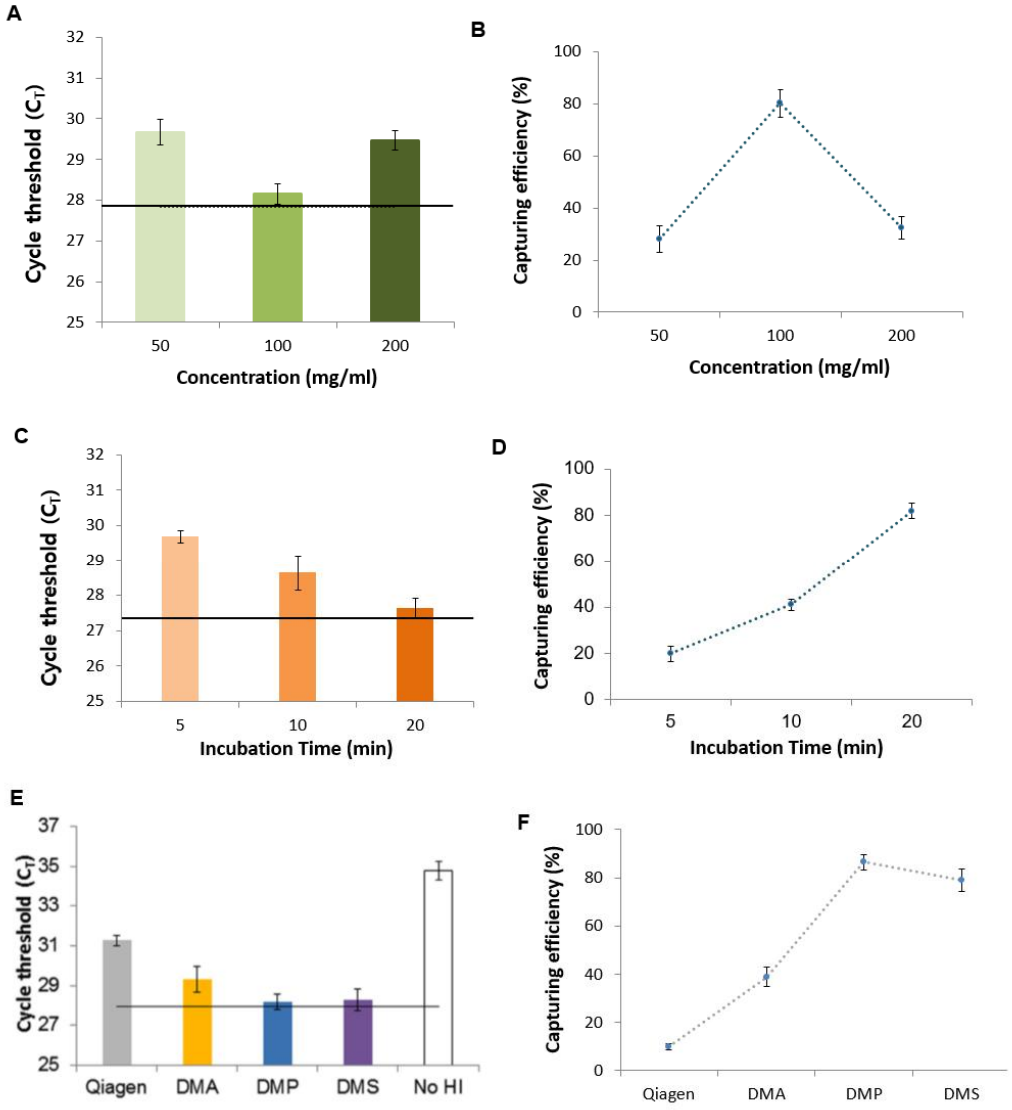

Figure 3.2 Characterization of the SLIM system for pathogen enrichment. (A) Amplification efficiency for a 1 mL *E. coli* test sample (10^4 CFU) following its enrichment on the SLIM system using the DMA. The black dotted line represents the C_T value for *E. coli* DNA from the absolute concentration (10^4 CFU) reference control extracted with a Qiagen kit. (B) The *E. coli* capture rate using the SLIM system depends on the HI concentration. (C) The amplification efficiency following *E. coli* (10^4 CFU/mL) enrichment depends on the incubation time on the platform. The black dotted line denotes the C_T value of the absolute concentration (10^4 CFU) *E. coli* reference control DNA extracted using a Qiagen kit. (D) The *E. coli* capture rate using the SLIM system also depends on the incubation time. (E) The amplification efficiency for a sample of *E. coli* (10^4 CFU/mL) following bacterial enrichment using the

SLIM system is dependent on the type of HI reagents (DMA; yellow, DMP; blue, DMS; purple). The control experiment without HI reagents is examined as negative control (No HI). The black dotted line denotes the C_T value for the reference control *E. coli* DNA extracted from the absolute concentration (10^4 CFU) sample control of using a Qiagen kit. (F) The *E. coli* capture rate using the SLIM system depends on the HI type. The error bars indicate the standard deviation from the mean, based on at least three independent experiments.

3.3.2. Bacteria enrichment and extraction

After optimizing the SLIM protocol for pathogen enrichment, its capacity was evaluated to analyze 1 mL *E. coli* samples ranging in concentration from 1×10^{1} to 1×10^{4} CFU/mL. Once the bacteria had been process using the SLIM system, A Qiagen kit for nucleic acid extraction was used, which followed by qPCR detect the bacteria. The PCR results indicated that DNAs from the enriched *E. coli* were amplified gradually and that this depended on the serial dilution of the pathogens. At all sample concentrations, much earlier C_T values were obtained for the enriched DNA than from DNA extracted using the Qiagen kit (Fig. 3.3A). The limit of detection limit was 10-fold higher using the SLIM system.

I next investigated whether the SLIM system could be used to both enrich the bacteria and perform the extraction on the same platform. To compare the detection efficiency of Qiagen without enrichment, a two-step process (enrichment and extraction in two separate chips) or the proposed one-step method (enrichment and extraction in a same chip), *E. coli* (10^{4} CFU/mL) and qPCR were used again. The C_T values when using Qiagen without enrichment were 3-4 cycles delayed compared with the absolute value of the pathogen. With the SLIM system with a 1 mL volume, the amplification efficiency over a two-step process was 1-2 cycles longer than that of the absolute value. However, when both enrichment and extraction were done on the same chip, the amplification efficiency was similar to the absolute value of the pathogen (Fig. 3.3B). Therefore, the SLIM system can significantly improve both the bacterial enrichment rate and detection limit within 50 min.

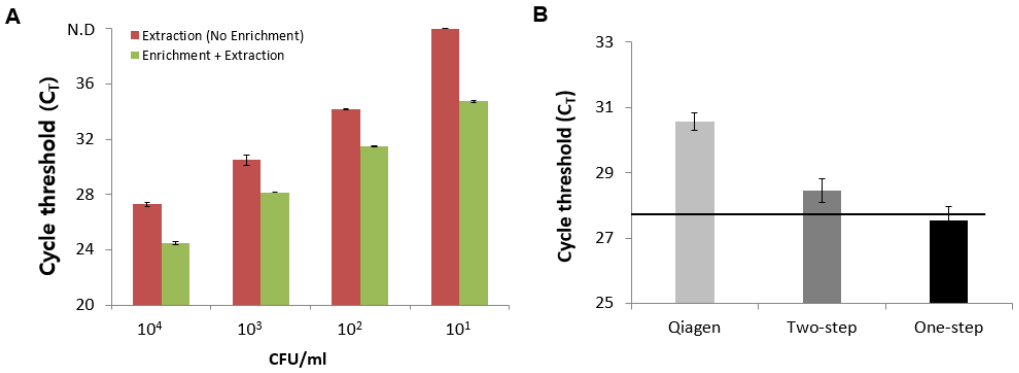

Figure 3.3. Application of the SLIM system to bacterial enrichment and extraction. (A) Capacity of the SLIM system to process test *E. coli* samples in concentrations ranging from 1×10^1 to 1×10^4 CFU/mL using both the Qiagen kit (red) and the SLIM system (light green) for DNA extraction. The error bars indicate the standard deviation from the mean, based on at least three independent experiments. (B) Use of the SLIM system for simultaneous enrichment and extraction with a test *E. coli* sample of 1×10^4 CFU/mL. Qiagen (light gray); DNA extraction only without enrichment, Two-step (dark gray); DNA extraction with Qiagen kit after bacterial enrichment with the SLIM platform, and One-step (black); simultaneous enrichment and extraction on the same system. The black dotted line denotes the C_T value of the absolute (10^4 CFU) *E. coli* reference control DNA extracted using a Qiagen kit. The error bars indicate the standard deviation from the mean, based on at least three independent experiments.

3.3.3. Validation in clinical samples

To validate our new SLIM system for real samples, swab samples taken from environmental surfaces in contact with patients during an hPIV-3 outbreak between May and June 2016 in South Korea were applied (Fig. 3.4). Detecting viral nucleic acids from environmental samples is important as environmental contamination by hPIV-3 is known to precede the nosocomial transmission of hPIV-3 in hospital wards (115). For the detection of hPIV-3, 140 μL aliquots from 2 ml environmental swab samples were used to extract viral RNA and amplify it by qRT-PCR (115). Due to limitations in existing nucleic acid extraction methods, the 2 mL entire sample volume could not be directly used for the detection of viral RNA. Using conventional methods, it has been reported that successful hPIV-3 detection the environmental swabs is only about 49% by qRT-PCR. Using our SLIM system however, the entire 2 mL volume of the environmental swab sample was used for hPIV-3 virus enrichment and viral RNA extraction (Fig. 3.4A). First, one positive and three negative samples were determined by PCR from 49 swabs to test the virus enrichment ability of the SLIM system. As shown in Figure 3.4B, one if the three negative samples as determined by PCR was in fact found to be hPIV-3 positive using the SLIM system. The positive sample determined by PCR showed an enhanced the amplification efficiency for the virus compared with the Qiagen kit (Fig. 3.4B). I further tested 6 positive and 6 negative swabs from a patient with hPIV-3 virus and found using the SLIM system that the amplification efficiency of the 6 positives was 1-2 cycles earlier than conventional approaches. Moreover, 4 out of the 6 negative swabs determined by qPCR showed C_T values with SLIM system (Fig. 3.4C). The detection sensitivity with SLIM system was calculate at 83.3 % (10/12) compared to 50% without the SLIM system (6/12) (Fig. 3.4C and Table 3.1). The positive samples were further confirmed by Sanger sequencing for the hemagglutinin-neuraminidase (HN) gene of hPIV-3.

The SLIM system was applied to saliva samples from patients with HZ (Fig. 3.5). Chickenpox and HZ are caused by VZV. Although the HZ rash is generally considered sufficient for clinical diagnosis, better diagnostic assays for saliva and plasma specimens are needed to distinguish HZ and HZ-mimicking diseases such as herpes simplex virus (116). VZV infection in saliva and plasma obtained from HZ patients. Saliva sample volumes of 200 μL of a total 1 mL sample have previously been used for PCR analysis without any enrichment process. Recently, one study described the diagnostic

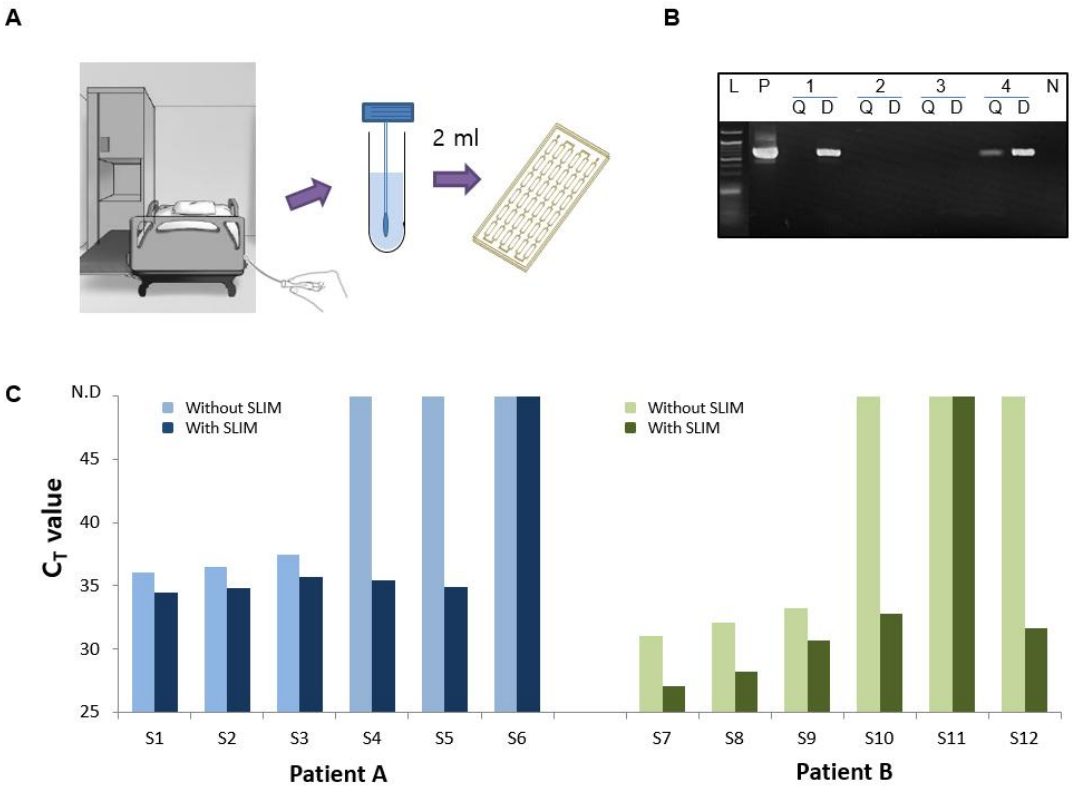

Figure 3.4. Validation of the SLIM system for RNA virus enrichment in environmental samples. (A) 12 environmental sample of hPIV-3 infected patients was collected and enriched with SLIM. (B) Gel electrophoresis analysis of end-point PCR products of viral RNAs extracted from 4 environmental samples of hPIV-3 using the Qiagen kit and the platform with DMP (L: 50 bp DNA ladder, 1-4: environmental specimens, Q: extracted with the Qiagen kit, D: enriched and extracted with the SLIM, and N: negative control). (C) Fluorescence signal obtained by real-time PCR for amplified hPIV-3 RNAs extracted from 6 specimens of using Qiagen kit from patient A(sky blue) and patient B (light green), and enriched from same 6 specimens of using SLIM with DMP from patient A(dark blue) and patient B (dark green).

Table 3.1. Comparison of C_T values in hPIV-3 environmental swabs.

Patients	Samples Nr.	C_T value	
		Without SLIM	With SLIM
A	1	36.09	34.42
	2	36.52	34.81
	3	37.47	35.69
	4	N.D	35.47
	5	N.D	34.91
	6	N.D	N.D
B	7	31.01	27.09
	8	32.12	28.18
	9	33.19	30.7
	10	N.D	32.75
	11	N.D	N.D
	12	N.D	31.61

usefulness of PCR for detecting VZV infection in saliva and plasma obtained from HZ patients. Saliva sample volumes of 200 μL of a total 1 mL sample have previously been used for PCR analysis without any enrichment process. The sensitivity of PCR analysis detecting VZV is far higher in saliva DNA (88%) than in plasma DNA (28%) (116). However, although, plasma samples from HZ patients are less sensitive than salivary DNA for PCR detection, false-positive results can be obtained from saliva and saliva sampling is more painful for the patient (112, 117). For these reasons, The use of both saliva and plasma samples were tested to diagnose HZ and determine the efficiency of enrichment in both cases with the SLIM system. 1 mL saliva sample volumes was used for VZV enrichment and viral DNA extraction (Fig. 3.5). 10 saliva-positive samples were selected as previously determined by qPCR. All PCR-positive samples that had been confirmed using the *ORF62* region of VZV had earlier C_T values with the SLIM system (Fig. 3.5A-B and Table 3.2). On the other hand, none of the previously determined PCR-negative samples showed a positive result for either group with the SLIM system (Fig. 3.5A-B and Table 3.2). These results are consistent with the previous findings that saliva samples have greater utility for the detection of VZV (117).

This SLIM system was validated with 14 plasma samples obtained from patients with HZ as previously determined by PCR analysis of saliva samples (Fig. 3.6). When a 200 μL plasma sample volume was used for viral DNA extraction without the SLIM system, the sensitivity for subsequent VZV detection by real-time PCR was only 35.7% (5/14) (Fig. 3.6A and Table 3.3). Using the SLIM system However, this improved to 57.1% (8/14) by real-time PCR (Fig. 3.6A and Table 3.3). In addition, all 8 samples enriched with the SLIM system showed better amplification efficiencies and higher virus detection sensitivities than samples that were not processed with the SLIM system (Fig. 3.6B).

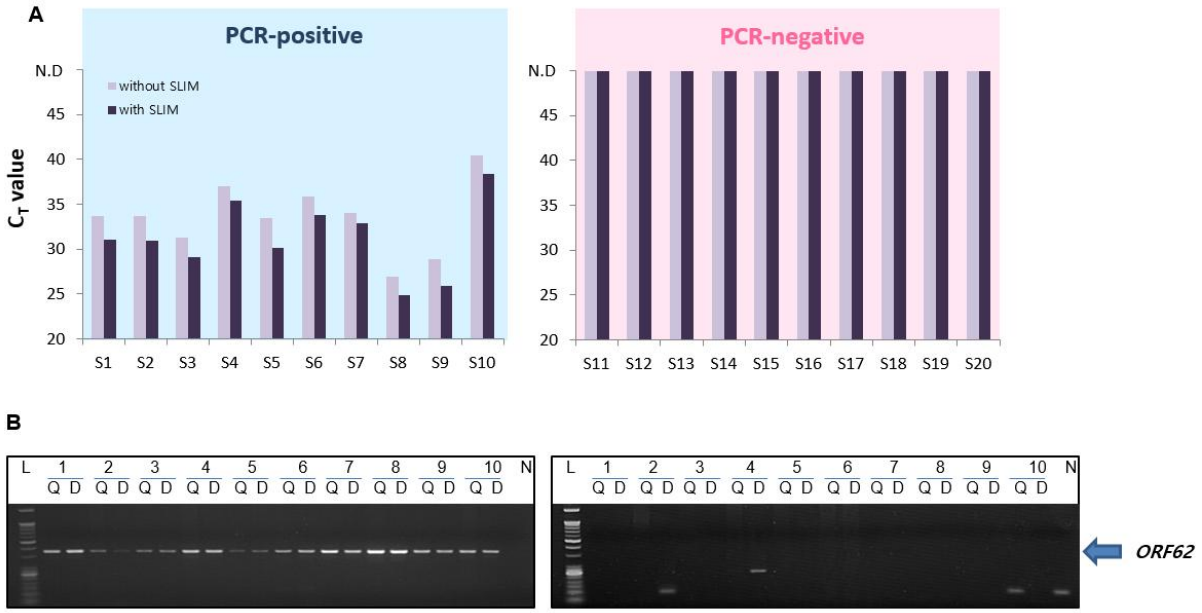

Figure 3.5. Validation of the SLIM system in HZ saliva samples. (A) SLIM system in environmental swab samples. 12 environmental swab samples taken from areas containing hPIV-3 infected patients were collected and enriched using the SLIM system. qPCR fluorescence signals for amplified hPIV-3 RNAs from the same 6 specimens extracted using a Qiagen kit (without SLIM enriched) or enriched using the SLIM system from patient A (S1-S6) and patient B (S7-S12). (B) SLIM system in saliva samples from HZ patients. 20 saliva samples from HZ infected patients were collected and enriched with and without the SLIM system. Fluorescence signals obtained by real-time PCR amplification of VZV DNAs extracted from 20Hz patient samples using a Qiagen kit (without SLIM system) (gray) and enriched from the same 20 specimens with the SLIM system (black). The sample numbers represent positive (S1-S10) and negative (S11-S20) samples that were confirmed by end-point PCR.

Table 3.2. Comparison of C_T values in PCR-positive saliva samples from HZ patients.

Nr.	C_T value	
	Without SLIM	With SLIM
1	33.69	31.08
2	33.72	31
3	31.27	29.07
4	37.06	35.45
5	33.46	30.15
6	35.9	33.85
7	34.03	32.93
8	26.91	24.87
9	28.87	25.96
10	40.47	38.45
11	N.D	N.D
12	N.D	N.D
13	N.D	N.D
14	N.D	N.D
15	N.D	N.D
16	N.D	N.D
17	N.D	N.D
18	N.D	N.D
19	N.D	N.D
20	N.D	N.D

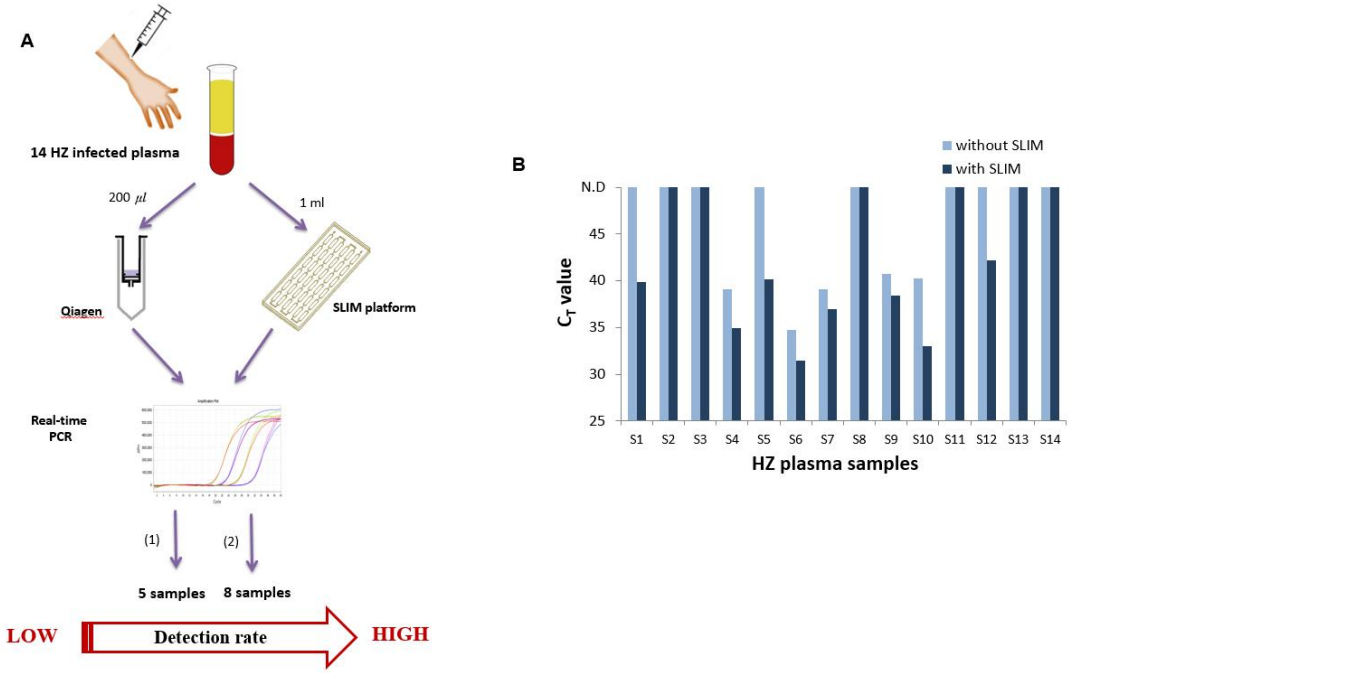

Figure 3.6. Clinical utility of the ultrasensitive pathogen diagnostic system integrated with the SLIM system to test blood plasma samples from HZ patients. (A) Fourteen plasma samples from HZ infected patients were collected and enriched with and without the SLIM platform and detected by PCR as follows: (1): qPCR detection without enrichment, (2): qPCR detection after processing on the SLIM system. (B) Fluorescence signals obtained by qPCR amplification of viral DNA from 14 specimens extracted using either a Qiagen kit (sky blue) or the SLIM system (dark blue).

Table 3.3. Comparison of C_T values in plasma samples from HZ patients.

Nr.	C_T value	
	Without SLIM	With SLIM
1	N.D	39.84
2	N.D	N.D
3	N.D	N.D
4	39.05	34.96
5	N.D	40.16
6	34.76	31.7
7	39.1	36.97
8	N.D	N.D
9	40.69	38.45
10	40.22	33.03
11	N.D	N.D
12	N.D	42.22
13	N.D	N.D
14	N.D	N.D

Chapter 4. Rapid Nucleic Acids Detection with Bio-optical Sensor

4.1. Introduction

For the rapid and sensitive detection of pathogens (both virus and bacteria), biosensors are emerging technologies that enable the development of fast, low-cost, highly sensitive, and specific detection systems for clinical applications. Numerous pathogen-sensing technologies have been constructed using optical, electrochemical, electrochemiluminescence, quartz crystal microbalance, surface plasmon resonance, and SMR techniques (26, 118-125). Most biosensors are employed to detect molecules, including DNA, RNA, and proteins, by using the interaction between the molecules and sensing ligands (126, 127). In particular, the SMR is a refractive index sensor that offers highly sensitive, label-free, real-time multiplexed detection of biomolecules on the sensor surface (128, 129). DNA-based detection using an SMR biosensor is more specific and sensitive than immunological-based detection (26, 27, 130). Despite the important role of biosensors in virus detection, their clinical utility has not been broadly explored in clinical applications because of the lack of integrated systems combining sample preparation with biosensor techniques (131-133). To create an ideal virus detection system, the integration of the sample preparation and biosensor techniques is desired.

A rapid bio-optical sensor that can simultaneously amplify and detect pathogen in human clinical specimens was developed. This assay is based on a combination of isothermal DNA amplification (IDA) and the use of a bio-optical sensor involving a SMR in a single chamber. IDA techniques were initially introduced to bypass the need for thermal cycling in molecular diagnostic applications. The RPA as the isothermal assay was used in this study as it does not require thermal cycling and operates at a constant temperature of 37 ℃ to 42 ℃ (34). Taken together, SMRs have been shown to be a powerful and versatile technique for bio-molecule detection. However, the clinical utility of these bio-optical sensors with isothermal amplification in human clinical samples is still being explored due to the complexity of using real samples that may include inhibitors (134, 135). The presence of these inhibitors in a sample can lead to false-negative or low sensitivity reactions.

In this study, the bio-optical sensor was used for detecting HAdV and HZ from clinical samples. Also, Microfluidic system was integrated with bio-optical sensor for increasing sensitivity of NA detection. Moreover, this

sensor can be applied detection of ctDNA using cfDNA from plasma. The detection limit of this bio-optical sensor was about 10 times higher than qPCR method. Therefore, this assay can be potentially applied for better diagnosis across a variety of clinical applications.

4.2. Materials and methods

4.2.1. Measurement of detection limit

To compare the limits of detection (LODs) of qPCR and the bio-optical sensor, HAdV PCR amplicon (400 bp) was generated with the hexon protein gene of ADV using PCR and was used as the template for evaluating the LOD. The DNA amplicon was purified using Expin PCR SV (GeneAll, Korea) and diluted the concentration of the 400-bp DNA amplicon to contain from 1×10^{1} to 1×10^{11} copies/reaction. The diluted purified DNA amplicon was stored at - 20 ℃ until use.

To detect oncogenic mutation using bio-optical sensor, the cell mixtures for the detection of the G12D mutation were prepared by mixing them with the AGS (G12D mutant cells) and HCT116 (wild-type cells) cell lines at the desired percentage, ranging from 0%, 1%, 10%, 30%, and 50% to 100% of mutant cells. Moreover, the cell mixtures for the detection of the G13D mutation were prepared by mixing them with the HCT116 (G13D mutant cell lines) and AGS (wild-type) cell lines at the desired percentage, ranging from 0%, 1%, 10%, 30%, and 50% to 100% of mutant cells. The serially diluted samples with either G12D or G13D were eluted with 100 μL of elution buffer. The eluted DNA was stored at -20 ℃ until use.

4.2.2. Clinical samples collection for detection *KRAS* mutation

A total of 70 cancer samples (24 samples with G12D mutations, 26 samples with G13D mutation, and 20 samples with no mutation in exon 2) based on frozen tissue availability were obtained from the BRC of Asan Medical Center (Seoul, Korea), after approval from the Institutional Review Board. The samples had been obtained by a colorectal surgical team, and were randomly selected according to the type of mutation. The clinicopathologic characteristics of all the patients, which are known to be related to the course of CRCs were obtained from a prospectively collected database (Table 2). The mean age of the CRC patients was 58.5 years, and 41 patients (58.6%) were male. Stage I, II, III, and IV tumors were observed in 0 (0%), 4 (5.7%), 13 (18.6%), and 52 (74.3%) patients, respectively. Among the 50 patients with the *KRAS* mutation and without *BRAF* mutations, 24 had the G12D mutation (codon 12 GGT→GAT) and the remaining 26 had the G13D mutation (codon 13 GGC→GAC). The types of CRC tissue samples were identified by direct sequencing at BRC, and were used as reference

(136). The genomic DNAs from the tissues were extracted using ATL buffer with proteinase K from a QIAamp DNA mini kit (Qiagen, Germany) according to the manufacturer's instructions. The samples were eluted using 100 μL of elution buffer. The eluted DNA was stored at -20°C until use.

4.3. Results and discussion

4.3.1. Comparison of sensitivity and specificity in clinical samples

Bio-optical sensor for viral DNA detection was used by measuring the wavelength shifts of serially diluted viral DNAs. To test the LOD of the bio-optical sensor, serially diluted samples containing 1×10^1 to 1×10^4 copies/reaction of viral DNA amplicon produced were used by PCR. The resonance wavelength shift of the samples was distinguished with the bio-optical sensor and could be compared with that of human genomic DNA as a negative control. The bio-optical sensor could detect viral DNA at 1×10^1 copies/reaction (Fig. 4.1A). In addition, good linearity of the wavelength shift from 1×10^1 to 10^4 copies/reaction was observed (R^2=0.9038) in 30 min measurements (Fig. 4.1B). On the other hand, using qPCR, a SYBR Green fluorescence signal was evident in the samples containing at least 1×10^3 copies/reaction (Fig. 4.1C). As a result, the LOD of the bio-optical sensor was 100 times higher than that of the qPCR method.

Given that the cancer samples are heterogeneous, a useful assay for the detection of *KRAS* mutations should be able to accurately detect the mutations in mixed cells with wild-type populations. In order to test this capability of the bio-optical sensor, serially diluted samples of mixed cells were used. To test the G12D mutation, AGS cells carrying the *KRAS* G12D mutation were diluted with HCT116 cells carrying no *KRAS* G12D mutation, and were used as wild-type cells. In contrast, to test the G13D mutation, HCT116 cells carrying the *KRAS* G13D mutation were diluted with AGS cells carrying no *KRAS* G13D mutation, and were used as wild-type cells. Genomic DNA was obtained from the cell mixtures containing 0% to 100% of the mutant cells in the background of wild-type cells. All genomic DNAs from the samples were examined via PCR, direct sequencing, and bio-optical sensor (Fig. 4.2). When PCR was used to amplify the G12D or G13D mutation, the mutant targets could be amplified within 2-3 h, particularly when the concentration of mutant cells was >30%. When direct sequencing was used to detect the G12D and G13D mutations, the mutant sequences could be identified within 1-2 days, particularly when the concentration of mutant cells was >30% (Fig. 4.2A). Consistent with previous reports, PCR and direct sequencing could not detect the presence of the mutant allele at a low copy number (<30%) in wild-type populations. Figure 4.2B shows that the mutant sequences for G12D and G13D could be rapidly detected using

bio-optical sensor, by measuring the differences in the wavelength shifts in the samples containing 1% to 100% of the mutant cells. The bio-optical sensor could detect the mutant allele in 30 min, at a concentration of only 1% mutant cells in the background of wild-type DNA (Fig. 4.2B).

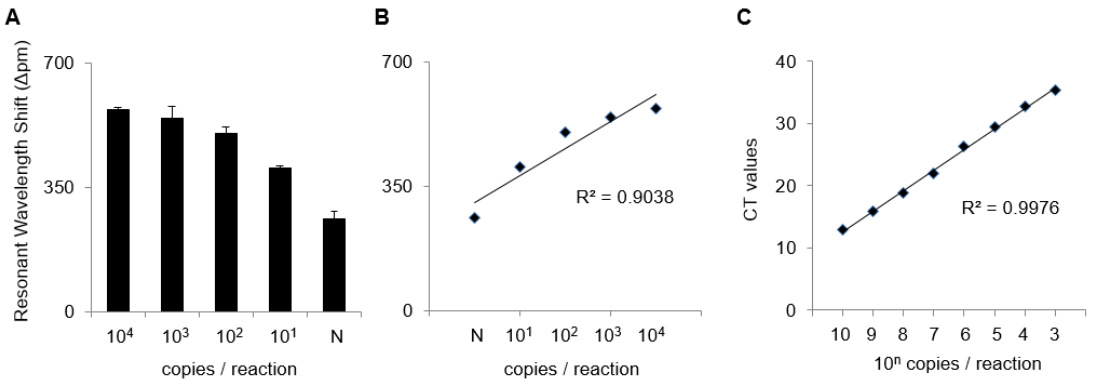

Figure 4.1. Detection limit of the bio-optical sensor for viral DNAs. (A) Resonance wavelength shift in the bio-optical sensor. The bars represent the amount of the target: 1×10^4 copies/reaction, 1×10^3 copies/reaction, 1×10^2 copies/reaction, 1×10^1 copies/reaction, and negative control (N). The error bars indicate the standard deviation from the mean, based on at least three independent experiments. (B) Linear relationship between the wavelength detected by the bio-optical sensor and the concentration of the target in 30 min. (C) Linear relationship between the concentration of the target and the C_T value of the fluorescence signal acquired by qPCR (1: 1×10^{10} copies/reaction, 2: 1×10^9 copies/reaction, 3: 1×10^8 copies/reaction, 4: 1×10^7 copies/reaction, 5: 1×10^6 copies/reaction, 6: 1×10^5 copies/reaction, 7: 1×10^4 copies/reaction, and 8: 1×10^3 copies/reaction).

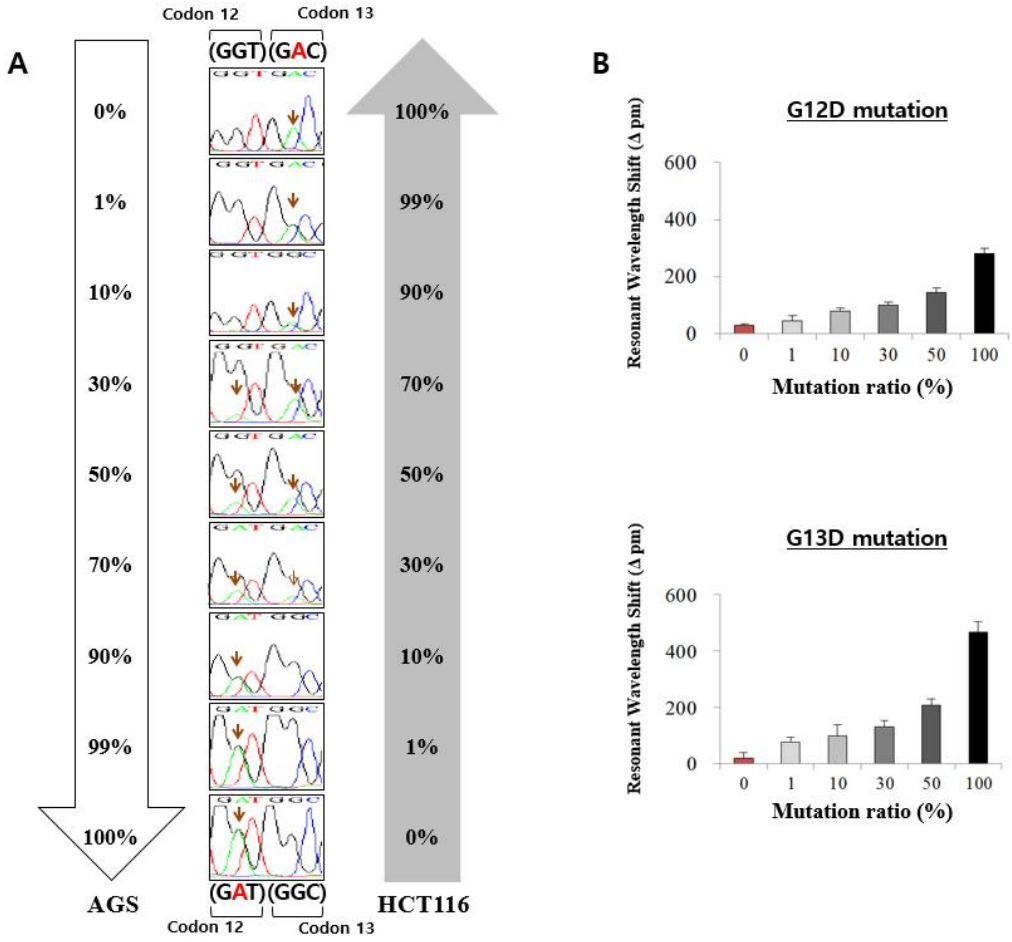

Figure 4.2. Analysis of the *KRAS* mutations with serially diluted mixed cells. The AGS cells (containing the G12D mutation) were diluted with HCT116 (containing the G13D mutation) cells. The percentages of the mutant cells were 0%, 1%, 10%, 30%, 50%, and 100%. (A) the results of direct sequencing, following the dilution of the AGS and HCT116 cell lines. (B) Shift in the resonant wavelength using the bio-optical sensor in the diluted mutation cells with either the G12D mutant primer (upper) or the G13D mutant primer (lower). The error bars indicate the standard deviation of the mean, based on at least 3 independent experiments.

4.3.2 Validation of the sensor for detecting pathogen

The clinical utility of the rapid virus diagnostic system was validated using 13 clinical samples, including 10 HAdV samples from patients as positives and three samples from patients with Q-fever, which is a zoonotic disease caused by *Corxiella burnatii* bacteria, as negatives. First, the viral DNA was extracted from the 10 samples using the DMS platform. Next, the viral DNA was used for analysis of the viral infection using the bio-optical sensor. According to the result of Fig. 4.3, the cut off for reporting a sample as HAdV (positive/negative) detected is a shift over 700 pm at 30 min. Based on this criterion, 10 HAdV and three non-HAdV specimens were identified within 1 h using the rapid virus diagnostics system. Our result was fully consistent with the result of qPCR (Fig 4.3).

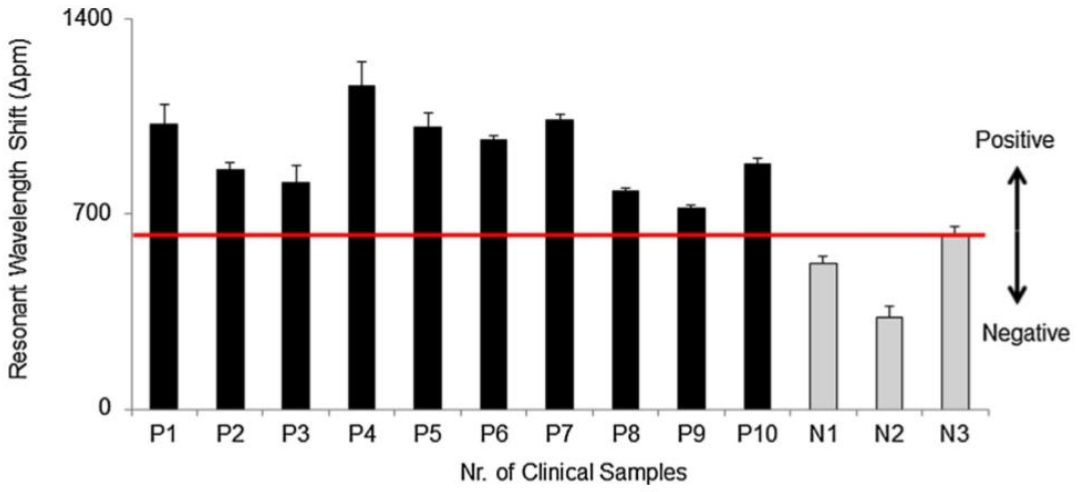

Figure 4.3. Clinical utility of the rapid virus diagnostic system for 13 clinical specimens. Analysis of 20 clinical nasopharyngeal samples from 10 human adenovirus (HAdVs) patients as targets (P1-P10, black) and three non-HAdVs patients as non-targets (N1-N3, gray) in 30 min. The red line represents the cut off (criterion) for reporting a sample as virus (positive/negative) detected. The error bars indicate the standard deviation from the mean, based on at least three independent experiments.

4.3.3 Validation of the sensor for detecting oncogenic mutation

To validate the clinical utility, as well as the rapidity and accuracy of the bio-optical sensor for detecting *KRAS* mutation using clinical samples, 70 frozen tissues samples from CRC patients in Bio-Resource Center (BRC) of Asan Medical Center were randomly selected. A total of 70 samples, including 24 samples with the G12D mutation (34.3%), 26 samples with the G13D mutation (37.1%), and 20 samples with no mutation (28.6%), were examined at the BRC and were used as reference. In these samples, the ability of the bio-optical sensor to diagnose specific mutations within 30 min was assessed, along with both the PCR and direct sequencing methods. When the PCR method was used for the 70 clinical samples, the G12D mutation was detected in 22 samples (31.4%) and the G13D mutation was detected in 25 samples (35.7%). When the direct sequencing method was used for the 70 clinical samples, the G12D mutation was detected in 21 samples (30%) and G13D mutation was detected in 22 samples (31.4%). Both methods are relatively less sensitive than the reference result from the BRC. Thereafter, the DNAs extracted from the 70 CRC samples were assessed via bio-optical sensor, by immobilizing either the G12D or G13D mutant primers on the optical sensors. When the G12D mutant primers were immobilized on the sensor, a resonant wavelength shift in the samples containing only the G12D mutation of > 600 pm was considered a positive result, whereas a resonant wavelength shift in the samples containing either no mutation or G13D mutation < 600 pm was considered a negative result. Similar to the G12D assay, when the G13D mutant primers were immobilized on the sensor, a resonant wavelength shift in the samples containing the G13D mutation of > 500 pm was considered as a positive result, whereas a resonant wavelength shift in the samples containing either no mutation or the G12D mutation of < 500 pm was considered as a negative result (Figure 4.4A).

When the bio-optical sensor was used for the 70 clinical samples, the G12D mutation was detected in 28 samples (40%) and the G13D mutation was detected in 27 samples (38.6%). The bio-optical sensor was superior in the detection of mutations in the clinical samples, as compared to the reference values. In particular, 2 samples (no. 26, and 62 containing the G12D mutation) and 2 samples (no. 11, and 33 containing the G13D mutation) were identified using bio-optical sensor and PCR. 2 samples (no. 24, and 32 containing the G12D mutation) and 1 sample (no. 59 containing the G13D mutation) were identified only using bio-optical sensor, however PCR and

sequencing could not identify the mutations in these samples as the number of mutant alleles within the samples may not have been sufficient. The genetic status of the *KRAS* mutations in the 70 CRC samples can be detected via PCR within 2-3 h, via sequencing within 1-2 days, and via the bio-optical sensor assay within 30 min. Using the CRC samples, I examined the clinical sensitivity and specificity of these methods for the detection of both the G12D and G13D mutations (Table 4.1). When the 70 clinical samples were used to assess the sensitivity and specificity of PCR, 22 (sensitivity, 91.6%) were found to be positive for the G12D mutation, in comparison with 24 samples identified at the BRC; moreover, 48 samples (specificity, 100%) were found to be negative for the G12D mutation. Furthermore, 25 samples (sensitivity, 96.2%) were found to be positive for the G13D mutation, in comparison with the 26 samples identified at the BRC; in addition, 45 samples (specificity, 100%) were found to be negative for the G13D mutation (Table 4.1). When 70 clinical samples were used to assess the sensitivity and specificity of direct sequencing, 21 samples (sensitivity, 87.5%) were found to be positive for the G12D mutation, in comparison with the 24 samples identified at the BRC; moreover, 49 samples (specificity, 100%) were found to be negative for the G12D mutation. In addition, 22 samples (sensitivity, 84.6%) were found to be positive for the G13D mutation, in comparison with the 26 samples identified at the BRC; moreover, 48 samples (specificity, 100%) were found to be negative for the G13D mutation (Table 4.1). In contrast, the bio-optical sensor showed a value of 100% for both the sensitivity and specificity with G12D and G13D mutations, when the 70 tumor specimens were examined (Table 4.1). In particular, when 70 CRC samples were assessed using bio-optical sensor, 5 cases (no. 13, 15, 18, and 68 for G12D and no. 5 for G13D) were found to have a mutation, which could not be detected by PCR and direct sequencing (Figure 4.4B). PCR and direct sequencing were unable to detect 3 and 7 samples containing *KRAS* mutations, respectively; the presence of *KRAS* mutations in these samples was confirmed by sequencing at the BRC. This may be due to the difference in the locations of the CRC samples from which DNA was extracted. This result is consistent with several studies that showed that the DNA from cancer samples isolated from different regions shows a change in the copy number, with very few discrepancies. Nevertheless, I could identify the *KRAS* mutations in these samples by using the bio-optical sensor. In particular, bio-optical sensor detected the mutations from 5 wild-type samples, including

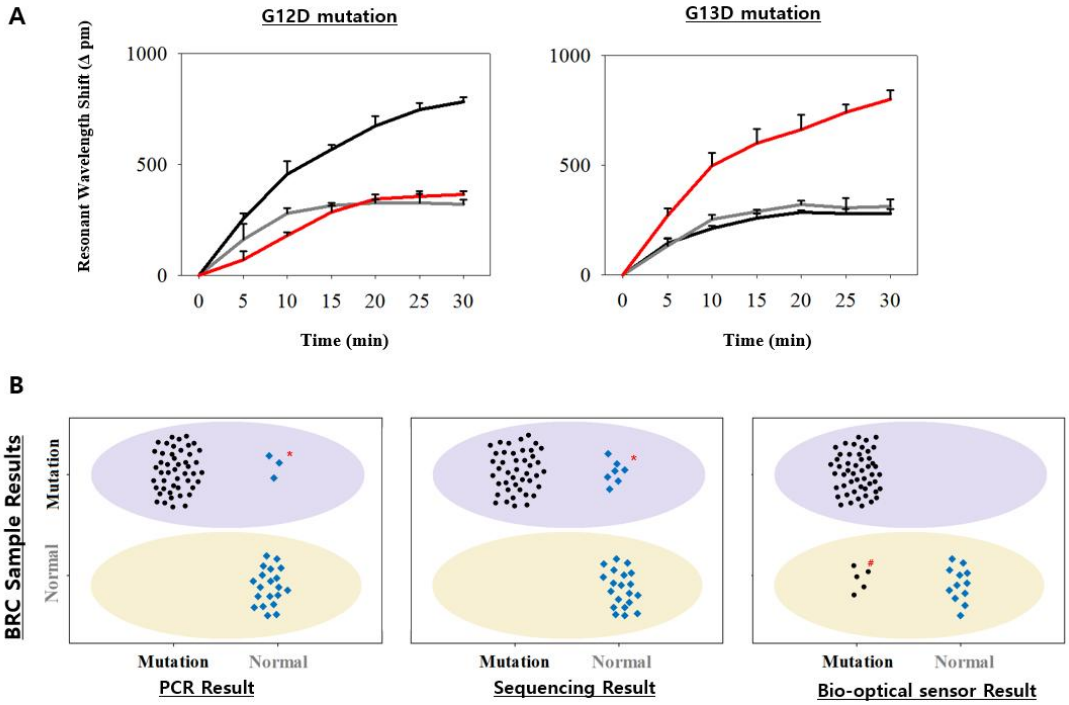

Figure 4.4 Validation of the bio-optical sensor in 70 clinical samples. (A) Representative wild and mutant cases from CRC sample. Resonant wavelength shift using the bio-optical sensor with either the G12D mutant primer (left) or the G13D mutant primer (right). The colors represent wild-type sample (gray), G12D mutant sample (black), and G13D mutant sample (red). The error bars indicate the standard deviation of the mean, based on at least 3 independent experiments. (B) 50 mutants and 20 wild-type samples were screened by PCR (left), sequencing (center), and bio-optical sensor (right). Based on the type of sample, as determined at the BRC, the light purple oval (mutant area) and yellow oval (wild-type area) areas were detected. The mutant allele (black) and wild allele (blue) are shown, based on the results of PCR, sequencing, and bio-optical sensor. *, # indicate mis-matched results for the sample types between the 3 detection methods

Table 4.1. Sensitivity and Specificity of PCR, direct sequencing and bio-optical sensor for *KRAS* mutation detection

Sample type	Positive sample					
	PCR result		Sequencing result		Bio-optical Result	
	Sensitivity	Specificity	Sensitivity	Specificity	Sensitivity	Specificity
G12D	91.6%	100%	87.5%	100%	100%	100%
G13D	96.2%	100%	84.6%	100%	100%	100%

Sensitivity: 100 X [TP/(TP+FN)], TP: true positive, FN: false negative

Specificity: 100 X [TN/(FP+TN)], TN: true negative, FP: false positive

4 samples with the G12D mutation and 1 sample with the G13D mutation (Fig. 4.4B, right); these mutations could not be detected using PCR and direct sequencing.

To confirm the bio-optical sensor results, I assessed several issues. First, the DNA from these samples were re-extracted to perform bio-optical sensor once more, using the new samples; however, the results obtained were similar. Second, the treatment history of the patient was assessed to confirm the response of the drug based on the *KRAS* mutation status. However, I could not predict the presence of mutations in the patients as they did not receive anti-EGFR drugs for their treatment. Although there is no other method for confirming the mutations identified by bio-optical sensor, I found that the performance of the bio-optical sensor assay in the present study is highly sensitive and specific. Thus the clinical sensitivity and specificity of the bio-optical sensor assay in clinical samples is superior to those of the conventional methods.

Furthermore, 11 plasma samples (frozen and long-term storage) of the CRC patients were tested whose tissue samples showed hot-spot mutations, as confirmed by the OncoPanel assay. The OncoPanel results of the tissue samples revealed a *BRAF* V600E mutation in one sample, *KRAS* G12D mutation in three samples, *KRAS* G12V mutations in two samples, and a *KRAS* G13D mutation in one sample. The cfDNAs obtained from 11 samples were isolated by the DTBP platform, and mutations were then analyzed using the Sanger sequencing or the bio-optical sensor (Figure 4.5B). Using the simple and low-cost ctDNA detection platform with Sanger sequencing, a *BRAF* V600E mutation was detected in one sample, a *KRAS* G12D mutation in two samples, a *KRAS* G12V mutation in one sample, and *KRAS* G13D mutations in two samples. This simple and low-cost method with Sanger sequencing yielded a 71.4% correlation in the mutation profiles of the tissues and frozen blood plasma samples obtained from 11 CRC patients (Figure 4.5A). In addition, using the simple and low-cost ctDNA detection platform with the bio-optical sensor, which has been reported in cancer tissues samples (136), one *BRAF* V600E mutation, three *KRAS* G12D mutations, one *KRAS* G12V mutation, and one *KRAS* G13D mutation were detected in the plasma samples (Figure 4.5B). The correlation of mutation profiling between the tissues and frozen blood plasma samples from 11 CRC patients using the platform with the bio-optical sensor was higher (85.7%) than that of the Sanger sequencing method (Figure 4.5A).

A

	Tissue	cfDNA (DTBP +Sanger)	cfDNA (DTBP+ Sensor)
Mutation	63.6% (7/11)	45.5% (5/11)	54.5% (6/11)
Correlation with Tissue	-	71.4% (5/7)	85.7% (6/7)

B

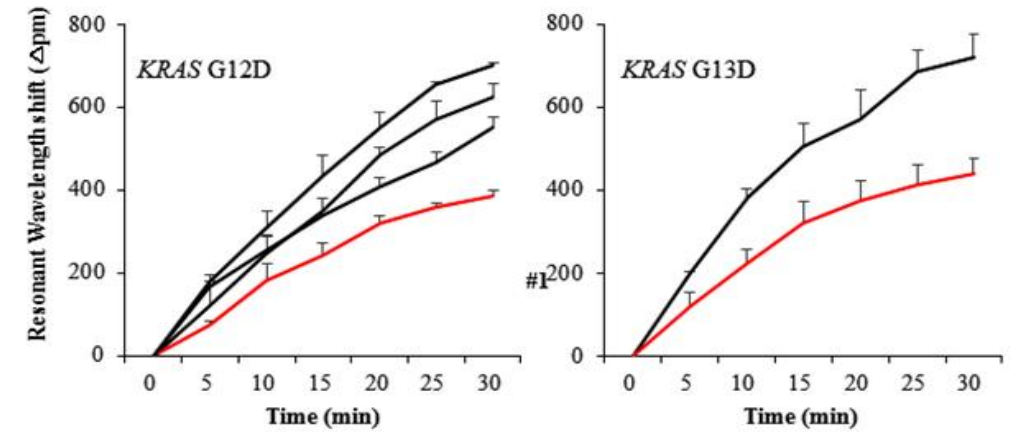

Figure 4.5. Validation of bio-optical sensor for detecting ctDNA. (A-B) ctDNA was isolated from 11 plasma samples of colorectal cancer patients using the DTBP platform, and followed by the use of the biosensor for ctDNA analysis. The correlation between the primary tissues (OncoPanel result) and blood plasma (with the Sanger sequencing and the biooptical sensor) (A) was analyzed. Resonant wavelength shift using the biooptical sensor with either the G12D (B-left) or the G13D mutant primers (B-right). The error bars indicate the standard deviation of the mean, based on at least three independent experiments

4.3.4 Integration of sample preparation platform and bio-optical sensor

Finally, as an alternative to qPCR, our rapid and accurate SLIM detection system was applied to proof-of concept testing at the point-of-care. The bio-optical sensor for simultaneous nucleic acid amplfication and detection was used. plasma DNA samples from 14 patients was tested with HZ as positives and 3 patients with human adenovirus (HAdV) as negatives to validate our combined SLIM and bio-optical sensor system. I again used 1mL of the plasma samples for VZV enrichment and viral DNA extraction (Fig. 4.6A). As shown in Fig. 4.6B-C, DNAs obtained via the SLIM system were simultaneously amplified and detected within 30 min in a label-free and real-time manner. Based on the HAdV negative samples, the cut-off line for detecting a VZV positive/negative sample was determined to be a shift of more than 380 p.m. at 30 min. Based on this criterion, I could identify VZV in 11 positive samples from 14 HZ samples within 80 min including the enrichment, extraction and detection steps. Although 3 samples deemed to be positive by previous saliva testing did not show a positive result, the detection sensitivity for HZ was significantly enhanced up to 78.6% on the SLIM system, indicating that plasma samples have utility for the diagnosis of HZ if using our combination system (Fig. 4.6).

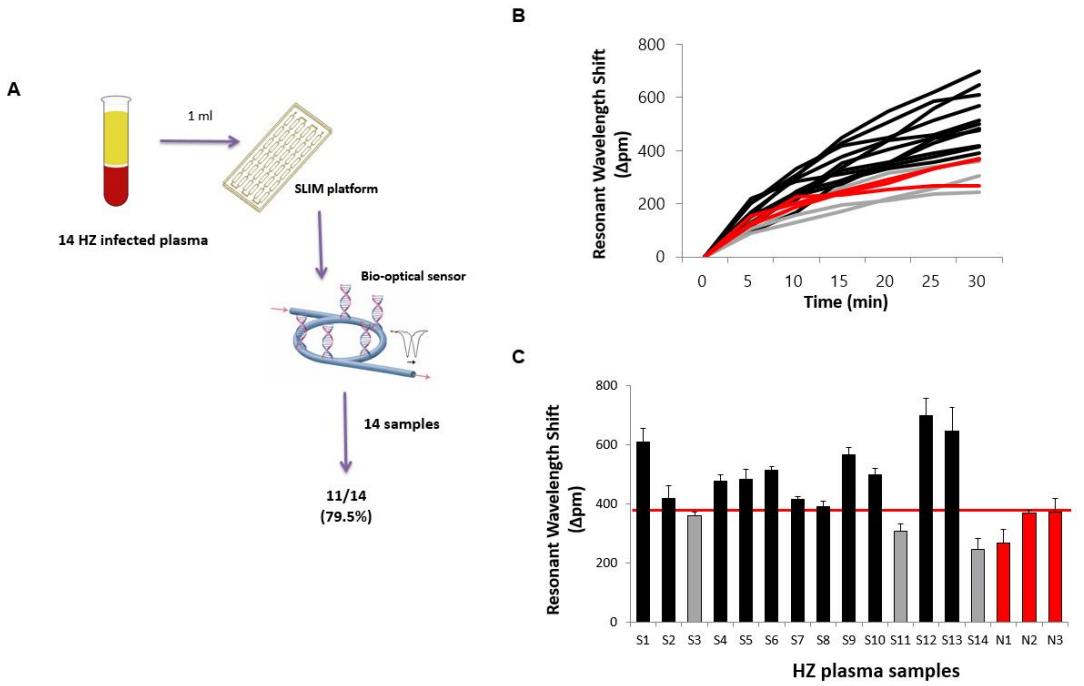

Figure 4.6. Clinical utility of the ultrasensitive pathogen diagnostic system integrated with the SLIM system and bio-optical sensor to test blood plasma samples from HZ patients. (A) Fourteen plasma samples from HZ infected patients were collected and enriched with the SLIM platform and detected by the bio-optical sensor. (B) Line graph showing the resonant wavelength shift results from sensor analysis of 17 blood plasma samples from HZ (n=14) and non-HZ (n=3) patients. The colors indicate HZ-positive (black) and HZ-negative (gray) samples from the 14 plasma samples, and 3 negative controls (red). (C) Clinical utility of the ultrasensitive pathogen diagnostic SLIM system in analyzing samples from 14 human HZ patients (S1-S14, black and gray) and 3 non-HZ patients (human adenovirus) (N1-N3, red) over a 30 min duration. The red line represents the cut-off (criterion) for reporting viral positivity. The error bars indicate the standard deviation from the mean, based on at least three independent experiments.

Chapter 5. Conclusions

Pathogenic diseases caused by both known and unknown bacteria and cancer can have devastating public health consequences. Various approaches have thus been introduced for rapid and sensitive disease diagnosis techniques to identify unknown pathogens or detect mutation. However, along with the advances in detection approaches, improved sample preparation techniques including enrichment and concentration are desired to process large volume clinical samples. For accurate diagnosis, sample preparation with high purity which can be applied to large volume of clinical samples is necessary. In this study, new simple platform for sample preparation which called SLIM assay was developed. This platform provides an innovative platform that combines HI reagents with a microfluidic device for pathogen enrichment and nucleic acid extraction. Using the HI reagents which bind with negatively charged molecules through an electrostatic interaction, pathogens that are negatively charged can be readily (>80%) captured from large volume samples. We demonstrated that our SLIM system significantly improved the detection sensitivity compared with real-time PCR by enabling pathogen enrichment and nucleic acid extraction on a single platform. To validate the clinical utility of the SLIM system, different types of clinical specimens were treated within 50 min, including environmental swabs, saliva, and blood plasma. Following enrichment and extraction with the SLIM system, the detection sensitivity of hPIV-3 samples was found to be 83.3% compared to 50% without using SLIM. In addition, the VZV detection sensitivity without SLIM in plasma samples was 35.7%, but increased to 57.1% using SLIM.

Moreover, microfluidic platform can be used for cfDNA isolation and cfDNA detection. Conventional cfNA-sampling technique is the high cost, slowness, low sensitivity, and complexity methods. To address these issues, we developed a DTBP platform for simple and low-cost cfNA isolation. This procedure only took 15 min without the use of chaotropic reagents, which lead to cfNA damage and increased cellular DNA background. In addition, the DTBP platform did not require bulky instruments for isolation. The hot-spot mutations were detected in the plasma by the DTBP platform, with >71% correlation between the tissues and frozen plasma samples obtained from the CRC patients.

Finally, the bio-optical sensor based SMR sensor was integrated sample preparation or ctDNA detection. It can simultaneously amplify and detect NA

which enables the diagnosis of infectious diseases or cancer within 30 min. The sensitivity of bio-optical sensor is 10-100 times higher than conventional PCR methods. The bio-optical sensor was validated with various clinical samples for detecting pathogens or mutation.

Despite the advantages of this proof-of-concept platform, clinical trials with additional clinical samples from patients with various cancers (e.g., colorectal, breast, and lung) and disease would be needed to further establish the clinical utility of cfNAs and enriched pathogen. To achieve this, technical advances, including sampling and detection methods, should be standardized for introduction into large-scale clinical trials. Further study for the validation of the real chemical reaction between HI and pathogens as well as further development of this process for use with various types of clinical samples will be needed. In addition, enhanced understanding regarding the use of cfNA as a biomarker in the diagnosis and treatment of cancers would be needed. Nevertheless, by combining it with cutting-edge detection techniques, this simple and low-cost sampling of cfNA and pathogen preparation platform could be useful for the clinical diagnosis and monitoring of disease treatment. I believe that an integrated diagnosis system (Table 5.1) such as this has considerable potential a POC based diagnostic system that could have diverse clinical applications in humans and also in animal healthcare and useful for the clinical diagnosis and monitoring of cancer treatment.

Table 5.1. Overview of rapid diagnosis system

Purpose	Assay	Sample	Time	Process
NA extraction	Microfluidic platform + HI (SLIM assay)	Bacteria, Virus, Clinical samples	30 min	Sample mixing → Incubation(RT) → lysis buffer → Incubation(56 ℃) → Washing → Elution
cfDNA isolation		Plasma	15 min	Sample mixing → Incubation(RT) → Washing → Elution
Pathogen enrichment		Bacteria, Virus, Clinical samples	50 min	Sample mixing → Incubation(56 ℃) → Washing → Elution
NA detection	Bio-optical Sensor	Extracted NA	20 min	Sample preparation → Laser alignment → Measure(38 ℃)

REFERENCES

(1) Azem A, Tsfadia Y, Hajouj O, Shaked I, Daniel E, Biochimica et Biophysica Acta. Cross-linking with bifunctional reagents and its application to the study of the molecular symmetry and the arrangement of subunits in hexameric protein oligomers. BBA-Proteins Proteom 2010;1804:768-780

(2) Dodson MS. Dimethyl suberimidate cross-linking of oligo (dt) to DNA-binding proteins. Bioconjugate Chem 2000;11:876-879.

(3) Charulatha V, & Rajaram A. Crosslinking density and resorption of dimethyl suberimidate-treated collagen. J Biomed Mater Res 1997;36:478-486.

(4) Shin Y, Lim SY, Lee TY, Park MK. Dimethyl adipimidate/Thin film Sample processing (DTS); A simple, low-cost, and versatile nucleic acid extraction assay for downstream analysis. Sci Rep 2005;5:14127.

(5) Jin CE, Lee TY, Koo B, Choi KC, Chang S, Park SY, et al. Use of Dimethyl Pimelimidate with Microfluidic System for Nucleic Acids Extraction without Electricity. Anal Chem 2017;89:7502-7510.

(6) Jin CE, Lee TY, Koo B, Sung H, Kim SH, Shin Y. Rapid virus diagnostic system using bio-optical sensor and microfluidic sample processing. Sens Actuat B: Chem 2018;255:2399-2406.

(7) Ashraf S, Huque MH, Kenah E, Agboatwalla M, Luby SP. Effect of recent diarrhoeal episodes on risk of pneumonia in children under the age of 5 years in Karachi, Pakistan. Int J Epidemiol 2013;42:194-200.

(8) Chappuis F, Alirol E, d'Acremont V, Bottieau E, Yansouni CP. Rapid diagnostic tests for non-malarial febrile illness in the tropics. Clin Microbiol Infec 2013;19:422-431.

(9) Khanam F, Sheikh A, Sayeed MA, Bhuiyan MS, Choudhury FK, Salma U, et al. Evaluation of a typhoid/paratyphoid diagnostic assay (TPTest) detecting anti-Salmonella IgA in secretions of peripheral blood lymphocytes in patients in Dhaka, Bangladesh. PLoS Neglect Trop D 2013;7:e2316.

(10) Jin CE, Koo B, Lee EY, Kim JY, Kim SH, Shin Y. Simple and label-free pathogen enrichment via homobifunctional imidoesters using a microfluidic (SLIM) system for ultrasensitive pathogen detection in various clinical specimens. Biosens Bioelectron 2018;111:66-73.

(11) Mardis ER. Next-generation DNA sequencing methods. Annu Rev Genomics Hum Genet 20018;9:387-402.

(12) Huppert J, Hesse E, Gaydos CA. What's the point? How point-of-care STI tests can impact infected patients. Point of care 2010;9:36.

(13) World Health Organization. From Bench to Bedside: Setting a path for the translation of improved sexually transmitted infections diagnostics into health care delivery in the developing world Sexually transmitted diseases diagnostics initiative 2001. 2009;www.who.int/std_diagnostics/about_SDI/priorities.htm.

(14) Diaz Jr, LA, & Bardelli A. Liquid biopsies: genotyping circulating tumor DNA. J Clin Oncol 2014;32:579.

(15) Schwarzenbach H, Hoon DS, Pantel K. Cell-free nucleic acids as biomarkers in cancer patients. Nat Rev Cancer 2011;11:426.

(16) Wan JC, Massie C, Garcia-Corbacho J, Mouliere F, Brenton JD, Caldas C, et al. Liquid biopsies come of age: towards implementation of circulating tumour DNA. Nat Rev Cancer, 2017;17:223.

(17) Cohen JD, Li L, Wang Y, Thoburn C, Afsari B, Danilova L, et al. Detection and localization of surgically resectable cancers with a multi-analyte blood test. Science, 2018;359:926-930.

(18) Gerlinger M, Rowan AJ, Horswell S, Larkin J, Endesfelder D, Gronroos E, et al. Intratumor heterogeneity and branched evolution revealed by multiregion sequencing. New Engl J Med 2012;366:883-892.

(19) Oltedal S, Aasprong OG, Møller JH, Kørner H, Gilje B, Tjensvoll K, et al. Heterogeneous distribution of K-ras mutations in primary colon carcinomas: implications for EGFR-directed therapy. Int J Colorectal Dis, 2011;26:1271-1277.

(20) Kim MJ, Lee HS, Kim JH, Kim YJ, Kwon JH, Lee JO, et al. Different metastatic pattern according to the KRAS mutational status and

site-specific discordance of KRAS status in patients with colorectal cancer. BMC cancer 2012;12:347.

(21) Dienstmann R, Vermeulen L, Guinney J, Kopetz S, Tejpar S, et al. Consensus molecular subtypes and the evolution of precision medicine in colorectal cancer. Nat Rev Cancer 2017;17:79.

(22) Siravegna G, Marsoni S, Siena S, Bardelli A. Integrating liquid biopsies into the management of cancer. Nat Rev Clin Oncol 2017;14:531.

(23) Thierry AR, Mouliere F, El Messaoudi S, Mollevi C, Lopez-Crapez E, Rolet F, et al. Multiplexed ion beam imaging of human breast tumors. Nat Med 2014;436-445.

(24) Diehl F, Schmidt K, Choti MA, Romans K, Goodman S, Li M, et al. Circulating mutant DNA to assess tumor dynamics. Nat Md 2008;14:985.

(25) Newman AM, Bratman SV, To J, Wynne JF, Eclov NC, Modlin LA, et al. An ultrasensitive method for quantitating circulating tumor DNA with broad patient coverage. Nat Med 2014;20:548.

(26) Shin Y, Perera AP, Kim KW, Park MK. Real-time, label-free isothermal solid-phase amplification/detection (ISAD) device for rapid detection of genetic alteration in cancers. Lab Chip 2013;13:2106-2114.

(27) Koo B, Jin CE, Lee TY, Lee JH, Park MK, Sung H, et al. An isothermal, label-free, and rapid one-step RNA amplification/detection assay for diagnosis of respiratory viral infections. Biosens Bioelectron 2017;90:187-194.

(28) Koo B, Jin CE, Park SY, Lee TY, Nam J, Jang YR, et al. A rapid bio-optical sensor for diagnosing Q fever in clinical specimens. J biophotonics 2018;11:e201700167.

(29) Shin Y, Perera AP, Wong CC, Park MK. Solid phase nucleic acid extraction technique in a microfluidic chip using a novel non-chaotropic agent: dimethyl adipimidate. Lab Chip 2014;14:359-368.

(30) Compton J. Nucleic acid sequence-based amplification. Nature, 1991;350:91.

(31) Notomi T, Okayama H, Masubuchi H, Yonekawa T, Watanabe K, Amino

N, et al. Loop-mediated isothermal amplification of DNA. Nucleic acids Res, 2000;28:e63-e63.

(32) Lizardi PM, Huang X, Zhu Z, Bray-Ward P, Thomas DC, Ward DC. Mutation detection and single-molecule counting using isothermal rolling-circle amplification. Nat Genet, 1998;19:225.

(33) Vincent M, Xu Y, Kong H. Helicase-dependent isothermal DNA amplification. EMBO Rep, 2004;5:795-800.

(34) Piepenburg O, Williams CH, Stemple DL, Armes NA. DNA detection using recombination proteins. PLoS Biol, 2006;4:e204.

(35) Shibata T, Cunningham RP, DasGupta C, Radding CM. Homologous pairing in genetic recombination: complexes of recA protein and DNA. P Nat Acad Sci 1979;76:5100-5104.

(36) M. Euler, Y. Wang, O. Nentwich, O. Piepenburg, F. T. Hufert and M. Weidmann, J. Clin. Virol., 2012, 54 , 308-312.

(37) Euler M, Wang Y, Nentwich O, Piepenburg O, Hufert FT, Weidmann M. Recombinase polymerase amplification assay for rapid detection of Rift Valley fever virus. J Clin Virol 2012;54:308-312.

(38) Lutz S, Weber P, Focke M, Faltin B, Hoffmann J, Müller C, et al. Microfluidic lab-on-a-foil for nucleic acid analysis based on isothermal recombinase polymerase amplification (RPA). Lab Chip 2010;10:887-893.

(39) Shen F, Davydova EK, Du W, Kreutz JE, Piepenburg O, Ismagilov RF. Digital isothermal quantification of nucleic acids via simultaneous chemical initiation of recombinase polymerase amplification reactions on SlipChip. Anal Chem 2011;83:3533-3540.

(40) Kim JY, Koo B, Jin CE, Kim MC, Chong YP, Lee SO, et al. Rapid Diagnosis of Tick-Borne Illnesses by Use of One-Step Isothermal Nucleic Acid Amplification and Bio-Optical Sensor Detection. Clin Chem 2018;64:556-565.

(41) Katsanis SH & Katsanis N. Molecular genetic testing and the future of clinical genomics. Nat Rev Genet 2013;14:415-426.

(42) Hanash SM, Baik CS, Kallioniemi O. Emerging molecular biomarkers—

blood-based strategies to detect and monitor cancer. Nat Rev Clin Oncol 2011;8:142-150.

(43) Guttmacher AE, McGuire AL, Ponder B, Stefánsson K. Personalized genomic information: preparing for the future of genetic medicine. Nat Rev Genet 2010;11:161-165.

(44) Kumar AA, Hennek JW, Smith BS, Kumar S, Beattie P, Jain S, et al. From the bench to the field in low-cost diagnostics: two case studies. Angew Chem Int Ed 2015;54:5836-5853.

(45) Cui F, Rhee M, Singh A, Tripathi A. Microfluidic sample preparation for medical diagnostics. Annu Rev Biomed Eng 2015;17:267-286.

(46) Rodriguez NM, Linnes JC, Fan A, Ellenson CK, Pollock, NR, Klapperich CM. based RNA extraction, in situ isothermal amplification, and lateral flow detection for low-cost, rapid diagnosis of influenza A (H1N1) from clinical specimens. Anal Chem 2015;87:7872-7879.

(47) Lounsbury JA, Karlsson A, Miranian DC, Cronk SM, Nelson DA, Li J, at al. From sample to PCR product in under 45 minutes: a polymeric integrated microdevice for clinical and forensic DNA analysis. Lab Chip 2013;13:1384-1393.

(48) Mao C, Liu A, Cao B. Virus-based chemical and biological sensing. Angew Chem Int Ed 2009;48:6790-6810.

(49) Qavi AJ & Bailey RC. Multiplexed detection and label-free quantitation of MicroRNAs using arrays of silicon photonic microring resonators. Angew Chem Int Ed 2010;49:4608-4611.

(50) Budin G, Chung HJ, Lee H, Weissleder R. A magnetic Gram stain for bacterial detection. Angew Chem Int Ed 2012;51:7752-7755.

(51) Pasche B, & Absher D. Whole-genome sequencing: a step closer to personalized medicine. JAMA. 2011;305:1596-1597.

(52) Shin Y, Perera AP, Kim KW, Park MK. Real-time, label-free isothermal solid-phase amplification/detection (ISAD) device for rapid detection of genetic alteration in cancers. Lab Chip 2013;13:2013-2114.

(53) Shin Y, Perera AP, Tang WY, Fu DL, Liu Q, Sheng JK, at al. A rapid

amplification/detection assay for analysis of Mycobacterium tuberculosis using an isothermal and silicon bio-photonic sensor complex. Biosens Bioelectron 2015;68:390-396.

(54) Reinholt SJ, & Baeumner AJ. Microfluidic isolation of nucleic acids. Angew. Chem. Int. Ed.. 2014;53:13988-14001.

(55) Thatcher SA. DNA/RNA preparation for molecular detection. Clin Chem 2015;61:89-99.

(56) Jiang W, Liang P, Wang B, Fang J, Lang J, Tian G, at al. Optimized DNA extraction and metagenomic sequencing of airborne microbial communities. Nat Protoc 2015;10:768-779.

(57) Hirama T, Mogi H, Egashira H, Yamamoto E, Kukisaki S, Hagiwara K, at al. A pressure-driven column-based technique for the efficient extraction of DNA from respiratory samples. Clin Chim Acta. 2015;445:122-126.

(58) Rahman MM & Elaissari A. Nucleic acid sample preparation for in vitro molecular diagnosis: from conventional techniques to biotechnology. Drug Discov Today. 2012;17:1199-1207.

(59) Gormally E, Caboux E, Vineis P, Hainaut P. Circulating free DNA in plasma or serum as biomarker of carcinogenesis: practical aspects and biological significance. Mutat Res 2007;635:105-117.

(60) Juliano RL, Ming X, Nakagawa O. The chemistry and biology of oligonucleotide conjugates. Acc Chem Res 2012;45:1067-1076.

(61) Hofreiter M, Serre D, Poinar HN, Kuch M, Pääbo S. ancient DNA. Nat Rev Genet 2001;2:353-359.

(62) Bull AT, Ward AC, Goodfellow M. Search and discovery strategies for biotechnology: the paradigm shift. Microbiol Mol Biol Rev 2000;64:573-606.

(63) Sambrook J, & Russell DW. Purification of nucleic acids by extraction with phenol: chloroform. Cold Spring Harbor Protocols. 2006;10.1101/pdb.prot4455.

(64) Clark KD, Nacham O, Yu H, Li T, Yamsek MM, Ronning DR, at al.

Extraction of DNA by magnetic ionic liquids: tunable solvents for rapid and selective DNA analysis. Anal Chem 2015:87:1552-1559.

(65) M Carpi F, Di Pietro F, Vincenzetti S, Mignini F, Napolioni V. Human DNA extraction methods: patents and applications. Recent patents on DNA & gene sequences. 2011;5:1-7.

(66) Lehmann U, Vandevyver C, Parashar VK, Gijs MA. Droplet-based DNA purification in a magnetic lab-on-a-chip. Angew Chem Int Ed 2006;45:3062-3067.

(67) Reedy CR, Price CW, Sniegowski J, Ferrance JP, Begley M, Landers JP. Solid phase extraction of DNA from biological samples in a post-based, high surface area poly (methyl methacrylate)(PMMA) microdevice. Lab Chip 2011;11:1603-1611.

(68) Melzak KA, Sherwood CS, Turner RF, Haynes CA. Driving forces for DNA adsorption to silica in perchlorate solutions. J. Colloid. And Interface Sci 1996;181:635-644.

(69) Bienvenue JM, Legendre LA, Ferrance JP, Landers JP. An integrated microfluidic device for DNA purification and PCR amplification of STR fragments. Forensic Sci Int Genet 2010;4:178-186.

(70) Langton MJ, Serpell CJ, Beer PD. Anion recognition in water: recent advances from a supramolecular and macromolecular perspective. Angew Chem Int Ed 2016;55:1974-1987.

(71) Schrader C, Schielke A, Ellerbroek L, Johne R. PCR inhibitors-occurrence, properties and removal. J Appl Microbiol 2012;113:1014-1026.

(72) Al-Soud WA, & Rådström P. Effects of amplification facilitators on diagnostic PCR in the presence of blood, feces, and meat. J Clin Microbiol 2000;38:4463-4470.

(73) Hagan KA, Meier WL, Ferrance JP, Landers JP. Chitosan-coated silica as a solid phase for RNA purification in a microfluidic device. Anal Chem 2009;81:5249-5256.

(74) Cao W, Easley CJ, Ferrance JP, Landers JP. Chitosan as a polymer for pH-induced DNA capture in a totally aqueous system. Anal Chem 2006;78:7222-7228.

(75) Jiang C, Xu S, Zhang S, Jia L. Chitosan functionalized magnetic particle-assisted detection of genetically modified soybeans based on polymerase chain reaction and capillary electrophoresis. Anal Biochem 2012;420:20-25.

(76) Rodriguez NM, Wong WS, Liu L, Dewar R, Klapperich CM. A fully integrated paperfluidic molecular diagnostic chip for the extraction, amplification, and detection of nucleic acids from clinical samples. Lab Chip 2016;16:753-763.

(77) Zhuang B, Gan W, Wang S, Han J, Xiang G, Li CX, at al. Fully automated sample preparation microsystem for genetic testing of hereditary hearing loss using two-color multiplex allele-specific PCR. Anal Chem 2014;87:1202-1209.

(78) Mark D, Haeberle S, Roth G, Von Stetten F, Zengerle R. From microfluidic application to nanofluidic phenomena issue. Chem. Soc. Rev. 2010;39:1153-1182.

(79) Hagan KA, Reedy CR, Uchimoto ML, Basu D, Engel DA, Landers JP. An integrated, valveless system for microfluidic purification and reverse transcription-PCR amplification of RNA for detection of infectious agents. Lab Chip 2011;11:957-961.

(80) Zare RN & Kim S. Microfluidic platforms for single-cell analysis. Annu Rev Biomed Eng 2010;12:187-201.

(81) Heineck DP, Lewis JM, Heller MJ. Electrokinetic device design and constraints for use in high conductance solutions. Electrophoresis. 2017;38:1475-1482.

(82) Kidess E, Heirich K, Wiggin M, Vysotskaia V, Visser BC, Marziali A, at al. Mutation profiling of tumor DNA from plasma and tumor tissue of colorectal cancer patients with a novel, high-sensitivity multiplexed mutation detection platform. Oncotarget. 2015;6:2549.

(83) Schmittgen TD, & Zakrajsek BA. Effect of experimental treatment on housekeeping gene expression: validation by real-time, quantitative RT-PCR. J Biochem Bioph Meth 2000;46:69-81.

(84) Jain M, Nijhawan A, Tyagi AK, Khurana JP. Validation of housekeeping

genes as internal control for studying gene expression in rice by quantitative real-time PCR. Biochem Bioph Res Comm 2006;345:646-651.

(85) Kim JW, Botvinnik OB, Abudayyeh O, Birger C, Rosenbluh J, Shrestha Y, at al. Characterizing genomic alterations in cancer by complementary functional associations. Nat Biotechnol 2016;34:539-546.

(86) Thierry AR, Mouliere F, El Messaoudi S, Mollevi C, Lopez-Crapez E, Rolet F, at al. Clinical validation of the detection of *KRAS* and *BRAF* mutations from circulating tumor DNA. Nat Med 2014;20:430-435.

(87) Kim WY, Choi W, Park SW, Wang EB, Lee WJ, Jee Y, at al. Nosocomial transmission of severe fever with thrombocytopenia syndrome in Korea. Clin Infec Dis. 2015;60:1681-1683.

(88) Fanning TG, Traut RR. Topography of the *E. coli* 5S RNA-protein complex as determined by crosslinking with dimethyl suberimidate and dimethyl-3, 3′-dithiobispropionimidate. Nucleic Acids Res 1981;9:993-1004.

(89) Jin CE, Koo B, Lee TY, Han K, Lim SB, Park IJ, et al. Simple and Low-Cost Sampling of Cell-Free Nucleic Acids from Blood Plasma for Rapid and Sensitive Detection of Circulating Tumor DNA. Adv Sci 2018;5:1800614.

(90) Wan JCM, Massie C, Garcia-Corbacho J, Mouliere F, Brenton JD, Caldas C, at al. Liquid biopsies come of age: towards implementation of circulating tumour DNA. Nat Rev Cancer 2017;17:223.

(91) Park G, Park JK, Shin SH, Jeon HJ, Kim NK, Kim YJ, at al. Characterization of background noise in capture-based targeted sequencing data. Genome Biol 2017;18:136.

(92) Schwarzenbach H, Hoon DS, Pantel K. Cell-free nucleic acids as biomarkers in cancer patients. Nat Rev Cancer 2011;11:426.

(93) Umetani N, Giuliano AE, Hiramatsu SH, Amersi F, Nakagawa T, Martino S, at al. Prediction of breast tumor progression by integrity of free circulating DNA in serum. J Clin Oncol 2006;24:4270-4276.

(94) Grasselli J, Elez E, Caratù G, Matito J, Santos C, Macarulla T, at al. Concordance of blood-and tumor-based detection of RAS mutations to

guide anti-EGFR therapy in metastatic colorectal cancer. Annal Oncol 2017;28:1294-1301.

(95) Strickler JH, Loree JM, Ahronian LG, Parikh AR, Niedzwiecki D, Pereira AAL, at al. Genomic landscape of cell-free DNA in patients with colorectal cancer. Cancer Discov 2018;8:164-173

(96) Ahn SM, Ansari AA, Kim J, Kim D, Chun SM, Kim J, at al. The somatic POLE P286R mutation defines a unique subclass of colorectal cancer featuring hypermutation, representing a potential genomic biomarker for immunotherapy. Oncotarget. 2016;7:68638.

(97) Fauci AS, & Morens DM. The perpetual challenge of infectious diseases. N Engl J Med 2012;366:454-461.

(98) Pennington H. Politics, media and microbiologists. Nat Rev Microbiol 2014;2:259-262.

(99) Marra MA, Jones SJM, Astell CR, Holt RA, Brooks-Wilson A, Butterfiel YSN, et al. The genome sequence of the SARS-associated coronavirus. Science 2003;300:1399-1404.

(100) Park WB, Perera RAPM, Choe PG, Lau EHY, Choi SJ, Chun JY, et al. Kinetics of serologic responses to MERS coronavirus infection in humans, South Korea. Emerg Infect Dis 2015;21:2186.

(101) Peiris JSM, Guan Y, Yuen KY. Severe acute respiratory syndrome. Nat med 2004;10:S88.

(102) Xu R, Ekiert DC, Krause JC, Hai R, Crowe JE, Wilson IA. Structural basis of preexisting immunity to the 2009 H1N1 pandemic influenza virus. Science 2010;328:357-360.

(103) Hanash SM, Baik CS, Kallioniemi O. Emerging molecular biomarkers—blood-based strategies to detect and monitor cancer. Nat Rev Clin Oncol 2011;8:142-150.

(104) Fricke WF, & Rasko DA. Bacterial genome sequencing in the clinic: bioinformatics challenges and solutions. Nat Rev Genet 2014;15:49-55.

(105) Gardy JL, & Loman NJ. Towards a genomics-informed, real-time, global pathogen surveillance system. Nat Rev Genet 2018;19:9-20.

(106) Mardis ER. Next-generation DNA sequencing methods. Annu Rev Genomics Hum Genet 2008;9:387-402.

(107) Rosseel T, Ozhelvaci O, Freimanis G, Borm SV. Evaluation of convenient pretreatment protocols for RNA virus metagenomics in serum and tissue samples. J Virol Methods 2015;222:72-80.

(108) Yeh YY, Nisic M, Yu X, Xia Y, Zheng SY. Point-of-care microdevices for blood plasma analysis in viral infectious diseases. Ann Biomed Eng 2014;42:2333-2343.

(109) de Mello AJ, & Beard N. Focus. Dealing with 'real' samples: sample pre-treatment in microfluidic systems. Lab Chip 2003;3:11N-20N.

(110) Ganesh I, Tran BM, Kim Y, Kim J, Cheng H, Lee NY, et al. An integrated microfluidic PCR system with immunomagnetic nanoparticles for the detection of bacterial pathogens. Biomed Microdevices 2016;18:116.

(111) Duncan AW, Maggi RG, Breitschwerdt EB. A combined approach for the enhanced detection and isolation of Bartonella species in dog blood samples: pre-enrichment liquid culture followed by PCR and subculture onto agar plates. J microbial Methods 2007;69:273-281.

(112) Mannoor MS, Zhang S, Link AJ, McAlpine MC. Electrical detection of pathogenic bacteria via immobilized antimicrobial peptides. Proc Natl Acad Sci 2010;107:19207-19212.

(113) Pérez FG, Mascini M, Tothill IE, Turner AP, Immunomagnetic separation with mediated flow injection analysis amperometric detection of viable Escherichia coli O157. Anal Chem 1998;70:2380-2386.

(114) Lien KY, Lin JL, Liu CY, Lei HY, Lee GB. Purification and enrichment of virus samples utilizing magnetic beads on a microfluidic system. Lab Chip 2007;7:868-875.

(115) Kim T, Jin CE, Koo B, Park J, Kim SM, Kim JY, et al. Molecular epidemiology and environmental contamination during an outbreak of parainfluenza virus 3 in a hematology ward. J Hosp Infec 2017;97:403-413.

(116) Park SY, Kim JY, Kim JA, Kwon J, Kim SM, Jeon NY, et al.

Diagnostic usefulness of varicella-zoster virus real-time polymerase chain reaction analysis of DNA in saliva and plasma specimens from patients with herpes zoster. J Infec Dis 2017; http://dx.doi.org/10.1093/infdis/jix508/4237571.

(117) Granger DA, Kivlighan KT, Fortunato C, Harmon AG, Hibel LC, Schwartz EB et al. Integration of salivary biomarkers into developmental and behaviorally-oriented research: problems and solutions for collecting specimens. Physiol Behav 2007;92:583-590.

(118) Jin XH, Ishii A, Aoki K, Ishida S, Mukasa K, Ohno S. Detection of human adenovirus hexon antigen using carbon nanotube sensors. J Virol Method 2011;171:405-407

(119) Zhang Y, Ozdemir P. Microfluidic DNA amplification-a review. Anal Chim Acta 2009;638:115-125

(120) Patolsky F, Zheng G, Hayden O, Lakadamyali M, Zhuang X. Electrical detection of single viruses Proc. Natl Acad Sci U.S.A. 2004;101:14017-14022

(121) Abadian PN, Yildirim N, Gu AZ, Goluch ED. SPRi-based adenovirus detection using a surrogate antibody method. Biosens Bioelectron 2015;74:808-814

(122) Krejcova L, Michalek P, Rodrigo MM, Heger Z, Krizkova S, Vaculovicova M, et al. Nanoscale virus biosensors: state of the art. Nanobiosensors in Dis Diagnosis 2015;4:47-66

(123) Ozcelik D, Parks JW, Wall TA, Stott MA, Cai H, Parks JW, et al. Optofluidic wavelength division multiplexing for single-virus detection. Proc Natl Acad Sci U.S.A. 2015;112:12933-12937

(124) Song MJ, & Jin JH. Label-free electrochemical detection of the human adenovirus 40/41 fiber gene. Anal Sci 2015;31:159-163

(125) Yang L, & Yamamoto T. Quantification of virus paricles using nanopore-based resistive-pulse sensing techniques. Front Microbiol 2016;7:1-7

(126) Yoo SM, & Lee SY. Optical biosensors for the detection of pathogenic microorganisms. Trends Biotechnol 2016;34:7-25

(127) Borisov SM, & Wolfbeis OS. Optical biosensors. Chem Rev 2008;108:423-461

(128) Iqbal M, Gleeson MA, Spaugh B, Tybor F, Gunn WG, Hochberg M, et al. Label-free biosensor arrays based on silicon ring resonators and high-speed optical scanning instrumentation, IEEE. J SelTop Quantum Electron 2010;16:654-661

(129) Shin Y, Perera AP, Kee JS, Song J, Fang Q, Lo GQ, et al. Label-free methylation specific sensor based on silicon resonators for detection and quantification of DNA methylation biomarkers in bladder cancer. Sens Actuat B: Chem 2013;177:404-411

(130) Shin Y, Perera AP, Tang WY, Fu DL, Liu Q, Sheng JK, et al. A rapid amplification/detection assay for analysis of mycobacterium tuberculosis using an isothermal and silicon bio-photonic sensors complex. Biosens Bioelectron 2015;68:390-396

(131) Lee WC, Lien KY, Lee GB, Lei HY. An integrated microfluidic system using magnetic beads for virus detection. Diagn Microbiol Infect Dis 2008;60:51-58

(132) Mairhofer J, Roppert K, Ertl P. Microfluidic systems for pathogen sensing: a review. Sensors 2009;9:4804-4823

(133) Hosseini S, Aeinehvand MM, Uddin SM, Benzina A, Rothan HA, Yusof R, et al. Microsphere integrated microfluidic disk: synergy of two techniques for rapid and ultrasensitive dengue detection. Sci Rep 2015;5:16485

(134) Zhang Z, Kermekchiev MB, Barnes WM. Direct DNA amplification from crude clinical samples using a PCR enhancer cocktail and novel mutants of Taq. J Mol Diagn 2010;12:152-161.

(135) Schrader C, Schielke A, Ellerbroek L, Johne R. PCR inhibitors-occurrence, properties and removal. J appl microbiol 2012;113:1014-1026.

(136) Jin CE, Yeom SS, Koo B, Lee TY, Lee JH, Shin Y, et al. Rapid and accurate detection of KRAS mutations in colorectal cancers using the isothermal-based optical sensor for companion diagnostics. Oncotarget, 2017;8:83860.

국문 요약

연구 목적

질병의 빠른 대처와 치료를 위해서는 무엇보다도 질병의 원인을 정확하고 신속하게 진단하는 것이 매우 중요하다. 특히 신,변종 감염병과 암은 높은 사망원인을 차지하고 있을 뿐만이 아니라, 원인이 되는 병원균 또는 돌연변이의 존재 여부에 따라서 치료방법이 달라지기 때문에 정확한 진단이 요구된다. 현재 알려진 진단 방법들은 임상적으로 적용하는데 있어 민감도와 특이도가 낮거나, 많은 시간과 비용을 요구된다. 또한 신, 변종 감염병의 경우 현장에서의 신속한 진단이 필요하지만, 현재의 진단 방법은 복잡한 장비와 기술이 요구된다는 문제를 가지고 있다. 이를 보완하기 위해 미세유체 플랫폼 기반의 샘플 전처리 기술과 실리콘 마이크로링 공진기 기반의 바이오 광학센서를 이용하여 신속하고 정확한 질병 진단 기술을 개발하였다.

연구 방법

임상 샘플의 전처리 과정을 위해 핵산 및 병원체와 선택적으로 결합하는 homobifuntinal imidoester 물질을 이용하여 병원체 농축과 핵산 추출이 가능한 미세유체 플랫폼을 개발하였다. 본 기술의 임상적 유용성 및 기존의 진단 기술과의 성능을 비교하기 위해서 ST, SFTS 환자의 혈액, 10명의 ADV 환자로부터 얻은 비인두 검체, hPIV-3에 감염된 환자로부터 노출되었던 12개의 환경 검체, HZ 환자의 타액 샘플 20개 및 plasma 14개를 이용하여 검증하였다. 또한, 암 환자의 혈액에 돌아다니는 cell-free DNA를 세포 용해 과정 없이 분리하여 암 관련 돌연변이 유전자 (*BRAF, KRAS*)의 유무를 확인할 수 있는 기술을 개발하였다. 실제 대장암 환자의 조직과 혈액을 이용하여 조직 WES 분석 및 혈액 oncopanel 검사결과와 비교하였다. 마지막으로 핵산 검출을 위해 등온성 PCR 기법을 이용한 바이오 광학센서를 개발하였고, ADV 및 HZ 감염 환자의 DNA와 암 환자의 genomic DNA 및 cfDNA로부터 타겟 유전자를 검출하였다.

연구 결과

미세유체 플랫폼을 이용한 샘플 전처리 과정(농축, 핵산 추출)은 한 칩 내에서 50분 이내에 처리가 가능하다. 이 플랫폼은 기존의 키트를 사용했을 때에 비해 병원체의 농축 비율을 80% 이상 향상시켰다. 또한, 46개의 다양한 임상 샘플을 이용하여 검증하였을 때 기존의 진단 방법에서 검출되지 않았던 샘플에서 본 기술을 이용하였을 때 검출함으로써 본 기술이 임상 샘플에서 병원체의 검출 민감도를 향상시킨 것을 확인하였다. 또한 동일한 미세유체 플랫폼을 이용하여 암 환자의 혈액으로부터 cfDNA를 분리한 결과 기존의 키트를 사용한 경우보다 백그라운드 DNA의 양을 감소하여 ctDNA의 검출 효율을 향상시킨 것을 확인하였다.

또한 조직의 WES 분석결과를 비교하였을 때 71.4%의 일치율을 나타내었다. ctDNA의 검출 민감도가 향상됨에 따라 본 기술을 이용할 경우 고가의 NGS 분석을 하지 않더라도 sequencing 및 PCR을 이용하여 돌연변이를 확인할 수 있음을 확인하였다. 마지막으로, 바이오 광학 센서를 이용하여 병원체 및 돌연변이를 검출하였을 때 기존 qPCR 검사법보다 10~100배의 검출 민감도가 향상된 것을 확인하였으며, 미세유체 플랫폼을 이용한 샘플 전처리 과정과 결합함으로써 신속하고 민감도 높은 진단 플랫폼의 가능성을 확인하였다.

결론

본 연구에서는 50분 이내에 샘플 전처리 과정이 가능한 미세유체 플랫폼 및 20분 이내에 핵산 검출이 가능한 바이오 광학센서를 결합하여 임상검체를 사용하였을 때 보다 신속하고 민감도 높게 진단이 가능한 기술을 개발하였다. 이 기술을 이용하여 사람뿐만 아니라 동물의 질병 진단에도 적용할 수 있는 POC 기반의 진단 시스템의 가능성을 확인함에 따라, 감염병 및 암을 비롯한 질병의 관리와 치료에 있어 효율적인 진단 도구가 될 것으로 기대된다.